INSTITUTE
FOR
AEROSPACE STUDIES

UNIVERSITY OF TORONTO

STATISTICAL AND METALLOGRAPHIC ASPECTS OF FATIGUE FAILURE MECHANISMS IN METALS

by

R. Ravindran

Obtain DRF

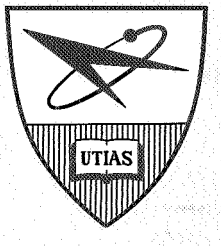

FEBRUARY 1968 UTIAS TECHNICAL NOTE NO. 123

STATISTICAL AND METALLOGRAPHIC ASPECTS OF FATIGUE FAILURE MECHANISMS IN METALS

by

R. Ravindran

Manuscript received November 1967

FEBRUARY 1968 UTIAS TECHNICAL NOTE NO. 123

ACKNOWLEDGEMENTS

The author wishes to thank Dr. G. N. Patterson, Director of the University of Toronto Institute for Aerospace Studies, for providing the opportunity to work on this project, and Dr. G.K. Korbacher for his guidance during the course of this work.

Thanks are due to Mr. P.J. Haagensen for providing most of the computer programs used in this project.

The help rendered to the author by Mr. W. Hoppe, Metallurgical Research Engineer, DeHavilland Aircraft of Canada, Limited and Mr. J.L. Bradbury of the Technical Staff of UTIAS is gratefully acknowledged.

This research project was sponsored jointly by the National Aeronautics and Space Administration and the National Research Council of Canada.

SUMMARY

This note presents the results of a study which is in nature and intent a continuation of the work reported by Haagensen and Muggeridge.

A total of 253 OFHC copper specimens were tested at the following stress levels, 3 at 10.0 ksi, 150 at 16.5 ksi and 100 at 19.0 ksi. The test results at 16.5 ksi were analysed separately as well as together with the test results of those 200 specimens tested previously at 16.5 ksi and reported by Haagensen. The 19.0 ksi test results originate from this study alone. Furthermore, the results of Bloomer and Roylance were treated in a similar manner. All the above test results were analysed using a single log-normal distribution, a single Weibull distribution, a truncated log-normal distribution and the mathematical dissection method.

Furthermore, metallographic and X-ray examinations of the fatigued specimens were carried out. A few specimens each at the stress levels of 12.7 ksi, 13.0 ksi, 14.0 ksi (from tests reported by Haagensen) 16.5 ksi and 19.0 ksi were examined using taper sectioning procedure to study the microstructure near the surface as well as in the work hardened layer, a leftover of the final machining after annealing, at the surface.

The main conclusions of this study are:

1) Both at the 16.5 ksi and the 19.0 ksi stress levels, a single log-normal distribution fitted the data better than a single Weibull distribution.

2) The truncation analysis did not give any evidence for the existence of two distributions at these two stress levels. The mathematical dissection method indicated the existence of only a single distribution which suggests that these two stress levels are above the bimodal transition region.

3) A definitive conclusion about the existence of two distributions could not be drawn from the results of Bloomer and Roylance because of too many sample disturbances and the uncertainty of the actually operative stress amplitude due to the presence of the notch.

4) At 10.0 ksi, even though the life indicates that this stress level is in the low F range, there is still some evidence of H range damage.

5) At 19.0 ksi there are about 60% H and 40% F range grains thus indicating that there is no clear division between H and F and both mechanisms exist in both H and F ranges but one predominating over the other in the respective ranges.

6) The work hardened surface layer and areas near the surface seemed to have a higher percentage of H grains than the other regions.

7) Surface microcracks originated at and developed from the roots of the cutting tool grooves and seemed to link up with the internal microcracks to cause failure by the formation of one or more macrocracks.

8) The development of cracks from tool grooves depends on the stress level and the sharpness of the grooves.

TABLE OF CONTENTS

NOTATION

b	Weibull shape parameter
E	Young's Modulus
f(x)	frequency distribution function or probability density function (p.d.f.)
F(x)	cumulative probability function or cumulative distribution function (c.d.f.)
ksi	thousands of pounds per square inch
LTF	Long Term Fatigue - designating the high-endurance component in a bimodal distribution
$\log_{10}$,log	common logarithm
ln	natural logarithm
n	total number of specimens in the sample of a population
n_{tr}	number of observations, the endurance values of which are known in a truncated sample.
N	endurance of a specimen in cycles
N_i	The ith ordered endurance when the endurance values of a sample are arranged in ascending sequence.
N_o	the minimum life parameter. N_o is defined by $F(N \leq N_o) = 0$
psi	pounds per square inch
P_i	plotting position
r	correlation coefficient
STF	Short Term Fatigue - designating the low-endurance component in a a bimodal distribution.
s^2	Estimate of σ^2 obtained from a sample, sample variance
s	sample standard deviation, estimate of σ
S_a	nominal stress amplitude in ksi
V	characteristic life parameter in Weibull distribution defined by $F(V) = \frac{1}{e}$.
x	$\text{Log}_{10}(N)$

x_i	the ith ordered value of x.
α	scale parameter of Weibull distribution being equal to $(V-N_o)$
β	shape parameter of Weibull distribution (same as b)
x_o	location parameter of Log Weibull distribution
$\Gamma(p)$	complete gamma function with argument p
μ_i	ith central moment or the ith moment about the mean
μ_i'	ith moment about any arbitrary point
σ^2	variance of a population
σ	population standard deviation
u	population mean
λ_i	ith cumulant or semi-invariant.

I. INTRODUCTION

The Stress (S) - Endurance (N) curve representation of fatigue life data is essentially a method of presentation adopted for the convenience of the designer. The S-N curve as such does not explain or provide any phenomenalogical information about the process of fatigue. Coffin (Ref. 8) and Mason (Ref. 22) pointed out that it is possible to represent the S-N curves of several metals using the same power function without recourse to the phenominalogical aspects of fatigue. Wood (Ref. 40) divided the generalised S-N curve into two or three distinct ranges (H, F and S) on the basis of microstructural differences. Each one of Wood's failure mechanism predominates in its respective range in co-existence with the other failure mechanisms.

It is a well recognised fact that fatigue failure is a statistical phenomena. Even under closely controlled conditions a large amount of scatter is observed in the fatigue life of specimens tested under identical conditions and this can be attributed to random variations of several factors such as load, specimen dimensions, material properties of specimens, defects in specimens and the material etc. Hence for the effective presentation of constant amplitude fatigue data it becomes imperative to provide a relation between the number of cycles and the probability of survival at each stress level in addition to the conventional S-N curve. This relation is, in general, based on either the log-normal distribution or the extreme value distribution. It has been observed that in the H range (above the lower 'knee' of the S-N curve) the log-normal distribution gives the best fit whereas in the F range (below the lower 'knee' of the S-N curve) the Weibull or extreme value distribution gives the better fit. At the lower 'knee' itself, neither distribution provides a good fit and a large amount of scatter has been observed.

The large scatter at the lower 'knee' of the S-N curve has been interpreted as being due to discontinuities in the S-N curve (Refs. 31, 39 and 34 for Aluminum, Ref. 29 for polycrystalline copper, Ref. 27 for copper single crystals <111>, and Ref. 2 for steel). Frost (Ref. 13) has approached this problem from the standpoint of microstructural changes. Swanson (Ref. 34) and Cicci (Ref. 6) interpreted the scatter at the lower 'knee' of the S-N curve as due to the blending of two endurance distributions caused by two coexisting fatigue failure mechanisms, namely H and F, the 'knee' being pictured as the transition region between the two ranges. Haagensen (Ref. 15) tested 631 specimens of OFHC copper in an attempt to check the existence of a bimodal endurance distribution at the lower 'knee' of the S-N curve on a sound statistical basis. Muggeridge (Ref. 24) studied the correlation between Haagensen's bimodal endurance distributions and Wood's fatigue failure mechanisms. At 16.5 ksi it was found that there is some discrepancy regarding the respective proportions of the STF and LTF distributions.

The present investigation was undertaken in order to clarify the discrepancy at the 16.5 ksi stress level and to study the endurance distributions and microstructural changes at a higher stress level (19.0 ksi) as well as the microstructural changes at a very low stress level (10.0 ksi) well below the lower 'knee' of the S-N curve. It was also proposed to investigate the effect of the work hardened layer and the grooves left by final machining by means of metallographic examination.

II. MATERIAL, APPARATUS AND TEST PROCEDURE

2.1 Specimen Material

The material used for testing is OFHC copper supplied by Anaconda Company (Canada) in the form of half-hard cold drawn rods of 3/4 inch diameter and 12 ft.length. The specifications are given in the table below.

OFHC COPPER
ASTM SPECIFICATION B-170-47

Contents	Amount by Weight
Copper	99.96 or more
Phosphorous	less than 0.003%
Sulphur	less than 0.004%
Zinc	less than 0.0003%
Mercury	less than 0.001%
Lead	less than 0.001%

2.2 Specimen Configuration and Preparation

The shape of the specimen is shown in Fig. 1a with dimensions, the above shape having been chosen on the basis of minimum stress concentration. The specimens were commercially machined and annealed. First, the specimens were rough machined to 0.0125" oversize on all diameters, then annealed and last fine machined with 5 cuts of 0.0025" depth and 0.002" feed per revolution. This procedure was adopted to remove the slight warping introduced during annealing.

The annealing was done for 2 hours at 1050°F in a vacuum of 25 microns Hg. in batches of 200 specimens with the specimens hung vertically to avoid eccentricity due to warping.

Prior to testing the specimen diameter and eccentricity were measured at the two ends and at mid-length of the test section. The nominal loads used in testing were based on the smallest diameter and specimens having an eccentricity of more than 0.001" were rejected.

2.3 The Fatigue Machines

Two machines were used in the program. The first machine was used to test 3 specimens at 10.0 ksi and 150 specimens at 16.5 ksi. A complete description of this machine can be found in Ref. 15. The operating frequency is about 60 cycles per second and it has an electromagnetic shaker of 25 lbs. force rating.

The second machine was used to test about 100 specimens at 19.0 ksi. Details of the machine and the instrumentation are shown in Figs. 2a, 2b, and 2c. This machine is similar to the first machine except for certain trivial differences in the physical arrangement of parts. The operating frequency is about 48 cycles per second and it has an electromagnetic shaker of 50 lbs. force rating.

Both machines work on the resonance principle. They employ two gripping heads each having a "rubber-flex" collet grip (with well shaped hardened steel plates which are hook-serrated for providing a firm grip) in conical bores. By tightening the collet compression disc and the back-up pin alternately the specimen can be gripped firmly to withstand alternating loads without slipping.

Of the two gripping heads, the upper one can be positioned at any level and clamped to the machine frame firmly. The lower one is movable and is connected through strain gauged dynamometer springs to a horizontal beam which is pivoted at one end and can be oscillated at the other end using the shaker. A mean stress spring is available to apply and vary the mean stress and to load the specimen statically if necessary.

The load monitoring system consists of the dynamometer strain gauges, a pre-amplifier and an electronic voltmeter for measurement. A photoelectric device with two cut out points is actuated by the dynamometer signal to warn against low load (buzzer) and to shut off the machine just before the specimen fails.

The loading arrangement consists of an audio oscillator whose sine wave output is amplified by a power amplifier and is fed to the shaker. The number of load cycles were counted using an electronic counter and an electric clock.

2.4 Machine Alignment and Calibration

The upper and lower grips were aligned to within 1/1000 inch using a strain gauged steel specimen of square cross-section which can be gripped in the machine and the resultant bending strains noted using a strain indicator.

The calibration was done using a strain gauged aluminum alloy (7075-T6) specimen of square cross-section. The specimen was first calibrated statically in an Instron testing machine using a strain indicator. The specimen was then gripped in the fatigue testing machine and an oscilloscope was calibrated for static loads by setting the loads using the strain indicator and applying the loads by means of the mean stress spring. Then the dynamic load was applied by running the machine to obtain a dynamic signal of amplitude equal to the previous static signal on the oscilloscope. This signal was then read on the voltmeter by disconnecting the oscilloscope and connecting instead the pre-amplifier-voltmeter circuit. In this way a calibration curve relating voltage and load was obtained.

2.5 Test Procedure and Environment

Special care was taken to keep experimental errors to a minimum. After gripping a specimen a mark was made on the specimen at the lower front end near the grip to provide a reference to record the crack location later. In most of the tests, failure occurred at the front of the lower fillet or the rear of the upper fillet, this being due to the fact that the maximum bending strains occur at these points (Ref. 15).

As far as possible only specimens from one heat treatment batch were used at each stress level. Prior to each test the bridge pre-amplifier and voltmeter were zeroed and calibrated. During the first few minutes of each test the load increasing due to work hardening in the specimen had to be kept constant by varying the shaker input and frequency.

The temperature rise during some fatigue tests at 19.0 ksi stress level was recorded using a thermocouple and a chart recorder. All tests were done at room temperature and uncontrolled (room) humidity.

III. ANALYSIS OF RESULTS

3.1 The Control Tensile Specimens and Examination of Unfatigued Specimens

To determine the mechanical properties of the specimens tested, 5 specimens from each of the batches were subjected to a tension test. The hardness values of the above specimens were evaluated prior to the tensile test. The results of these tests and the arithmetic means and the standard deviations of the various properties along with the 95% confidence limits for the more important properties are listed in Table I.

Transverse sections (see Fig. 1c) from two unfatigued specimens were prepared by standard polishing methods and were examined under the microscope after etching. The specimens showed a partially recrystallised structure and the grain size was found to be that of ASTM No. 8. Figure 1d shows a typical back reflection X-ray pattern obtained from an unfatigued specimen.

3.2 Statistical Analysis of Results

The endurance data for the specimens tested at 10.0 ksi, 16.5 ksi and 19.0 ksi are listed in Table II. 150 specimens were tested at 16.5 ksi mainly for the purpose of clarifying certain discrepancies reported in Ref. 15. So the endurances at this stress level were analysed separately as well as in conjunction with those of the 200 specimens fatigued in Ref. 15. Hence the following analyses were carried out at both the 16.5 ksi (150 specimens and 350 specimens) and the 19.0 ksi (100 specimens) stress levels.

1) Single log-normal distribution
2) Single Weibull (extreme value) distribution
3) Truncated log-normal distribution
4) Mathematical dissection method (Appendix B).

The theoretical background for analyses (1), (2) and (3) can be found in Ref. 15.

Figures 3,4, and 5 show the histograms with a class length of 0.01 log N for the three sets of data. These do not show any indication of the existence of bimodality. Figure 6 shows the results of the truncation analysis carried out and again there is no evidence to suggest the existence of bimodality at these high stress levels. A simple analysis (Appendix A) shows that if the means of the two component distributions are separated by less than 2.2 times the mean standard deviation, $(\sigma_1 + \sigma_2)/2$, only a single top will exist. Figures 7 and 8 show the data plotted as single distributions on log-normal probability

paper and extreme value probability paper respectively. The goodness of fit as determined by the correlation coefficient (Ref. 15) seems to be better in the case of log-normal distribution than in the case of extreme value distribution for all the sets of data analysed. The somewhat lower value of the correlation coefficient obtained for 19.0 ksi is partly due to the small sample size since if the sample size is small the fit is sensitive to random disturbances in the sample.

If one considers the large scatter at the lower 'knee' of the S-N curve as being composed of the blending of two endurance distributions caused by two coexisting fatigue failure mechanisms, it is obvious that as the stress level approaches the H region of the S-N curve, the means of the component distributions approach each other and at the same time the F component diminishes. Hence under such conditions the truncation analysis becomes obviously inapplicable to determine the existence of bimodality (Appendix A). Therefore the mathematical dissection method outlined in Appendix B was applied to the test results.

In this mathematical method of dissection, instead of assuming the bimodal distribution as a combination of a log-normal distribution (STF component) and a Weibull distribution (LTF component), the bimodal distribution has been assumed to consist of two log-normal distributions for simplicity of analysis. On this basis the parameters pertaining to the two component distributions were calculated. Table III shows the parameters obtained for all the analyses carried out. It can be seen from Tables IIIa and IIIb that the correlation coefficients for the single log-normal distribution are higher than the correlation coefficients for the single Weibull distribution at both the 16.5 ksi and 19.0 ksi stress levels. This indicates that the single log-normal distribution fits the data better than the single Weibull distribution as is to be expected for stress levels well above the lower 'knee' of the S-N curve. The results of the mathematical dissection shown in Table IIIc indicates that there is only a single distribution at both 16.5 and 19.0 ksi stress levels since the proportion of the LTF component present, as indicated by the value of h_2 is practically insignificant.

Figure 9 shows a plot of the temperature rise during fatigue at the 19 ksi stress level. Results from Ref. 15 for 16.5 ksi and 14 ksi are also shown in Fig. 9 for comparison. At 19 ksi, the amount of energy dissipated seemed to rise rapidly during the first 10,000 cycles and then remained almost steady at about 20°F above room temperature, until final fracture occurred. In contrast, the energy dissipation at 16.5 ksi and 14.0 ksi seemed to have a more or less gradual rise throughout the life-time. But in all the cases the maximum temperature rise during fatigue was considered too small to affect the fatigue life of the specimen by any significant amount.

Figure 10 shows a schematic plot of the S-N curve. Results from Ref. 15 have been included in this plot to obtain the points at the 12.7 ksi, 13 ksi and 14 ksi stress levels. Besides the schematic S-N curve, the STF and LTF components are also shown in Fig. 10. The dotted lines indicate the suspected merging of the LTF and STF components above the lower 'knee' which leads to a single distribution in the neighbourhood of the 16.5 ksi stress level and above it.

3.3 Analysis of the Results of Bloomer and Roylance

Bloomer and Roylance (Ref. 4) tested a sample of 973 notched Aluminum (B.26S-WP:2024-ST) specimens using four Wohler type rotating bending cantilever machines. The nominal stress used corresponds to 16.8 ksi. The results of these tests are shown plotted in the form of histograms for all four machines and for the total of 973 specimens in Fig. 11 with a class length of 0.02 log N which is twice the class length used for Figs. 4, 5, and 6. The histograms clearly indicate that there is a large amount of random disturbances or irregularities in the sample. The truncation analysis was applied to these results and the plots obtained are shown in Fig. 12. The plot corresponding to Machine-1 (Fig. 12a) seems to indicate the existence of two distributions. But all the other plots show a much higher random variation of parameters suggesting that the samples are very irregular. Figure 13 shows the plot of the data on log-normal probability paper. The correlation coefficients indicate that the log-normal distribution does not fit any of the results too well. Figure 14 shows the plot of the data on Weibull or extreme value probability paper. The straight line was fitted by the upper vertical moment method. Regression analysis could not be carried out on these plots since there were a few specimens from each of the machines with Log N lower than Log N_o. Consequently, correlation coefficients could not be obtained to determine the relative merits of the log-normal and the log-Weibull distributions from the point of view of what one provides the best fit. The parameters obtained for single log-normal distribution and single log-Weibull distribution are shown in Table IV. An attempt was made to fit the ordinary single Weibull distribution. But it was found that the minimum life obtained by using the upper vertical moment method was higher than the lives of about 15 to 20 specimens in the case of each of the four machine data sets and hence the fit was found to be extremely poor. The mathematical dissection method was also applied to these results and it was found that the method does not converge, possibly because of the irregularities in the samples.

IV. METALLOGRAPHIC EXAMINATION

4.1 Examination of Fatigued Specimens

Specimens tested at 10.0 ksi, 16.5 ksi and 19.0 ksi taken from the tail ends of the endurance histograms were examined for microstructural features characteristic of the failure mechanisms which operate at these stress levels. The specimens were sectioned longitudinally to the diameter (sectioning procedure is shown in Fig. 1b). The sections were then prepared by mechanical polishing followed by electropolishing in ortho-phosphoric acid solution for 30 seconds. Etching was then carried out using a standard ferric chloride reagent.

Another set of specimens tested at 12.7 ksi, 13.0 ksi, 14.0 ksi, 16.5 ksi and 19.0 ksi also taken from the tail ends of the endurance histograms were examined using the taper sectioning procedure (Fig. 1b shows the sectioning procedure), to study the effect of the work hardened layer and the grooves left by final machining. For this purpose the specimens were first silver plated and then a longitudinal flat was ground, polished mechanically and etched using ferric chloride reagent.

4.2 X-Ray Tests

X-ray back reflection patterns give a sure indication of the presence of the deformed grains which are characteristic of the H range. If H range damage is present the Laue spots extend to become arcs. Figure 15 shows the back reflection patterns obtained at 10.0 ksi, 16.5 ksi and 19.0 ksi stress levels. The patterns were taken from specimens sectioned to the diameter and polished mechanically and electrolytically to remove any work hardened layer left by sectioning. The disorientation and deformation of grains occurring as the stress level is increased is clearly revealed in Fig. 15.

4.3 Optical Microscopy

Typical photomicrographs taken from the longitudinal midsection of specimens tested at 10.0 ksi and 19.0 ksi stress levels are given in Figs. 16 and 17. Figure 16 shows some of the photomicrographs taken from specimens fatigued at 10.0 ksi. The 10.0 ksi stress level is well below the lower 'knee' of the S-N curve. However, the figures show some typical F range damage. Figure 16a shows etched up distorted slip zones which are characteristic of F range damage. Figure 16b shows extensive cross slip and straight slip (S range damage). Figure 16c shows straight slip and cross slip along with some distorted slip zones, twin boundary distortion and grain boundary distortion. It is to be noted that twin boundary distortion, twin boundary damage, grain boundary distortion and grain boundary damage are not characteristic of any particular type of damage and hence can be found over a wide range of stress levels in all the ranges, namely H, F, and S. Figure 17 shows some of the photomicrographs taken from specimens fatigued at 19.0 ksi stress level which is well above the lower 'knee' of the S-N curve. Figure 17a shows typical H range damage in several grains being characterised by etch pits along with a twin with H damage (showing etch pits), distorted twins and twin boundary damage. Figure 17b shows fatigued slip zones which are typical of the F range damage along with some cell boundary damage which is typical of the H range. Figure 17c shows a grain with distorted twins and cross slip along with some twin boundary damage. Figure 17d shows cell boundary damage which is typical of the H range along with some distorted twins with boundary damage. Figure 17e shows the interaction between fatigued slip zones and a twin.

Figures 18 to 20 show the photomicrographs of specimens taken from the tail ends of the endurance distributions at 12.7 ksi, 14.0 ksi and 19.0 ksi stress levels. Taper sectioning procedure was used to obtain these photomicrographs and the average taper magnification in all the above pictures varies from 3.0 to 3.5. Figure 18 shows the photomicrographs taken from specimens fatigued at 12.7 ksi. Figure 18a shows some distorted slip zones at very high magnification. Figure 18b shows the grooves left by final machining and the work hardened surface layer at low magnification. Figure 18c shows the work hardened surface layer and a microcrack developing from the grooves left by final machining. Figure 18d shows some F range damage, particularly distorted slip zones. The effect of improper polishing procedure and the area that has been magnified to obtain Fig. 18a is shown in Fig. 18e. The photomicrographs from specimens fatigued at 14.0 ksi stress level are shown in Fig. 19. Figure 19a shows the grooves which are blunt, left by final machining and the absence of microcracks. Figure 19b shows the grooves which are sharp, left by final machining with cracks originating from them. Figure 19c shows typical H range damage in the vicinity of the work hardened surface layer along with distorted twins, twin boundary damage and microcracks. Figure 19d shows a grain with H range damage (note etch

pits) along with distorted twins, twin boundary damage and grain boundary damage at a high magnification. Etch pits reveal the difference in orientation within a grain. Figure 20 shows the photomicrographs taken from specimens fatigued at 19.0 ksi stress level. Figure 20a shows the macrocrack which caused failure along with other macrocracks and microcracks which originate at the grooves left by final machining. Figure 20b shows several microcracks and macrocracks along with some microcracks which are about to link up with the adjoining macrocracks. Figure 20c shows the linking up of microcracks with adjoining macrocrack. It also shows the formation of microcracks from grain boundary damage and slip zones Figure 20d shows a macrocrack running along the grain boundary linking up with microcracks formed in the interior of the grain. Figure 20e shows a typical macrocrack along with some twin boundary damage. Figure 20f shows a macrocrack, cell boundary damage and fatigued slip zones about to open up into cracks. Jaxtaposed depressions can be observed in the macrocracks shown in Fig. 20d, 20e and 20f confirming the earlier observations made by Laird (Ref. 21) and Muggeridge (Ref. 24) regarding crack profiles and crack propagation mechanisms.

V. CONCLUDING REMARKS

On the basis of the statistical analysis carried out on the axial-load fatigue endurance distributions of OFHC copper at two stress levels and the results of Bloomer and Roylance and the metallographic examination of a number of fatigued OFHC copper specimens, the following conclusions could be drawn:

1) Both at the 16.5 ksi and 19.0 ksi stress levels a single log-normal distribution fitted the data better than a single Weibull distribution.

2) The truncation analysis did not give any evidence for the existence of two distributions at these two rather high stress levels. The mathematical dissection method indicated the existence of only a single distribution and hence leads to the conclusion that these two stress levels are above the bimodal transition region and hence have only a single distribution.

3) A definitive conclusion about the existence of two distributions could not be drawn from the results of Bloomer and Roylance because of too many sample disturbances and the uncertainty of the operative stress value because of the presence of the notch.

4) At 10.0 ksi, even though the lift indicates that this stress level is in the low F range, there is still some evidence of H range damage.

5) At 19.0 ksi there are about 60% H and 40% F range grains, thus indicating that there is no clear division between H and F ranges and that both mechanisms exist in co-existance in both H and F ranges but one predominating over the other in their respective ranges.

6) The work hardened surface layer and the areas near the surface seemed to have a higher percentage of H damage than the other regions.

7) Surface microcracks originated at and developed from the roots of the cutting tool grooves and seemed to link up with the internal microcracks to cause failure by the formation of one or more macrocracks.

8) The development of cracks from tool grooves depends on the stress level and the sharpness of the grooves.

REFERENCES

1. Averbach et al — Fracture, John Wiley & Sons, 1959

2. Benham, B.P.
Ford, H. — J. Mech. Engg. Sci., Vol. 3, 1961.

3. Blom, G. — Statistical Estimates and Transformed Beta Variables. Stockholm, 1958.

4. Bloomer, N.T.
Roylance, T.F. — A Large Scale Fatigue Test of Aluminum Specimens. The Aeronautical Quarterly, Vol. XVI, Nov. 1965.

5. Burrau, C. — The Half-Invarients of Two Typical Laws of Errors, with an Application to the Problem of Dissecting a Frequency Curve into Components. Skandinavisk Aktuarietidskrift, 17, 1934, p. 1-6.

6. Cicci, F. — An Investigation of the Statistical Distribution of Constant Amplitude Fatigue Endurance for a Maraging Steel. UTIAS Tech. Note No. 73, July 1964.

7. Clareborough, L.M.
Hargreaves, M.E.
Head, A.K.
West, G.W. — Energy Stored During Fatigue of Copper. Journal of Metals, Jan. 1955.

8. Coffin, L.F., Jr. — Trans. AIME, Vol. 76, 1954.

9. Cramer, H. — Mathematical Methods of Statistics. Princeton University Press, 1961.

10. Forsyth, P.J.E. — Some Metallographic Observations on the Fatigue of Metals. Journal of the Institute of Metals, Vol. 80, 1951-1952.

11. Fraser, D.A.S. — Statistics: An Introduction. John Wiley & Sons, 1958.

12. Freudenthal, A.M.
Grumbel, E.J. — Minimum Life in Fatigue. Journal of the American Statistical Association, Vol. 49, Nov. 1954.

13. Frost, N.E. — Different Between High and Low Stress Fatigue. Nature, Vol. 192, 1961.

14. Gumbel, E.J. — Statistics of Extremes. Columbia University Press, 1966.

15. Haagensen, P.J. — Statistical Aspects of Coexisting Fatigue Failure Mechanisms in OFHC Copper. UTIAS Tech. Note. No. 112, 1967.

16. Hald, A. — Maximum Liklihood Estimation of the Parameters of a Normal Distribution which is Truncated at a Known Point. Skandinavisk Aktuarietidskrift, 1949.

17. Hald, A. — Statistical Theory with Engineering Applications. John Wiley & Sons, 1952.

18. Kemsley, D.S. — The Behaviour of Cold Worked Copper in Fatigue. Journal of the Institute of Metals, Vol.87, 1958-59.

19. Kendall, M.G. Stuart, A. — The Advanced Theory of Statistics, Vol. 1, Distribution Theory. Charles Griffin & Co. 1958.

20. Kendall, M.G. Stuart, A. — The Advanced Theory of Statistics. Vol. 2, Inference and Relationship. Charles Griffin & Co. 1961.

21. Laird, C. — The Influence of Metallurgical Structure on the Mechanism of Fatigue Crack Propagation. Symposium on Fatigue Crack Propagation, ASTM STP 32, June 1966.

22. Mason, S.S. — NACA Report No. 1170, 1954.

23. Mott, N.F. — Acta. Met., Vol. 6, p. 195, 1958.

24. Muggeridge, D.B. — An Attempt to Correlate Bimodal Fatigue Endurance Distributions in OFHC Copper to Wood's H,F, and S Ranges. UTIAS Tech. Note No. 111, Oct. 1966.

25. Nine, H.D. Bendler, H.M. — Effect of Strain Amplitude on Fatigue in Copper Single Crystals, Acta Met., Vol. 12, Aug. 1964.

26. Nine, H.D. — Peculiar Fracture Behaviour for High Amplitude Fatigue in Copper Single Crystals, Acta Met., Vol. 13, No. 9, 1965.

27. Nine, H.D. — Discontinuities in the S-N Fatigue Curve of <111> Copper Single Crystals, Trans. AIME, Vol. 233, July 1965.

28. Pearson, K. — Tables of Incomplete Gamma Function. Cambridge, 1951.

29. Porter, J. — The Fatigue Curves of Copper. Journal of the Institute of Metals, Vol. 89, 1960 - 1961.

30. Sarhan, A.E. Greenberg, B.G. — Contributions to Order Statistics. John Wiley & Sons, 1962.

31. Shabalin, V.I. — Discontinuity in the Fatigue Curve for Duralumin. Metal Industry, Jan. 1959.

32. Stromgren, B. — Tables and Diagrams for Dissecting a Frequency Curve into Components by the Half-Invarient Method. Skandinavisk Aktuarietidskrift, 17, 1934, p. 7 - 54.

33. Swanson, S.R. — Systematic Axial Load Fatigue Tests Using Unnotched Aluminium Alloy 2024-T4 Extruded Bar Specimens. UTIA Tech. Note No. 35, May 1960.

34. Swanson, S.R. — An Investigation of the Fatigue of Aluminum Alloy Due to Random Loading. UTIAS Report No. 84, Feb. 1963.

35. Wadsworth, N.J. — Energy Dissipation During Fatigue Tests (Article), Dislocations and Mechanical Properties of Crystals. John Wiley & Sons, 1956.

36. Weibull, W. — New Methods for Computing Parameters of Complete or Truncated Distributions. FFA Report 58, Aeronautical Research Institute of Sweden, Feb. 1955.

37. Weibull, W. — A Statistical Representation of Fatigue Failure in Solids. Trans. Royal Institute of Technology, No. 27, Stockholm, 1949.

38. Weibull, W. — Fatigue Testing and Analysis of Results. Pergamon Press, 1961.

39. Williams, T.R.G. Stevens, D.T. — Nature, 1964, Vol. 201, p. 1181.

40. Wood, W.A. — Experimental Approach to Basic Study of Fatigue. Institute for the Study of Fatigue and Reliability, Report No. 24, Columbia University, Aug. 1965.

APPENDIX A

Dissection of Frequency Curves

A frequency curve can be dissected into components either by the method of truncation (Ref. 15) or by a formal mathematical method (Ref. 5, 32 and Appendix B). Each method has its own inherent limitations and is only applicable under certain conditions.

The mathematical method, for instance described in Appendix B gives realistic results only if the difference between the means of the component distributions is not appreciably larger than the standard deviation due to reasons discussed in Ref. 32. Moreover the relative sizes of the components should be of reasonable magnitude since otherwise the estimates of the standard deviations will be unrealistic as can be seen from the expressions of the standard deviations given in Appendix B.

For the method of truncation to be successful, the frequency curve should have two tops. A detailed discussion of the conditions under which a bimodal distribution will have only a single top and where therefore the truncation method is not useful is given below.

The above single or two top conditions will have to be considered for the following four cases:

1) Component distributions with equal number of specimens and same standard deviation.

2) Component distributions with unequal number of specimens and same standard deviation.

3) Component distributions with equal number of specimens and unequal standard deviation.

4) Component distributions with unequal number of specimens and unequal standard deviation.

Cases (1), (2), and (3) are particular cases of case (4) but still all cases are discussed separately.

Case 1

$$n_1 = n_2 = \frac{N}{2} \; ; \; \sigma_1 = \sigma_2 = \sigma$$

where n_1 and n_2 are the number of specimens in component 1 and 2 respectively and N the total number of specimens.

The probability density function is given by,

$$f(x) = \tfrac{1}{2}\left\{ \frac{1}{\sqrt{2\pi}\sigma} \; e^{-\frac{(x-m_1)^2}{2\sigma^2}} + \frac{1}{\sqrt{2\pi}\sigma} \; e^{-\frac{(x-m_2)^2}{2\sigma^2}} \right\}$$

Referring to the sketch below, the condition for flat top is $x_1 + x_2 = 2x_3$.
Let $(m_2 - m_1) = K\sigma$

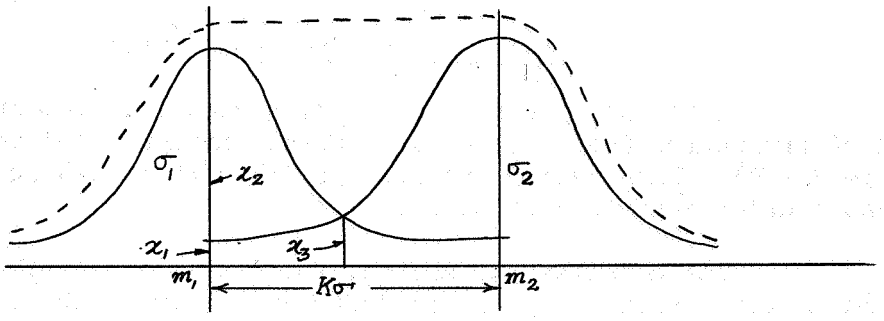

Hence,

$$\frac{1}{2}\left\{\frac{1}{\sqrt{2\pi}\sigma} + \frac{1}{\sqrt{2\pi}\sigma}\ e^{-K^2/2}\right\} = \frac{1}{\sqrt{2\pi}\sigma}\ e^{-K^2/8}$$

or,

$$\frac{1}{2}\left\{\frac{1}{\sqrt{2\pi}} + \frac{1}{\sqrt{2\pi}}\ e^{-K^2/2}\right\} = \frac{1}{\sqrt{2\pi}}\ e^{-(K/2)^2/2}$$

The above equation can be solved graphically to obtain K = 2.212. Hence if $(m_2-m_1) \leq 2.212\sigma$ only a single top exists.

Case 2

$$\frac{n}{N} = \alpha\ ,\quad \frac{n}{N} = \beta\ ;\ \sigma_1 = \sigma_2 = \sigma$$

Hence $\alpha + \beta = 1$ Let $(m_2-m_1) = K$

The probability density function is given by,

$$f(x) = \frac{\alpha}{\sqrt{2\pi}\sigma}\ e^{-\frac{(x-m_1)^2}{2\sigma^2}} + \frac{\beta}{\sqrt{2\pi}\sigma}\ e^{-\frac{(x-m_2)^2}{2\sigma^2}}$$

Referring to sketch, the condition for having a single top is that AB should be either a straight line or should be a convex curve.

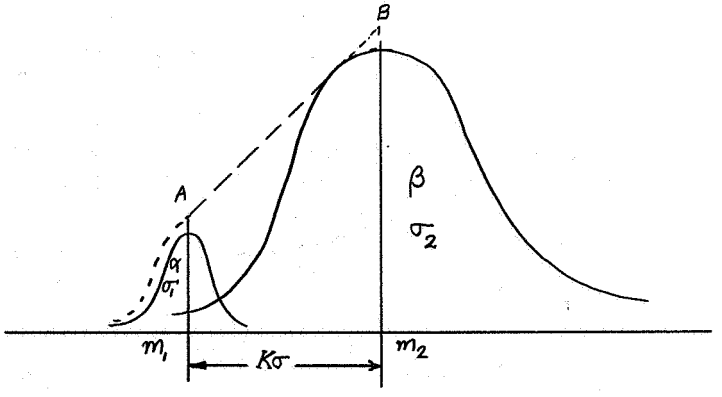

Hence,

$$\frac{1}{2}\left\{\left(\frac{\alpha}{\sqrt{2\pi}\sigma}\ e^{-K^2/2} + \frac{\beta}{\sqrt{2\pi}\sigma}\right) - \left(\frac{\alpha}{\sqrt{2\pi}\sigma} + \frac{\beta}{\sqrt{2\pi}\sigma}\ e^{-K^2/2}\right)\right\}$$

$$= \left\{\left(\frac{\alpha}{\sqrt{2\pi}\sigma}\ e^{-(K/2)^2/2} + \frac{\beta}{\sqrt{2\pi}\sigma}\ e^{-(K/2)^2/2}\right) - \left(\frac{\alpha}{\sqrt{2\pi}\sigma} + \frac{\beta}{\sqrt{2\pi}\sigma}\ e^{-K^2/2}\right)\right\}$$

or

$$\frac{1}{2}\left\{\frac{1}{\sqrt{2\pi}} + \frac{1}{\sqrt{2\pi}}\ e^{-K^2/2}\right\}\ (\alpha+\beta) = \frac{1}{\sqrt{2\pi}}\ e^{-(K/2)^2/2}$$

Since $(\alpha+\beta) = 1$, the above equation yields the same result as in Case 1, namely $K = 2.212$. Hence if $(m_2 - m_1) \leq 2.212\sigma$ only a single top exists.

Case 3

$$n_1 = n_2 = \frac{N}{2}\ ; \sigma_2 = n\ \sigma_1$$

Let $(m_2 - m_1) = K\left(\frac{\sigma_1 + \sigma_2}{2}\right)$, where $\left(\frac{\sigma_1 + \sigma_2}{2}\right)$ is called the mean standard deviation.

The condition for having a single top is,

$$\frac{1}{2}\left\{\frac{1}{2}\left(\frac{1}{\sqrt{2\pi}\sigma_1}\ e^{-\frac{[\frac{K}{2}(\sigma_1+\sigma_2)]^2}{2\sigma_1^2}} + \frac{1}{\sqrt{2\pi}\sigma_2}\right) - \left(\frac{1}{\sqrt{2\pi}\sigma_1} + \frac{1}{\sqrt{2\pi}\sigma_2}\ e^{-\frac{[\frac{K}{2}(\sigma_1+\sigma_2)]^2}{2\sigma_2^2}}\right)\right\}$$

$$= \left\{\frac{1}{2}\left(\frac{1}{\sqrt{2\pi}\sigma_1}\ e^{-\frac{[\frac{K}{4}(\sigma_1+\sigma_2)]^2}{2\sigma_1^2}} + \frac{1}{\sqrt{2\pi}\sigma_2}\ e^{-\frac{[\frac{K}{4}(\sigma_1+\sigma_2)]^2}{2}}\right) - \frac{1}{2}\left(\frac{1}{\sqrt{2\pi}\sigma_1} + \frac{1}{\sqrt{2\pi}\sigma_2}\ e^{-\frac{[\frac{K}{2}(\sigma_1+\sigma_2)]^2}{2\sigma_2^2}}\right)\right\}$$

The above equation can be solved for various values of n after substituting $\sigma_2 = n\,\sigma_1$ and the value of K lies between 0 and 2.212.

Case 4

$$\frac{n_1}{N} = \alpha,\ \frac{n_2}{N} = \beta\ ;\ \sigma_2 = n\ \sigma_1\ ,\ \text{Let}\ (m_2 - m_1) = K\left(\frac{\sigma_1 \pm \sigma_2}{2}\right)$$

The condition for having a single top is,

$$\frac{1}{2}\left\{\left(\frac{\alpha}{\sqrt{2\pi}\sigma_1}\ e^{-\frac{[\frac{K}{2}(\sigma_1+\sigma_2)]^2}{2}} + \frac{\beta}{\sqrt{2\pi}\sigma_2}\right) - \left(\frac{\alpha}{\sqrt{2\pi}\sigma_1} + \frac{\beta}{\sqrt{2\pi}\sigma_2}\ e^{-\frac{[\frac{K}{2}(\sigma_1+\sigma_2)]^2}{2\sigma_2^2}}\right)\right\}$$

$$= \left\{\left(\frac{\alpha}{\sqrt{2\pi}\sigma_1}\ e^{-\frac{[\frac{K}{4}(\sigma_1+\sigma_2)]^2}{2}} + \frac{\beta}{\sqrt{2\pi}\sigma_2}\ e^{-\frac{[\frac{K}{4}(\sigma_1+\sigma_2)]^2}{2}}\right) - \left(\frac{\alpha}{\sqrt{2\pi}\sigma_1} + \frac{\beta}{\sqrt{2\pi}\sigma_2}\ e^{-\frac{[\frac{K}{2}(\sigma_1+\sigma_2)]^2}{2\sigma_2^2}}\right)\right\}$$

Putting $\sigma_2 = n\,\sigma_1$ and $\beta = (1-\alpha)$ and assigning various values of α and n one can solve the above equation to determine K. The value of K is found to vary from 0 to 2.212.

Hence taking into consideration the worst circumstances, if the means are separated by less than 2.212 times the mean standard deviation, $(\sigma_1 + \sigma_2)/2$, only a single top exists and hence it is not very reliable to use the method of truncation under such conditions.

APPENDIX B

Mathematical Dissection of Frequency Curves into Components

In 1894 Pearson treated the problem of dissecting a given frequency curve into two typical laws of errors (Normal). He used the expressions for moments of a sum of two typical laws of errors to accomplish the dissection. His method involved the solution of a certain 9th degree algebraic equation.

Charlier (1906, 1923) recommended a modified method of elimination which lead to two equations with two unknowns to be solved simultaneously.

Barrau (Ref. 5) used the cumulants or half-invarients instead of moments in a similar approach. Tables and charts were provided by Stromgren (Ref. 32) for solutions by Barrau's method.

In the present problem of fatigue testing it is a more or less generally accepted fact that the lower life component (STF) follows a log-normal distribution whereas the higher lift component (LTF) seem to follow a Weibull distribution. Therefore one has to dissect a frequency curve into two components, one of which is log-normal and the other a Weibull or extreme value distribution.

If n_1 and n_2 are the number of specimens in each of the component distributions, the probability density function is given by,

$$f(x) = n_1 \frac{1}{\sigma\sqrt{2\pi}} e^{-\frac{1}{2}\left(\frac{x-\mu}{\sigma}\right)^2} + n_2 \left(\frac{\beta}{\alpha}\right)\left(\frac{x - x_o}{\alpha}\right)^{\beta-1} e^{-\left(\frac{x-x_o}{\alpha}\right)^{\beta}}$$

The moment generating function is,

$$M(t) = E(e^{xt}) = \int_{-\infty}^{\infty} \left\{ n_1 \frac{1}{\sigma\sqrt{2\pi}} e^{-\frac{1}{2}\left(\frac{x-\mu}{\sigma}\right)^2} + n_2 \left(\frac{\beta}{\alpha}\right)\left(\frac{x-x_o}{\alpha}\right)^{\beta-1} e^{-\left(\frac{x-x_o}{\alpha}\right)^{\beta}} \right\} e^{xt} dx$$

$$= n_1 e^{\mu t + t^2 \frac{\sigma^2}{2}} + n_2 \frac{\beta}{\alpha^{\beta}} \int_{-\infty}^{\infty} (x-x_o)^{\beta-1} e^{xt} e^{-\left(\frac{x-x_o}{\alpha}\right)^{\beta}} dx$$

The second term leads to a complicated series. Since one is interested in the moments of the distribution, the expressions for the various moments can be obtained without recourse to the above expression.

For the second component (Weibull) the general expression for the kth order moment is

$$E(X^K) = \sum_{j=0}^{K} \binom{K}{j} x_o^{K-j} \alpha^{(j/\beta)} g_j$$

where $g_j = \Gamma\left(\frac{j}{\beta} + 1\right)$ and $\binom{K}{j} = \frac{K!}{j!\,(K-j)!}$

Hence one obtains the following expressions for the various moments of the compound distribution:

$$1 = h_1 + h_2$$

$$\mu_1' = h_1\mu + h_2(x_o + \alpha^{(1/\beta)}g_1)$$

$$\mu_2' = h_1(\mu^2 + \sigma^2) + h_2\{(x_o)^2 + 2x_o\alpha^{(1/\beta)}g_1 + \alpha^{(2/\beta)}g_2\}$$

$$\mu_3' = h_1(\mu^3 + 3\mu\sigma^2) + h_2\{x_o^3 + 3x_o^2\,\alpha^{(1/\beta)}g_1 + 3x_o\alpha^{(2/\beta)}g_2 + \alpha^{(3/\beta)}g_3\}$$

$$\mu_4' = h_1(\mu^4 + 6\mu^2\sigma^2 + 3\sigma^4) + h_2\{x_o^4 + 4x_o^3\,\alpha^{(1/\beta)}g_1 + 6x_o^2\,\alpha^{(2/\beta)}g_2 + 4x_o\alpha^{(3/\beta)}g_3 + \alpha^{(4/\beta)}g_4\} \qquad (A)$$

$$\mu_5' = h_1(\mu^5 + 10\mu^3\sigma^2 + 15\mu\sigma^4) + h_2\{x_o^5 + 5x_o^4\,\alpha^{(1/\beta)}g_1 + 10x_o^3\,\alpha^{(2/\beta)}g_2 + 10x_o^2\,\alpha^{(3/\beta)}g_3 + 5x_o\,\alpha^{(4/\beta)}g_4 + \alpha^{(5/\beta)}g_5\}$$

$$\mu_6' = h_1(\mu^6 + 15\mu^4\sigma^2 + 45\mu^2\sigma^4 + 15\sigma^6) + h_2\{x_o^6 + 6x_o^5\,\alpha^{(1/\beta)}g_1 + 15x_o^4\,\alpha^{(2/\beta)}g_2 + 20x_o^3\,\alpha^{(3/\beta)}g_3 + 15x_o^2\,\alpha^{(4/2)}g_4 + 6x_o\,\alpha^{(5/\beta)}g_5 + \alpha^{(6/\beta)}g_6\}$$

where $h_1 = \frac{n_1}{N}$ and $h_2 = \frac{n_2}{N}$

One has to solve for the seven unknowns namely, n_1, n_2, μ, σ, x_o, α and β. Therefore seven equations are needed and in the method of moments the seven equations in (A) are used.

The above equations form a set of nonlinear algebraic simultaneous equations for the solution of which no general method is available. Methods like Newton's method and the method of steepest descent have been extensively used for such problems. In the present case, the problem is further complicated by the fact that the unknowns appear as powers of other unknowns.

In the method of cumulants, the first equation of (A) along with six other equations obtained by substituting the expressions for moments from (A) in the following expressions for cumulants can be used.

$$\lambda_1 = \mu_1'$$

$$\lambda_2 = \mu_2' - \mu_1'$$

$$\lambda_3 = \mu_3' - 3\mu_2'\mu_1' + 2\mu_1'^3$$

$$\lambda_4 = \mu_4' - 4\mu_3'\mu_1' - 3\mu_2'^2 + 12\mu_2'\mu_1'^2 - 6\mu_1'^4$$

$$\lambda_5 = \mu_5' - 5\mu_4'\mu_1' - 10\mu_3'\mu_2' + 20\mu_3'\mu_1'^2 + 30\mu_2'^2\mu_1' - 60\mu_2'\mu_1'^3 + 24\mu_1'^5 \qquad (B)$$

$$\lambda_6 = \mu_6' - 6\mu_5'\mu_1' - 15\mu_4'\mu_2' + 30\mu_4'\mu_1'^2 - 10\mu_3'^2 + 120\mu_3'\mu_2'\mu_1' - 120\mu_3'\mu_1'^3 + 30\mu_2'^3 - 270\mu_2'^2\mu_1'^2 + 360\mu_2'\mu_1'^4 - 120\mu_1'^6$$

Thus it is obvious that this procedure is unlikely to lead to any substantial simplification over the method of moments.

Instead of facing the formidable task of solving the equations in either of the above cases one can simplify the model by assuming the Weibull component as another log-normal distribution. So in the method of moments we obtain the following six equations in place of equations (A) to solve for the six unknowns n_1, n_2, μ_1, μ_2, σ_1, and σ_2.

$$
\begin{aligned}
1 &= h_1 + h_2 \\
\mu_1' &= h_1 \mu_1 + h_2 \mu_2 \\
\mu_2' &= h_1 (\mu_1^2 + \sigma_1^2) + h_2(\mu_2^2+\sigma_2^2) \\
\mu_3' &= h_1 (\mu_1^3+ 3\mu_1\sigma^2) + h_2(\mu_2^2+ 3\mu_2\sigma_2^2) \\
\mu_4' &= h_1 (\mu_1^4+ 6\mu_1^2 \sigma_1^2+ 3\sigma_1^4) + h_2 (\mu_2^4 + 6 \mu_2^2 \sigma_2^2+ 3\sigma_2^4) \\
\mu_5' &= h_1 (\mu_1^5 + 10\mu_1^3 \sigma_1^2+ 16 \mu_1\sigma_1^4)+ h_2(\mu_2^5 + 10\mu_2^3 \sigma_2^2+ 16 \mu_2 \sigma_2^4)
\end{aligned}
\qquad (C)
$$

For the method of cumulants substituting (C) in (B) one obtains after manipulation the following equations which incidentially are the same as Barrau's equations except for changes in notation.

$$
\begin{aligned}
1 &= h_1 + h_2 \\
\lambda_1 &= h_1\mu_1 + h_2\mu_2 \\
\lambda_2 &= h_1h_2(\mu_2- \mu_1)^2 + h_1 \sigma_1^2+ h_2\sigma_2^2 \\
\lambda_3 &= h_1h_2(h_1-h_2) (\mu_2- \mu_1)^3 + 3h_1h_2 (\mu_2- \mu_1)(\sigma_2^2-\sigma_1^2) \\
\lambda_4 &= h_1h_2(h_1^2- 4h_1h_2+ h_2^2)(\mu_2-\mu_1)^4 + 6 h_1h_2(h_1-h_2)(\mu_2-\mu_1)^2 (\sigma_2^2- \sigma_1^2) \\
&\qquad + 3 h_1h_2(\sigma_2^2- \sigma_1^2)^2 \\
\lambda_5 &= h_1h_2(h_1^3- 11 h_1^2h_2+ 11 h_1h_2^2 - h_2^3)(\mu_2 -\mu_1)^5+ 10h_1h_2(h_1^2- 4h_1h_2+ h_2^2)(\mu_2-\mu_1)^3 \\
&\qquad \times(\sigma_2^2 - \sigma_1^2) + 15 h_1h_2(h_1- h_2)(\mu_2-\mu_1)(\sigma_2^2-\sigma_1^2)
\end{aligned}
\qquad (D)
$$

Solving equations (D) is simpler than solving equations (C) (Ref. 5). For any specific problem knowing the first five cumulants λ_1, λ_2, λ_3, λ_4 and λ_5, equations (D) can be solved to obtain estimates of n_1, n_2, μ_1, μ_2, σ_1 and σ_2 using the charts and tables given in Ref. 32 even though it is a time consuming procedure. Therefore, a direct method suitable for use with computers will be outlined below.

Defining $\alpha = (\mu_2 - \mu_1)$ and $\beta = (\sigma_2^2- \sigma_1^2)$

and knowing h_1 and α, the other unknowns can be found with the following equations derived from (D).

$$
\begin{aligned}
h_2 &= (1 - h_1) \\
\mu_1 &= (\lambda_1 - \alpha h_2) \\
\mu_2 &= (\alpha h_1 + \lambda_1) \\
\sigma_1 &= \left\{ \lambda_2 - \frac{\lambda_3}{3h_1\alpha} - \frac{h_2(2h_1+h_2)}{3} \alpha^2 \right\}^{\frac{1}{2}} \\
\sigma_2 &= \left\{ \lambda_2 + \frac{\lambda_3}{3h_2\alpha} - \frac{h_1(h_1+2h_2)}{3} \alpha^2 \right\}^{\frac{1}{2}}
\end{aligned}
$$

Hence the problem reduces to one determining α and h_1. From equation 4 of (D)

$$\beta = \frac{\lambda_3}{3h_1h_2\alpha} - \frac{(h_1 - h_2)\alpha^2}{3}$$

From equation 1 of (D), $h_2 = 1 - h_1$

Using the above, equation 5 of (D) can be reduced to

$$h_1^6(2\alpha^6) - h_1^5(6\alpha^6) + h_1^4(8\alpha^6) - h_1^3(6\alpha^6 - 8\lambda_3\alpha^3) + h_1^2(2\alpha^6 - 12\lambda_3\alpha^3 - 3\lambda_4\alpha^2) + h_1(4\lambda_3\alpha^3 + 3\lambda_4\alpha^2) - \lambda_3^2 = 0 \qquad (I)$$

Similarly equation 6 of (D) can be reduced to

$$\alpha^6(h_1^4 - 2h_1^3 + h_1^2)(24h_1^3 - 36h_1^2 + 24h_1 - 6) + 60\lambda_3(h_1^4 - 2h_1^3 + h_1^2)\alpha^3 + 9\lambda_5(h_1 - h_1^2)\alpha - 15\lambda_3^2(2h_1 - 1) = 0 \qquad (II)$$

For a known value of α equation (I) is a polynomial in h_1 and can be denoted by $g(h_1) = 0$.

Similarly for a known value of h_1 , equation (II) is a polynomial in α and can be denoted by $f(\alpha) = 0$

By Newton-Raphson method,

$$(h_1)_{New} = h - \frac{g(h_1)}{g'(h_1)}$$

$$= h - \left\{ \frac{2\alpha^6h_1^6 - 6\alpha^6h_1^5 + 8\alpha^6h_1^4 - (6\alpha^6 - 8\lambda_3\alpha^3)h_1^3 + (2\alpha^6 - 12\lambda_3\alpha^3 - 3\lambda_4\alpha^2)h_1^2 + (4\lambda_4\alpha^3 + 3\lambda_4\alpha^2)h_1 - \lambda_3^2}{12\alpha^6h_1^5 - 30\alpha^6h_1^4 + 32\alpha^6h_1^3 - (18\alpha^6 - 24\lambda_3\alpha^3)h_1^2 + (4\alpha^6 - 24\lambda_3\alpha^3 - 6\lambda_4\alpha^2)h_1 + 4\lambda_3\alpha^3 + 3\lambda_4\alpha^2} \right\}$$

$$(\alpha)_{New} = \alpha - \frac{f(\alpha)}{f'(\alpha)}$$

$$= \left\{ \frac{(h_1^4 - 2h_1^3 + h_1^2)(24h_1^3 - 36h_1^2 + 24h_1 - 6)\alpha^6 + 60\lambda_3(h_1^4 - 2h_1^3 + h_1^2)\alpha^3 + 9\lambda_5(h_1 - h_1^2)\alpha - 15\lambda_3^2(2h_1 - 1)}{6(h_1^4 - 2h_1^3 + h_1^2)(24h_1^3 - 36h_1^2 + 24h_1 - 6)\alpha^5 + 180\lambda_3(h_1^4 - 2h_1^3 + h_1^2)\alpha^2 + 9\lambda_5(h_1 - h_1^2)} \right\}$$

By providing starting values for α and h_1 the above expressions can be used in an iteration procedure to obtain better values, the iteration being terminated after sufficient convergence is achieved.

A computer program was set up to compute the cumulants and to obtain values of, h_1, h_2, μ_1, μ_2, σ_1 and σ_2 using the above method. Several of the examples given in Ref. 32 were tried and they gave the same answers as in Ref. 32, confirming the practicability of the method. The method fails if the means of the two components are separated by an amount appreciably larger than the standard deviation due to reasons outlined in Ref. 32.

TABLE I

CONTROL TENSILE SPECIMEN DATA

Nominal Stress Amplitude S_a (ksi)	Specimen number. *Designates heat treatment batch	Mean diameter (inches)	0.2% Proof stress (psi)	Tensile Strength (psi)	E x 10^{-6} (psi)	Elongation on 1 inch (%)	Area reduction (%)	Diamond pyramid hardness of unfatigued material
10.0,16.5	*F-171	0.2901	9,508	41,183	21.8	63.5	92.2	38.02
	F-172	0.2905	8,600	41,041	17.52	63.5	91.8	37.27
	F-173	0.2909	8,275	41,077	16.15	61.0	91.4	37.23
	F-174	0.2906	8,745	41,392	17.63	64.5	91.5	35.94
	F-175	0.2913	8,547	41,086	16.67	61.5	91.8	36.51
19.0	E-137	0.2904	13,287	41,673	18.78	60.5	92.4	36.42
	E-138	0.2911	15,026	41,773	18.98	60.0	91.8	37.87
	E-139	0.2907	9,334	41,253	18.80	62.0	91.8	38.48
	E-140	0.2909	8,802	41,378	21.30	65.5	92.4	39.17
	E-141	0.2919	9,115	41,393	17.73	65.0	91.9	37.96
19.0	G-17	0.2910	8,421	41,504	17.08	61.0	91.4	38.15
	G-18	0.2909	8,877	41,529	20.50	64.0	92.2	36.51
	G-19	0.2901	8,623	41,301	20.60	62.5	91.4	36.61
	G-20	0.2906	8,443	41,164	18.20	61.5	91.2	35.52
	G-21	0.2907	8,732	41,253	20.40	62.0	92.1	36.57
Mean			9,489	41,333	18.81	62.5	91.8	37.20
Standard Deviation			1,952	218	1.75			
95% Confidence Limits			8,408	41,213	17.84			
			10,570	41,454	19.78			

TABLE II

RANKED FATIGUE ENDURANCES

(CYCLES TO FAILURE) x 10^{-6}

Rank	10 ksi	16.5 ksi	19.0 ksi
1	4.724855	0.133670	0.053781
2	7.754862	0.143412	0.056897
3	19.939855	0.144499	0.057314
4		0.148993	0.058724
5		0.155734	0.060064
6		0.157741	0.060233
7		0.160678	0.060403
8		0.163277	0.060786
9		0.165278	0.061057
10		0.165824	0.062062
11		0.167091	0.062643
12		0.169573	0.062756
13		0.170941	0.062884
14		0.170985	0.063497
15		0.171196	0.063530
16		0.171237	0.064019
17		0.171796	0.064071
18		0.171858	0.064326
19		0.172882	0.064360
20		0.173165	0.065126
21		0.174431	0.065275
22		0.175384	0.065325
23		0.176240	0.065564
24		0.177119	0.065654
25		0.177812	0.065851
26		0.178107	0.066013
27		0.180846	0.066071
28		0.181259	0.066155
29		0.181437	0.066502
30		0.185261	0.066632
31		0.185446	0.066673
32		0.185855	0.066832
33		0.186063	0.066914
34		0.186410	0.067408
35		0.186504	0.067735
36		0.186573	0.067769
37		0.187171	0.067804
38		0.187245	0.067833
39		0.188442	0.067963
40		0.188602	0.068365
41		0.188873	0.068369
42		0.188884	0.068655
43		0.190483	0.068861
44		0.190556	0.069525
45		0.191976	0.069544
46		0.192880	0.069636
47		0.192917	0.069693
48		0.193961	0.069732
49		0.194958	0.069981
50		0.195274	0.070146

TABLE II - continued

Rank	10 ksi	16.5 ksi	19.0 ksi
51		0.195797	0.070381
52		0.196076	0.070704
53		0.196096	0.071196
54		0.196225	0.071207
55		0.197082	0.071428
56		0.198465	0.071752
57		0.199300	0.071904
58		0.199554	0.072160
59		0.200314	0.072327
60		0.200412	0.072352
61		0.200554	0.072814
62		0.200715	0.072857
63		0.200975	0.073188
64		0.201135	0.073286
65		0.201630	0.073506
66		0.201817	0.073733
67		0.201823	0.074001
68		0.201949	0.074182
69		0.203206	0.074638
70		0.204003	0.074667
71		0.204791	0.074716
72		0.205522	0.074979
73		0.205868	0.075156
74		0.206264	0.075608
75		0.206533	0.075658
76		0.206862	0.076176
77		0.207005	0.076225
78		0.208479	0.076236
79		0.210603	0.076300
80		0.212287	0.076374
81		0.212348	0.077583
82		0.212662	0.078340
83		0.213520	0.078919
84		0.214395	0.079063
85		0.214908	0.079100
86		0.215995	0.079181
87		0.217440	0.079584
88		0.217678	0.079650
89		0.217742	0.079833
90		0.219021	0.080865
91		0.219803	0.082291
92		0.219902	0.082467
93		0.219983	0.082982
95		0.222300	0.084063
95		0.222609	0.085400
96		0.222823	0.087042
97		0.223079	0.087509
98		0.223154	0.091770
99		0.223301	0.097286
100		0.223963	0.116950
101		0.224080	
102		0.226722	
103		0.226948	
104		0.227155	
105		0.227166	

TABLE II - concluded

Rank	10 ksi	16.5 ksi	19.0 ksi
106		0.227686	
107		0.228390	
108		0.229288	
109		0.229554	
110		0.229638	
111		0.230820	
112		0.232774	
113		0.232948	
114		0.233787	
115		0.234165	
116		0.235247	
117		0.239302	
118		0.239566	
119		0.239960	
120		0.240027	
121		0.240051	
122		0.242189	
123		0.242751	
124		0.244210	
125		0.245498	
126		0.245765	
127		0.246116	
128		0.247234	
129		0.249065	
130		0.251035	
131		0.251147	
132		0.254924	
133		0.256093	
134		0.256164	
135		0.257553	
136		0.257684	
137		0.258779	
138		0.263382	
139		0.264940	
140		0.265414	
141		0.265725	
142		0.266822	
143		0.272201	
144		0.274876	
145		0.276605	
146		0.280214	
147		0.280321	
148		0.287637	
149		0.330226	
150		0.333713	

TABLE III

A) PARAMETERS OF SINGLE LOG-NORMAL DISTRIBUTION

	16.5 ksi 150 specimens)	16.5 ksi 350 specimens	19.0 ksi 100 specimens
Mean of log(N), $\bar{X}$	5.32089	5.32058	4,85163
Standard deviation, s	0.0704147	0.0903587	0.0510833
Correlation coefficient, r	0.99712	0.99918	0.97805

B) PARAMETERS OF SINGLE WEIBULL DISTRIBUTION (UPPER VERTICAL MOMENT METHOD)

	16.5 ksi 150 specimens	16.5 ksi 350 specimens	19.0 ksi 100 specimens
Shape parameter, b	2.25439	2.19052	1.81487
Minimum life, N_o (Mill. cycles)	0.138887	0.121481	0.0568477
Characteristic life, V (Mill. cycles)	0.221759	0.225820	0.0735204
Correlation coefficient, r	0.98281	0.98383	0.88723

C) PARAMETERS OF MATHEMATICAL DISSECTION METHOD

	16.5 ksi 150 specimens	16.5 ksi 350 specimens	19.0 ksi 100 specimens
STF Component			
h_1	0.999854	0.999774	0.997580
Mean of log(N), m_1	5.320897	5.320587	4.850606
Standard deviation, s_1	0.074330	0.088239	0.047027
LTF Component			
h_2	0.000145	0.000225	0.002419
Mean of log(N), m_2	5.312835	5.298581	5.272022
Standard deviation, s_2	2.028144	1.260850	0.145477

TABLE IV

A) PARAMETERS OF SINGLE LOG-NORMAL DISTRIBUTION

Machine No.	1	2	3	4
Number of Specimens	243	255	245	230
Mean of log(N), $\bar{X}$	5.95902	5.94342	5.97992	5.97745
Standard deviation, s	0.177530	0.164388	0.189107	0.190898
Correlation coefficient, r	0.93047	0.94431	0.88778	0.91626

B) PARAMETERS OF SINGLE LOG-WEIBULL DISTRIBUTION (UPPER VERTICAL MOMENT METHOD)

Machine No.	1	2	3	4
Number of specimens	243	255	245	230
Shape parameter, b	1.54682	1.76714	1.45728	1.29897
Minimum life, log N_o	5.70737	5.68136	5.74261	5.74781
Characteristic life, log V	5.98883	5.97763	6.00701	5.99812

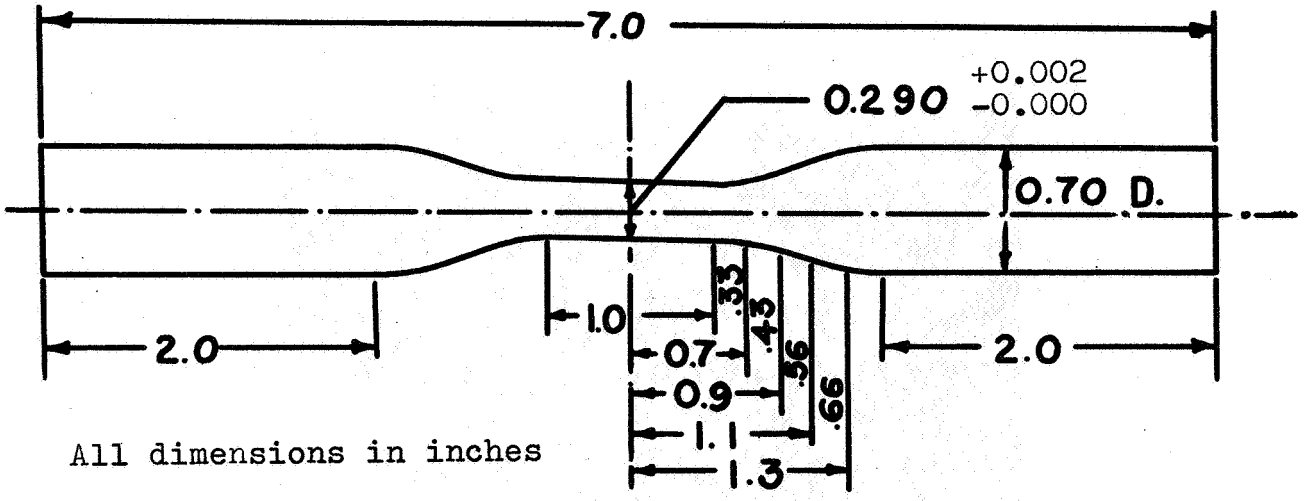

FIG. 1(a). THE COPPER (O.F.H.C) FATIGUE SPECIMEN.

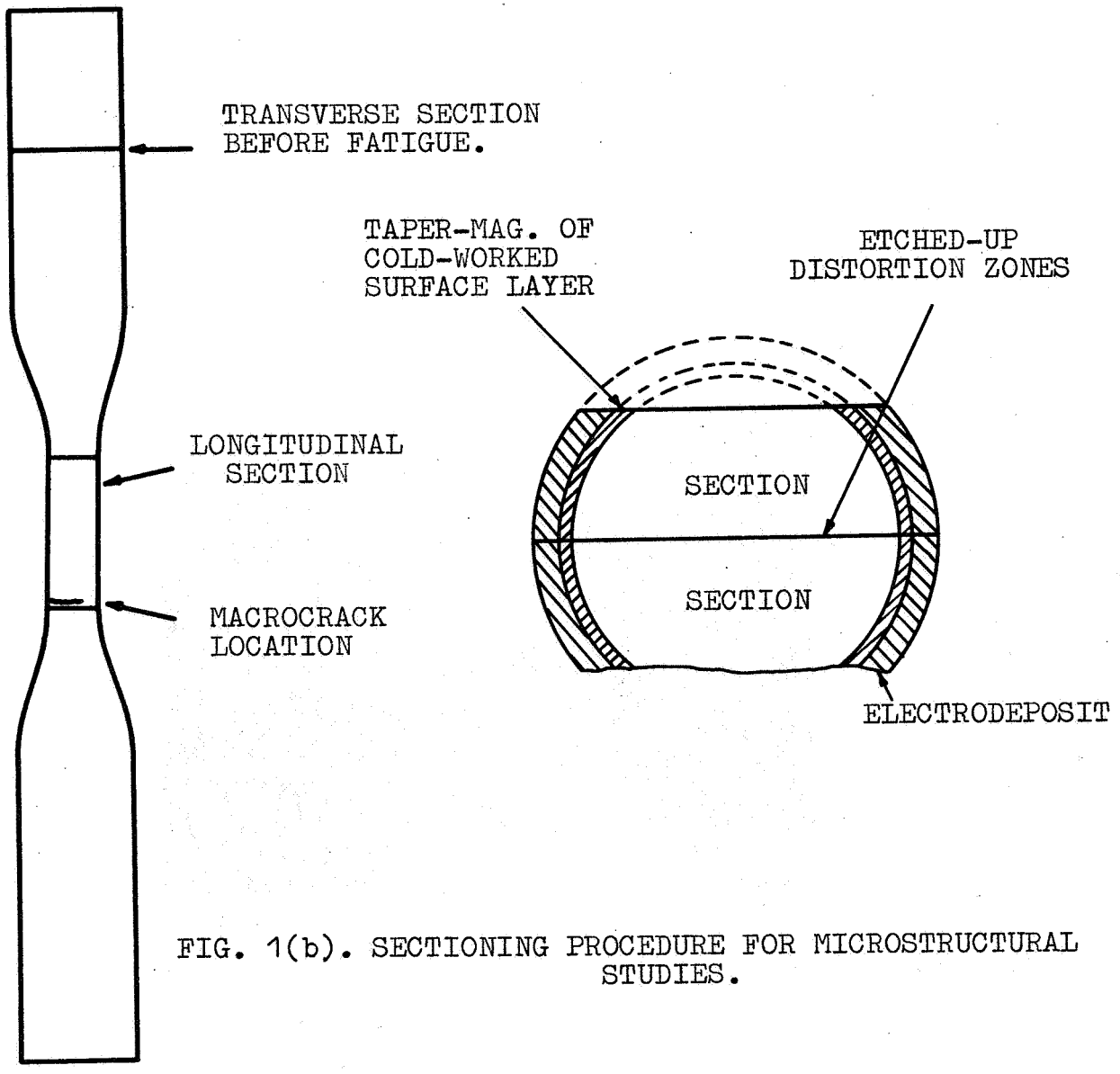

FIG. 1(b). SECTIONING PROCEDURE FOR MICROSTRUCTURAL STUDIES.

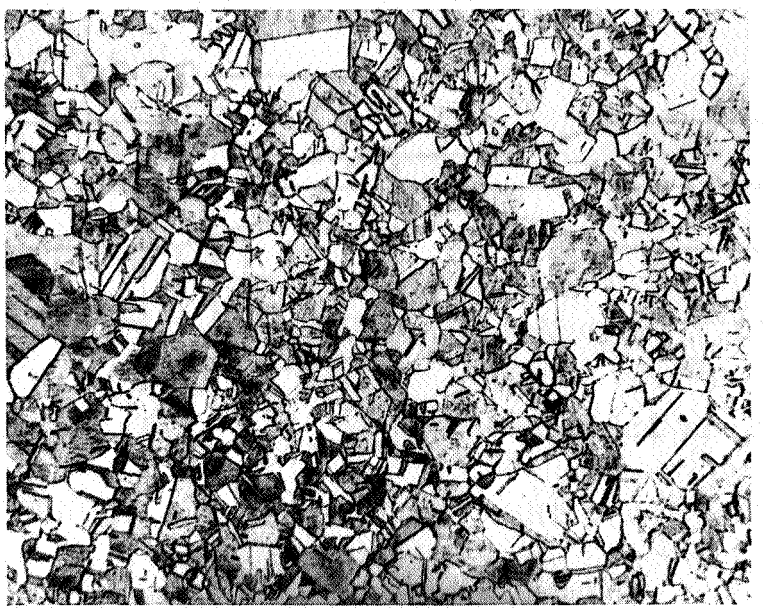

FIG. 1(c). TYPICAL TRANSVERSE SECTION OF A SPECIMEN BEFORE FATIGUING (ASTM. GRAIN SIZE NO. 8.0, x100)

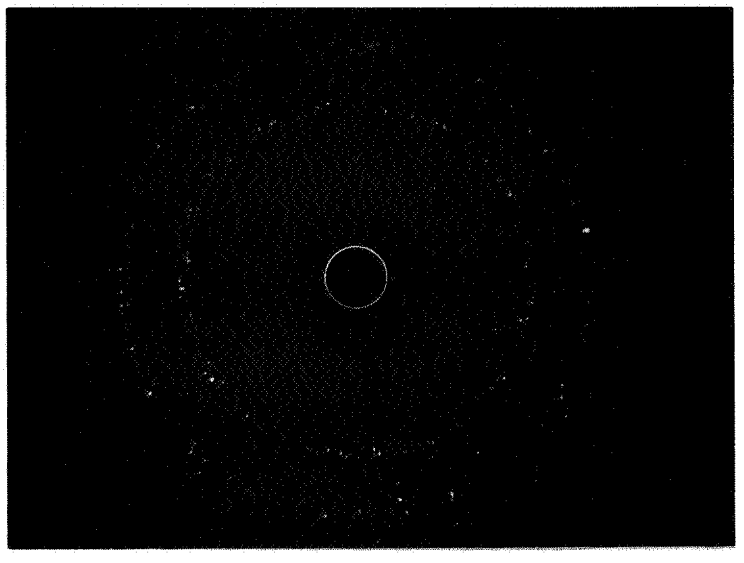

FIG. 1(d). X-RAY BACK REFLECTION PATTERN OF A SPECIMEN BEFORE FATIGUING (Cu RADIATION).

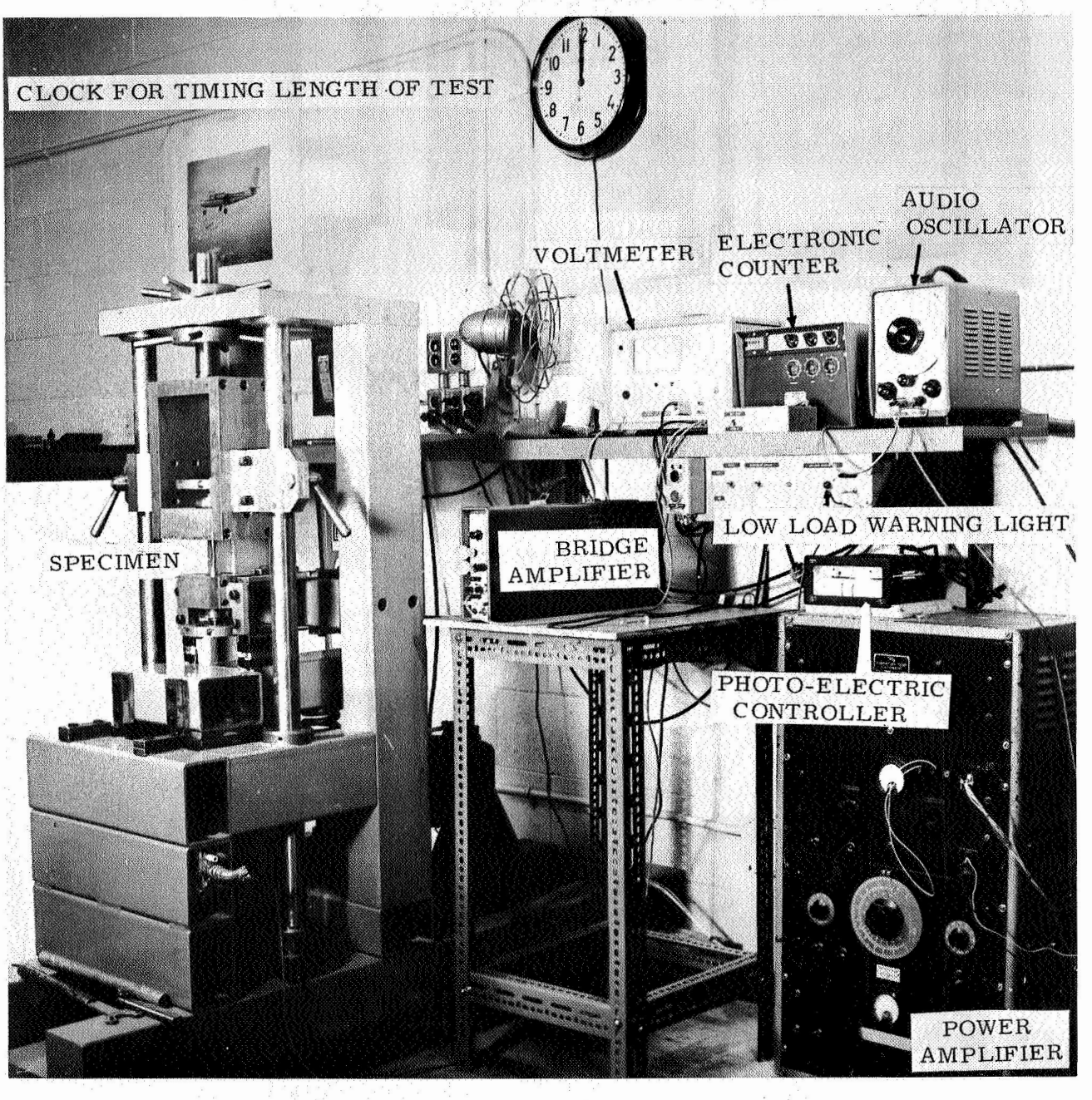

FIG-2(a). GENERAL ARRANGEMENT OF FATIGUE MACHINE AND INSTRUMENTS.

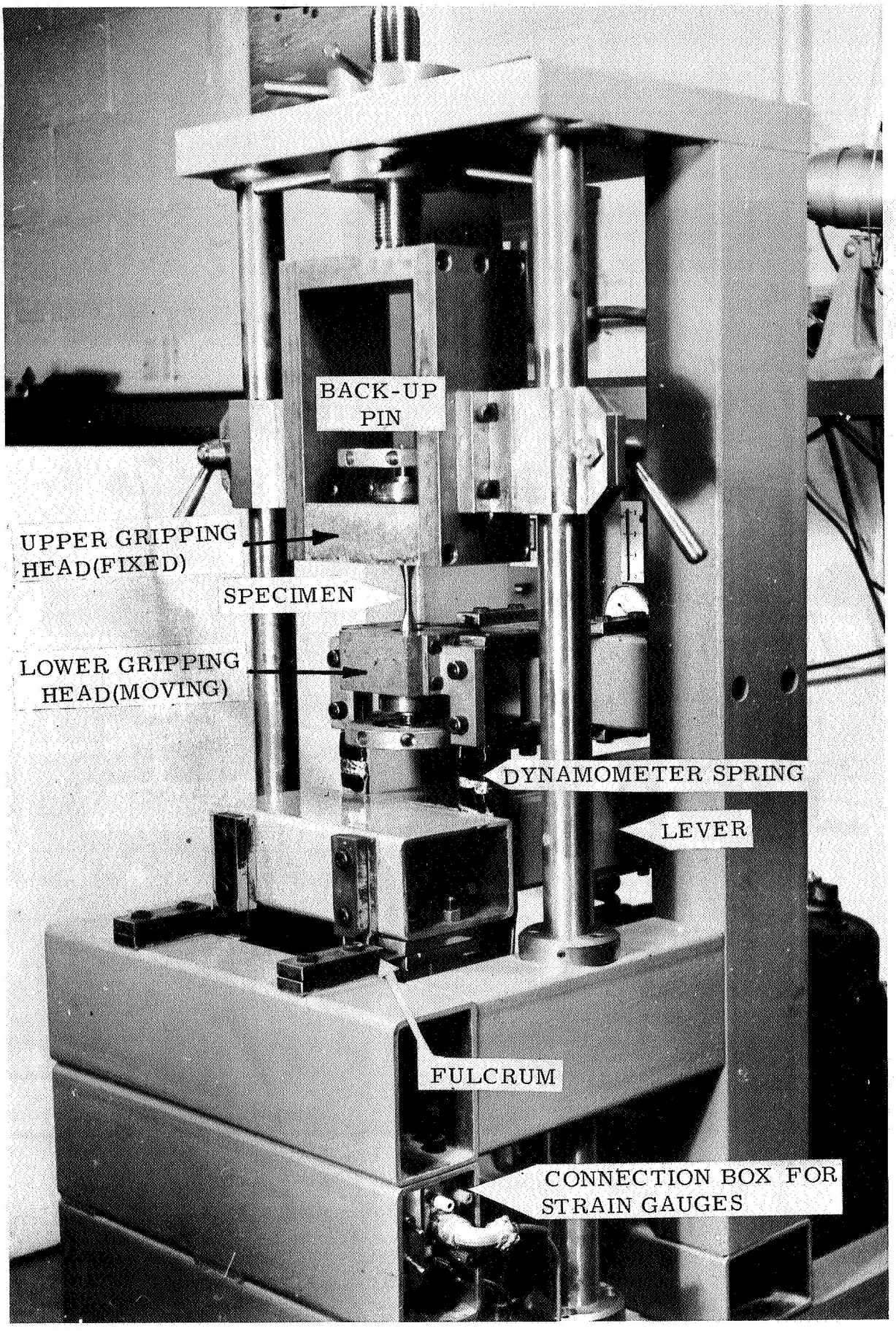

FIG-2(b). CLOSS-UP VIEW OF THE FATIGUE MACHINE.

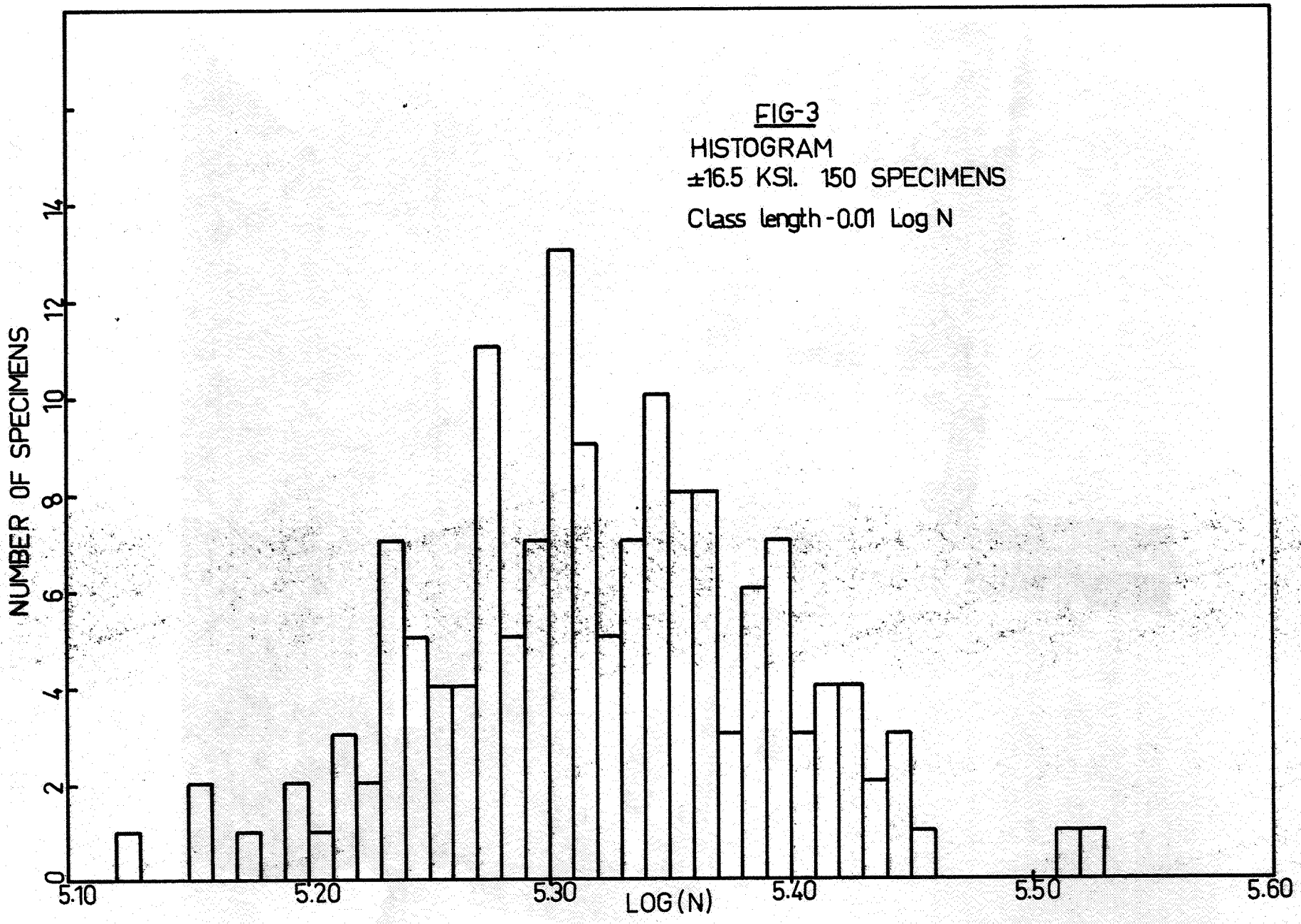
FIG-3
HISTOGRAM
±16.5 KSI. 150 SPECIMENS
Class length - 0.01 Log N
NUMBER OF SPECIMENS
0
2
4
6
8
10
12
14
5.10
5.20
5.30
LOG (N)
5.40
5.50
5.60

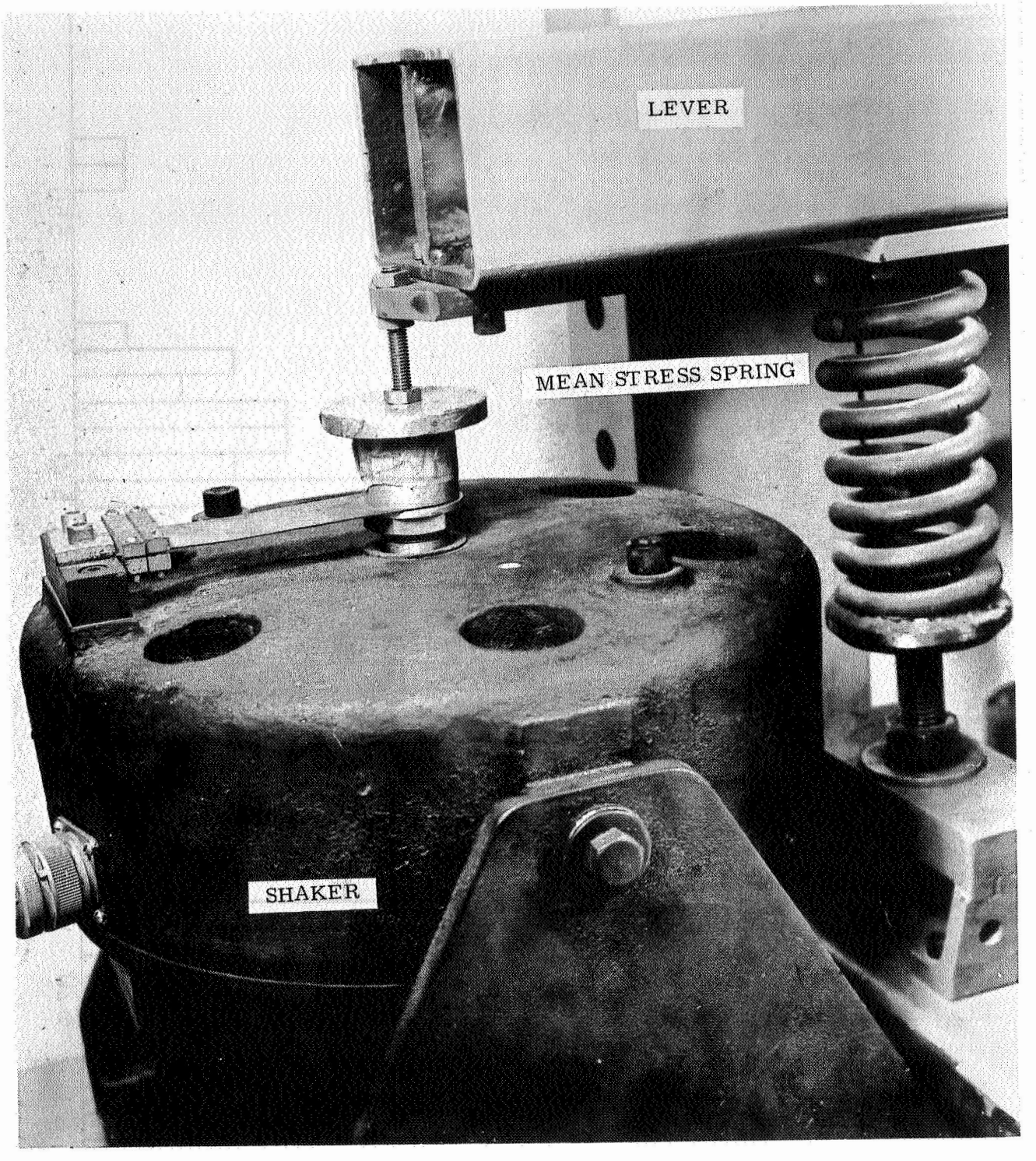

FIG-2(c). VIEW SHOWING SHAKER AND MEAN STRESS SPRING.

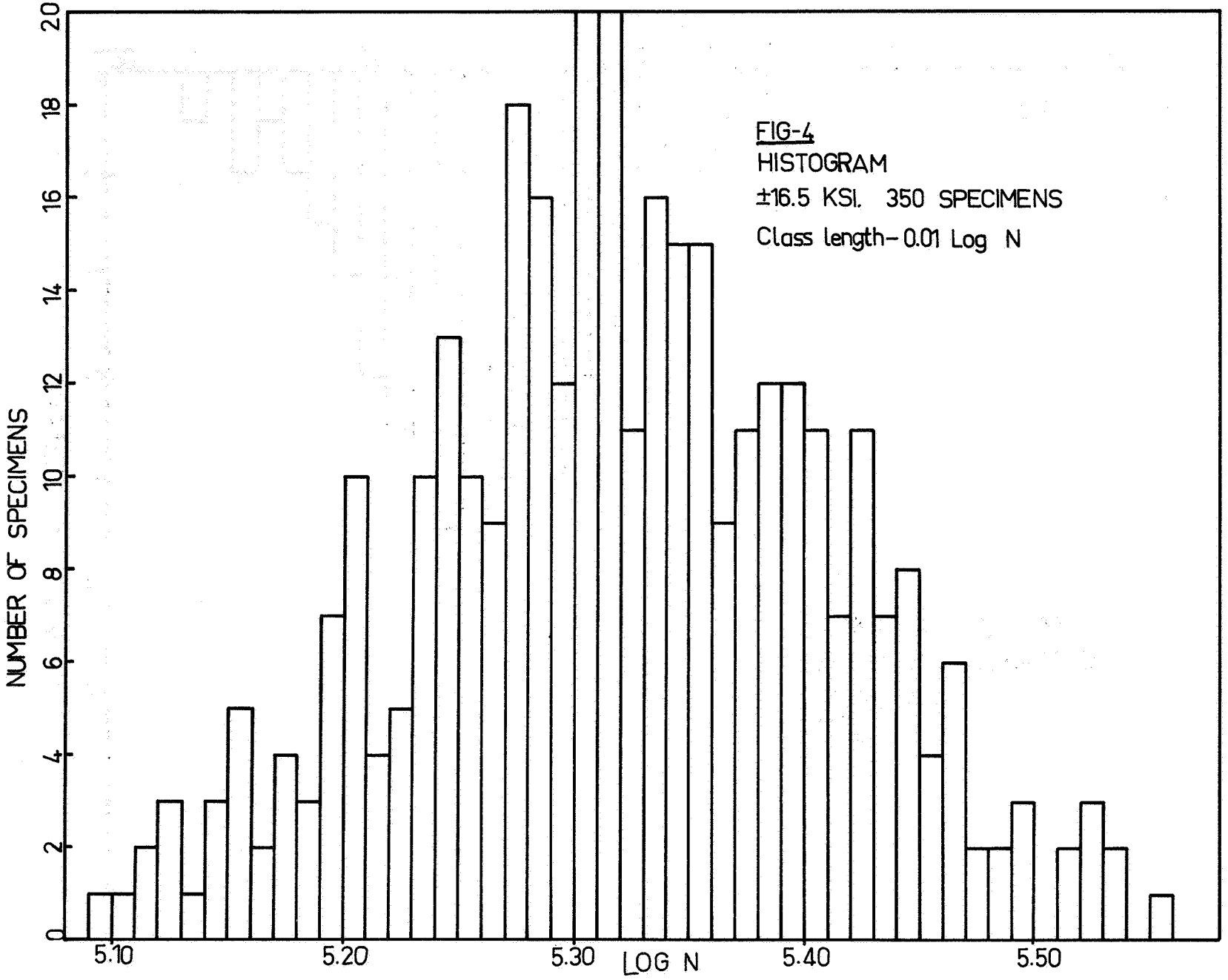
FIG-4
HISTOGRAM
±16.5 KSI. 350 SPECIMENS
Class length- 0.01 Log N
NUMBER OF SPECIMENS
0
2
4
6
8
10
12
14
16
18
20
5.10
5.20
5.30
LOG N
5.40
5.50

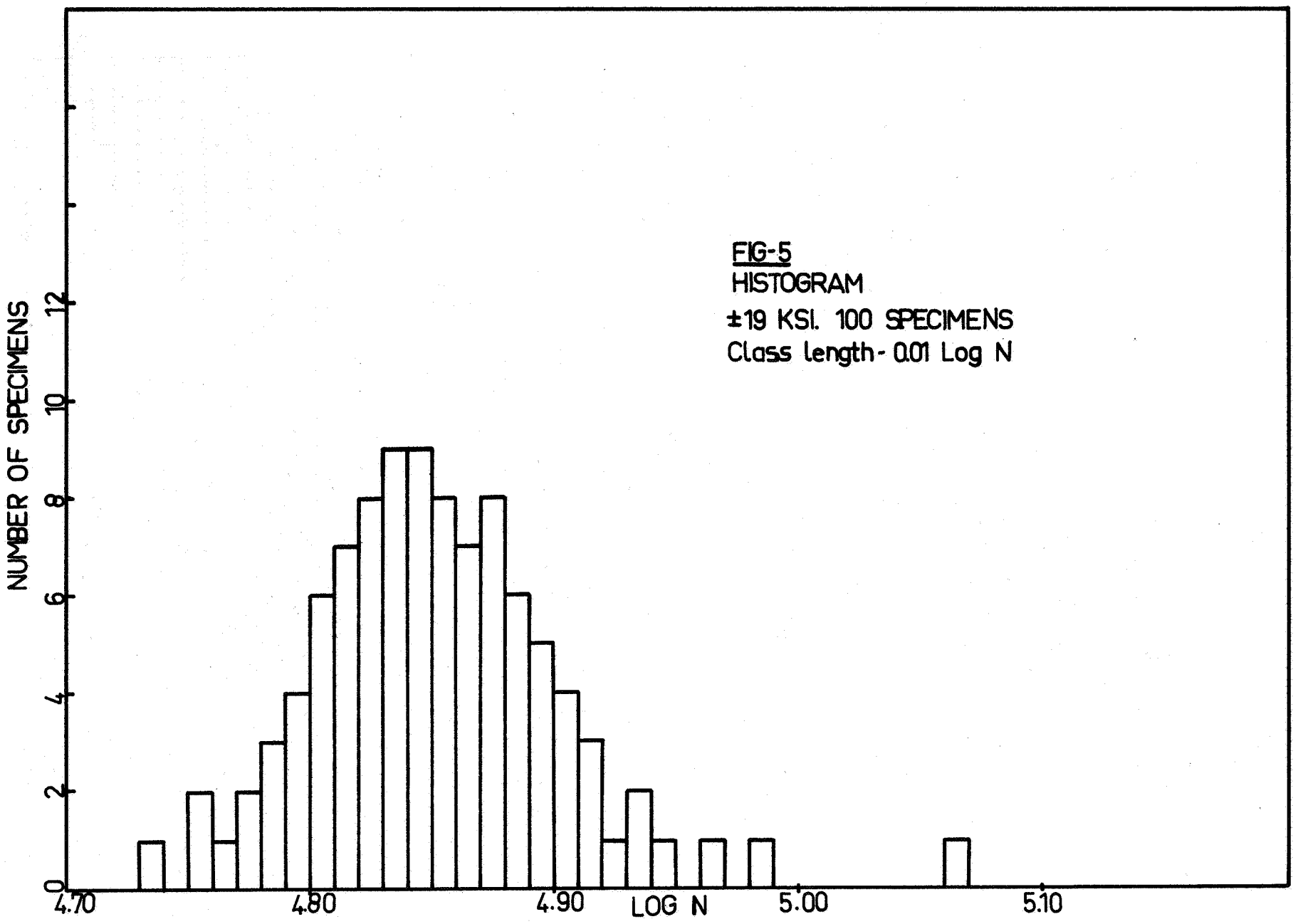
FIG-5
HISTOGRAM
±19 KSI. 100 SPECIMENS
Class length - 0.01 Log N
NUMBER OF SPECIMENS
0
2
4
6
8
10
12
4.70
4.80
4.90
LOG N
5.00
5.10

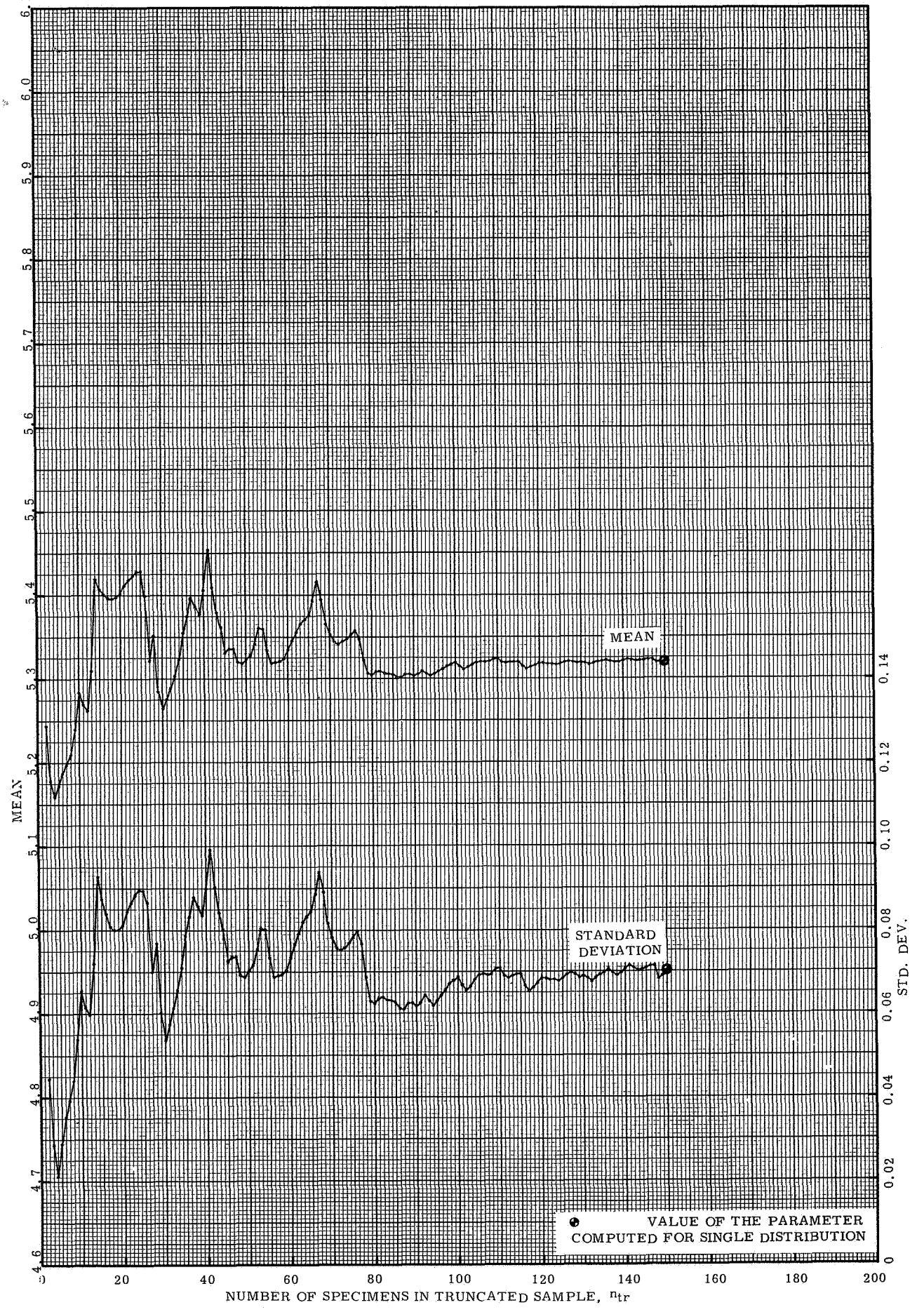

FIG. 6(a). PARAMETERS OF THE TRUNCATED LOG-NORMAL DISTRIBUTION. HIGH ENDURANCE PART EXCLUDED. 16.5 KSI STRESS LEVEL. $0 < n_{tr} < 150$

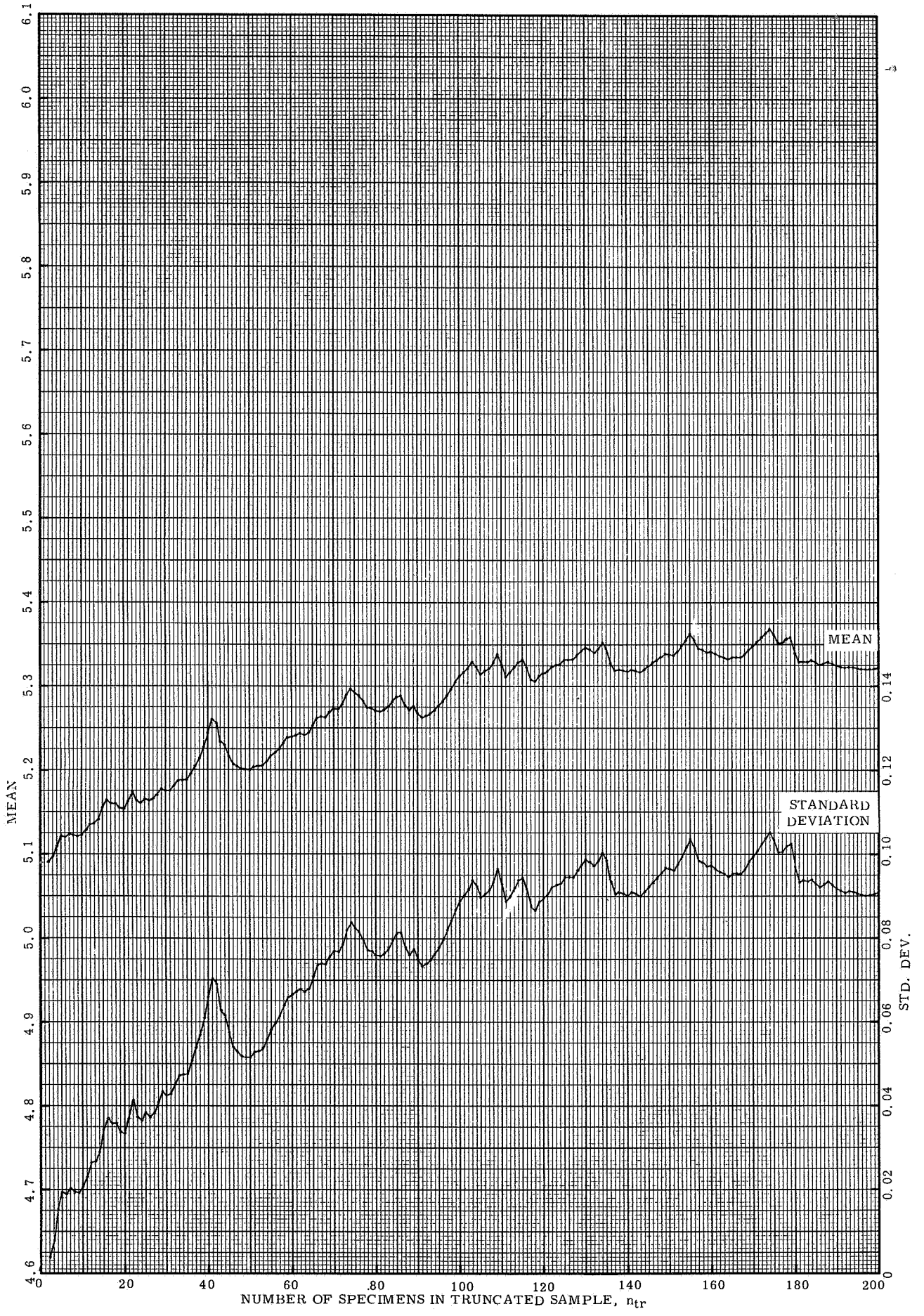

FIG. 6(b). PARAMETERS OF THE TRUNCATED LOG-NORMAL DISTRIBUTION. HIGH ENDURANCE PART EXCLUDED. 16.5 KSI STRESS LEVEL. $0 < n_{tr} < 200$

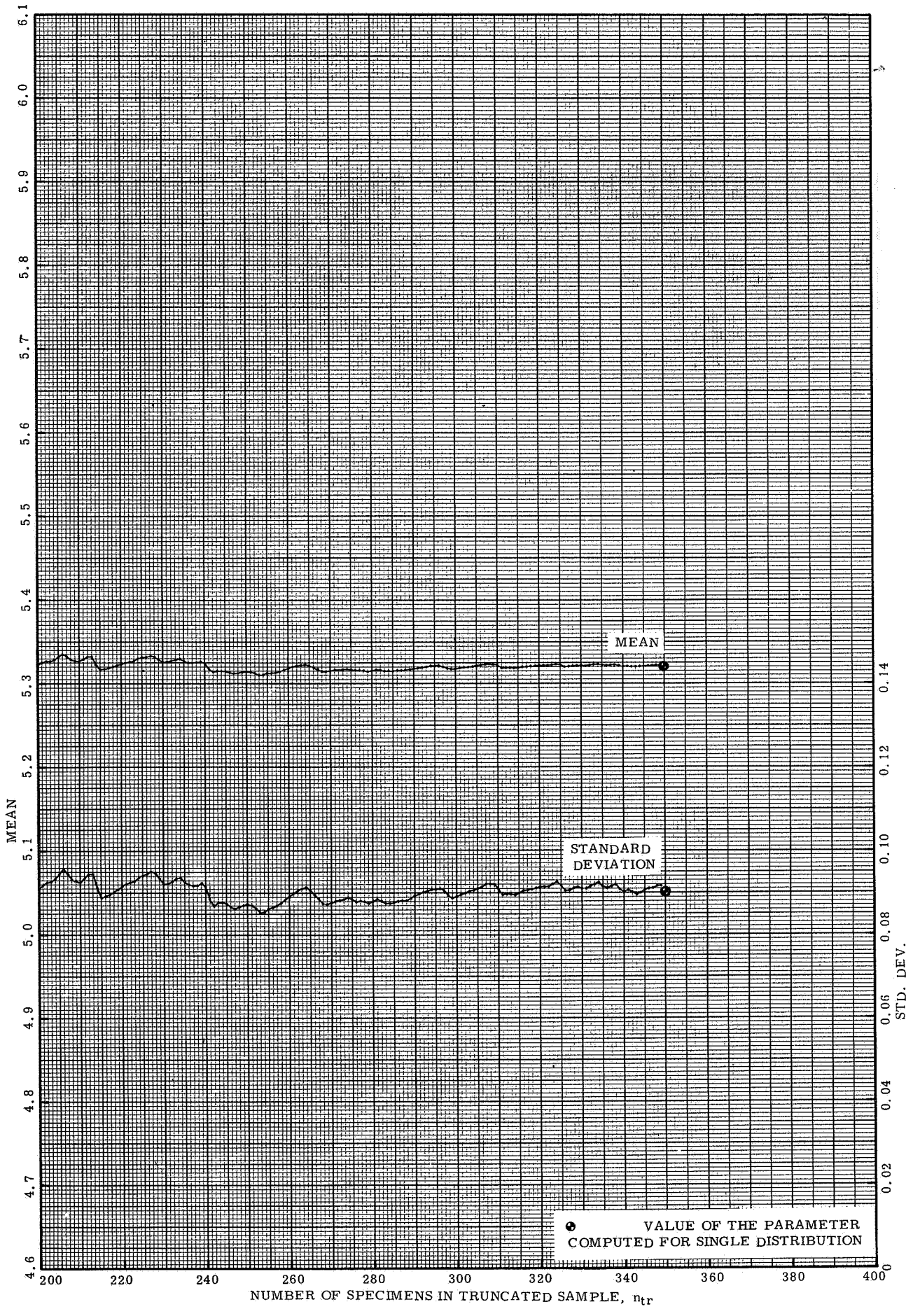

FIG. 6(b). PARAMETERS OF THE TRUNCATED LOG-NORMAL DISTRIBUTION. HIGH ENDURANCE PART EXCLUDED. 16.5 KSI STRESS LEVEL. $200 < n_{tr} < 350$

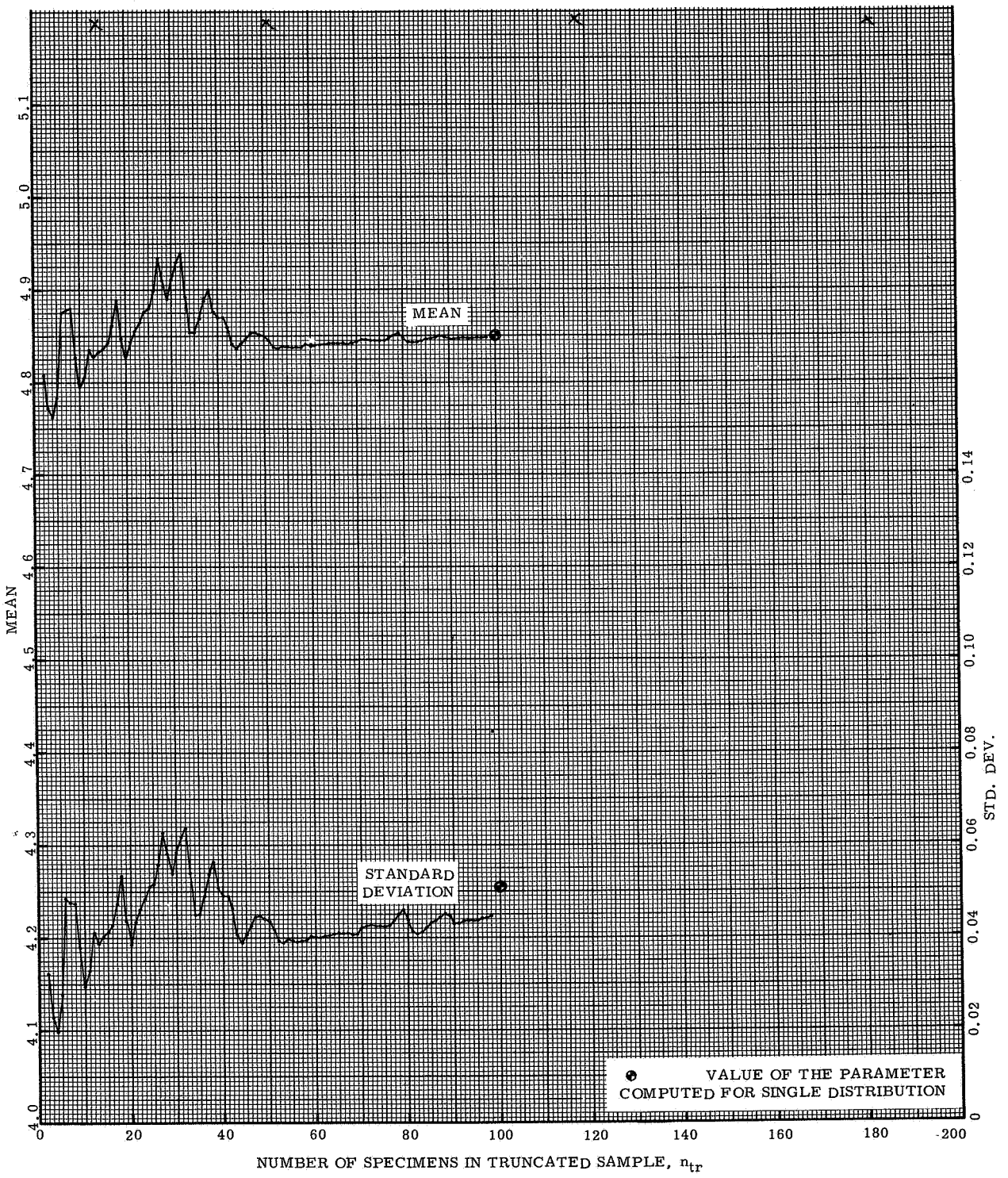

FIG. 6(c) PARAMETERS OF THE TRUNCATED LOG-NORMAL DISTRIBUTION. HIGH ENDURANCE PART EXCLUDED. 19.0 KSI STRESS LEVEL.

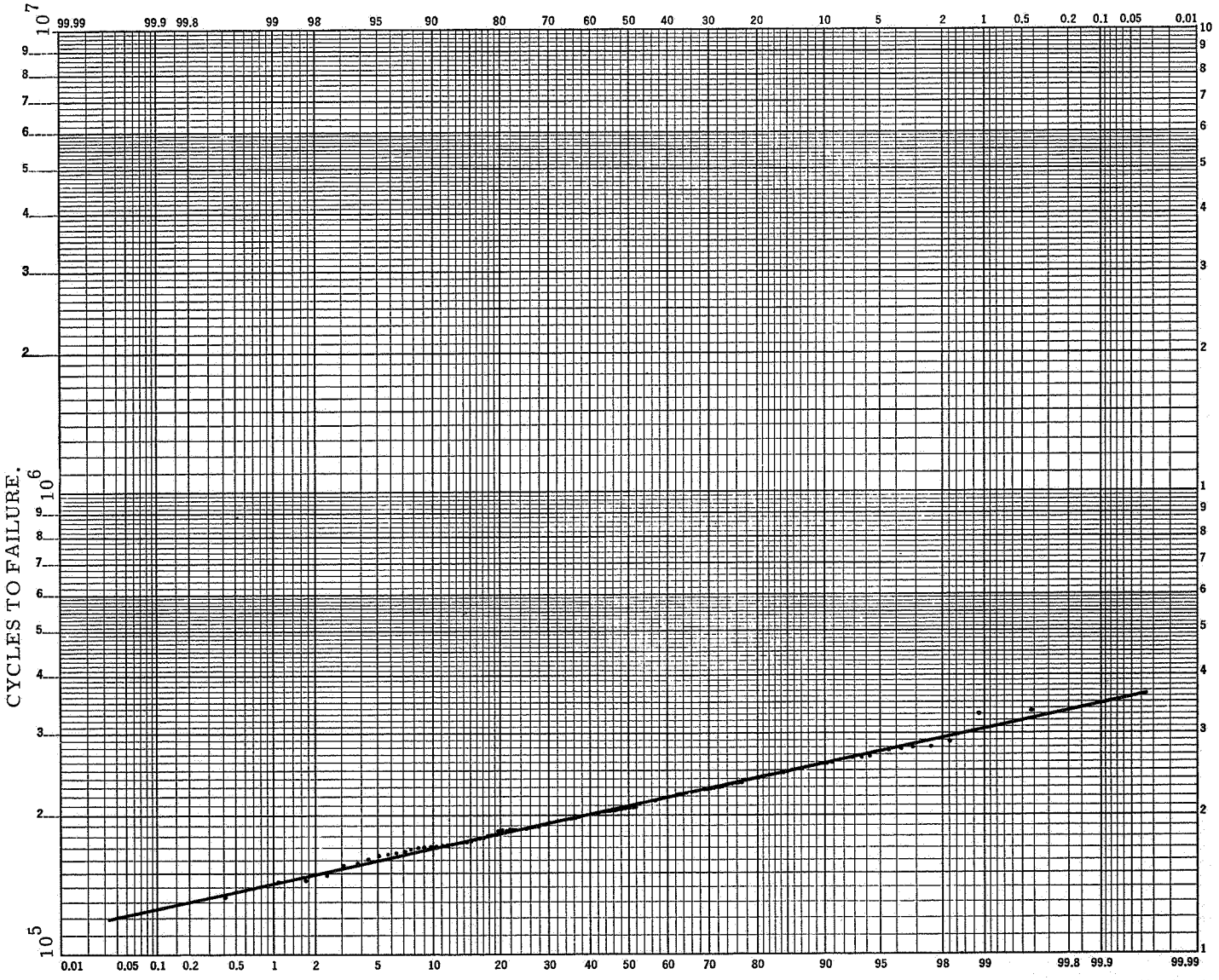

FIG. 7(a). LOG-NORMAL PROBABILITY PLOT. SINGLE DISTRIBUTION. 16.5 KSI, 150 SPECIMENS. r=0.99712.

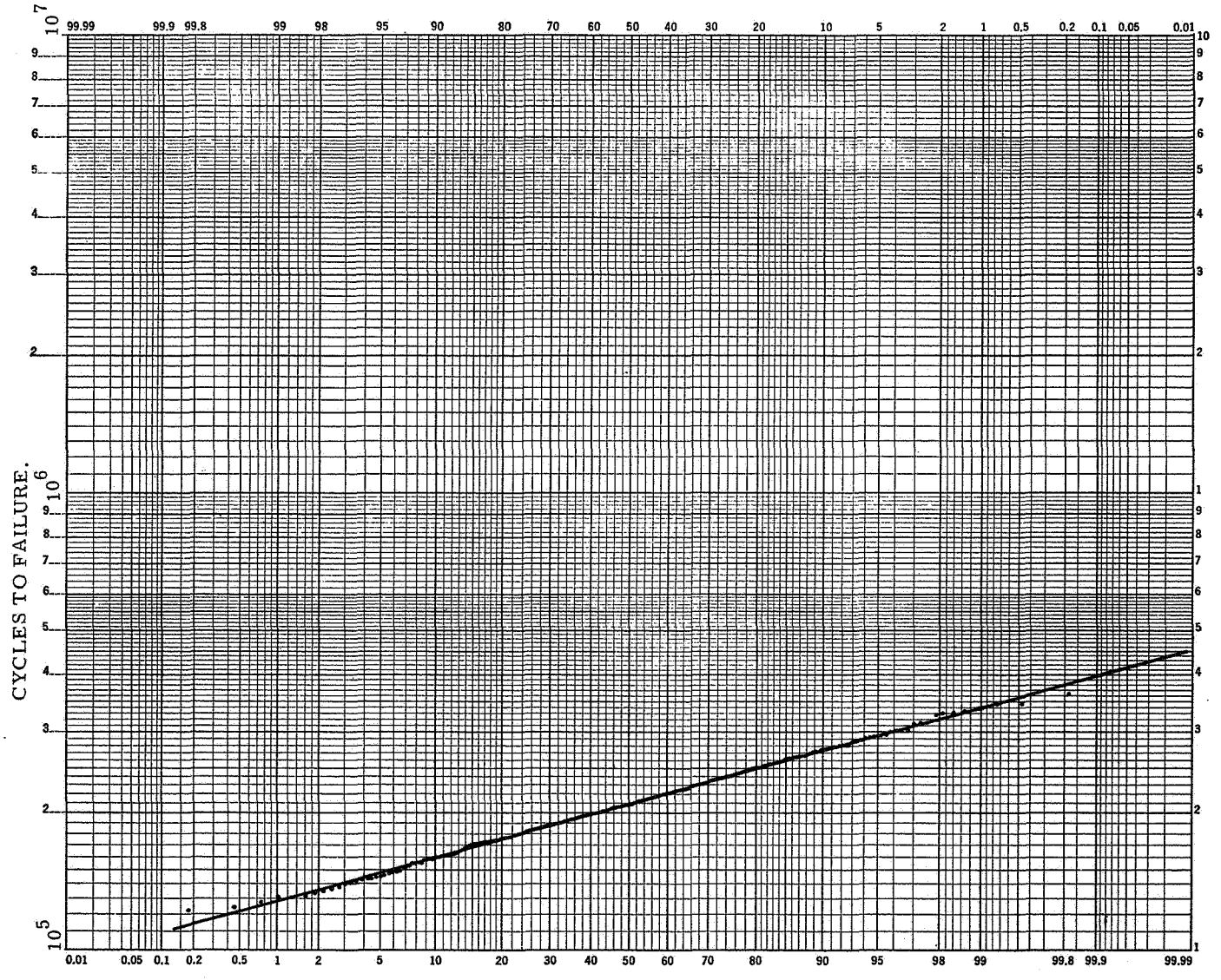

FIG. 7(b). LOG-NORMAL PROBABILITY PLOT. SINGLE DISTRIBUTION. 16.5 KSI, 350 SPECIMENS. r=0.99918.

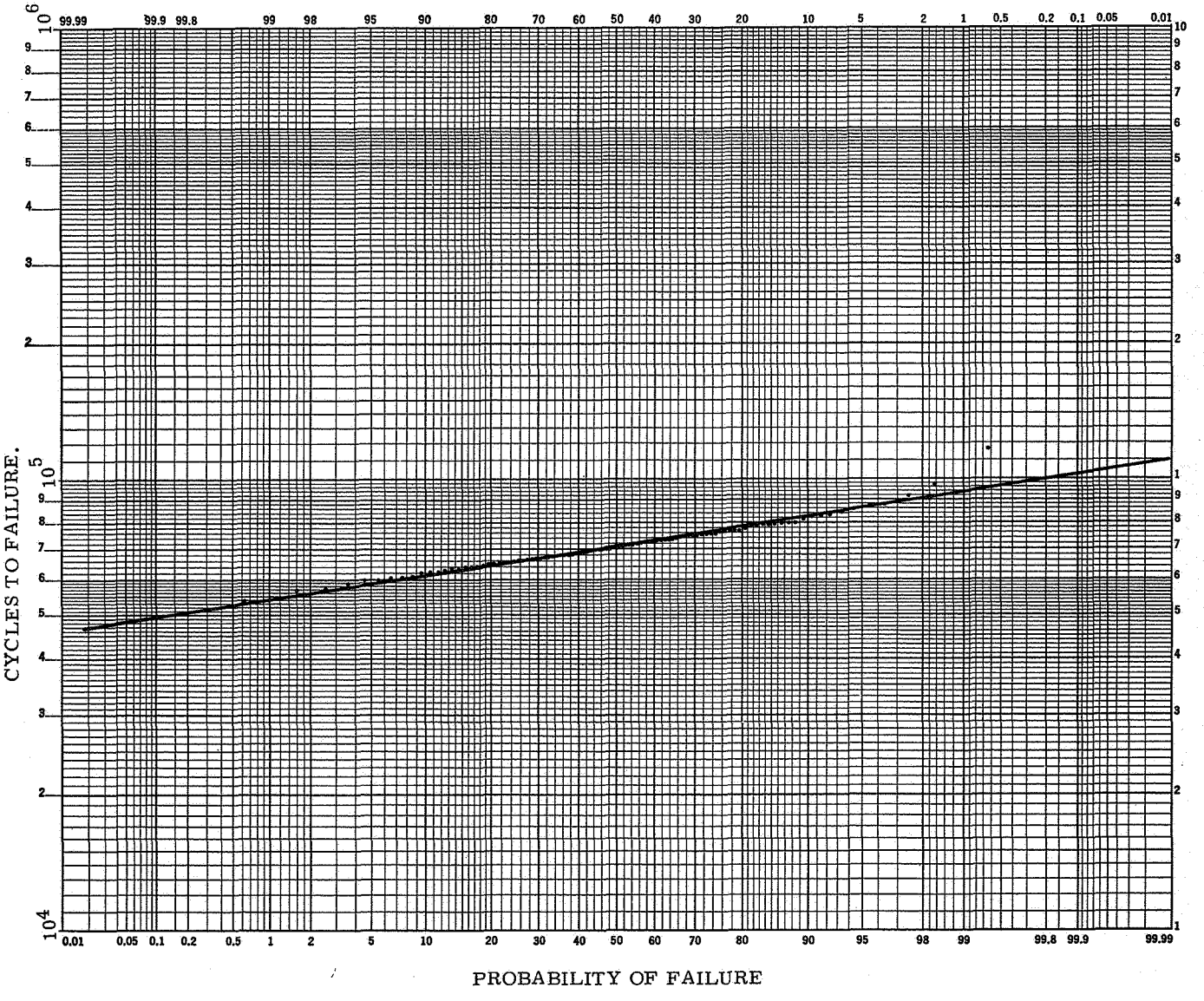

FIG. 7(c) LOG-NORMAL PROBABILITY PLOT. SINGLE DISTRIBUTION. 19.0 KSI, 100 SPECIMENS. r=0.97805.

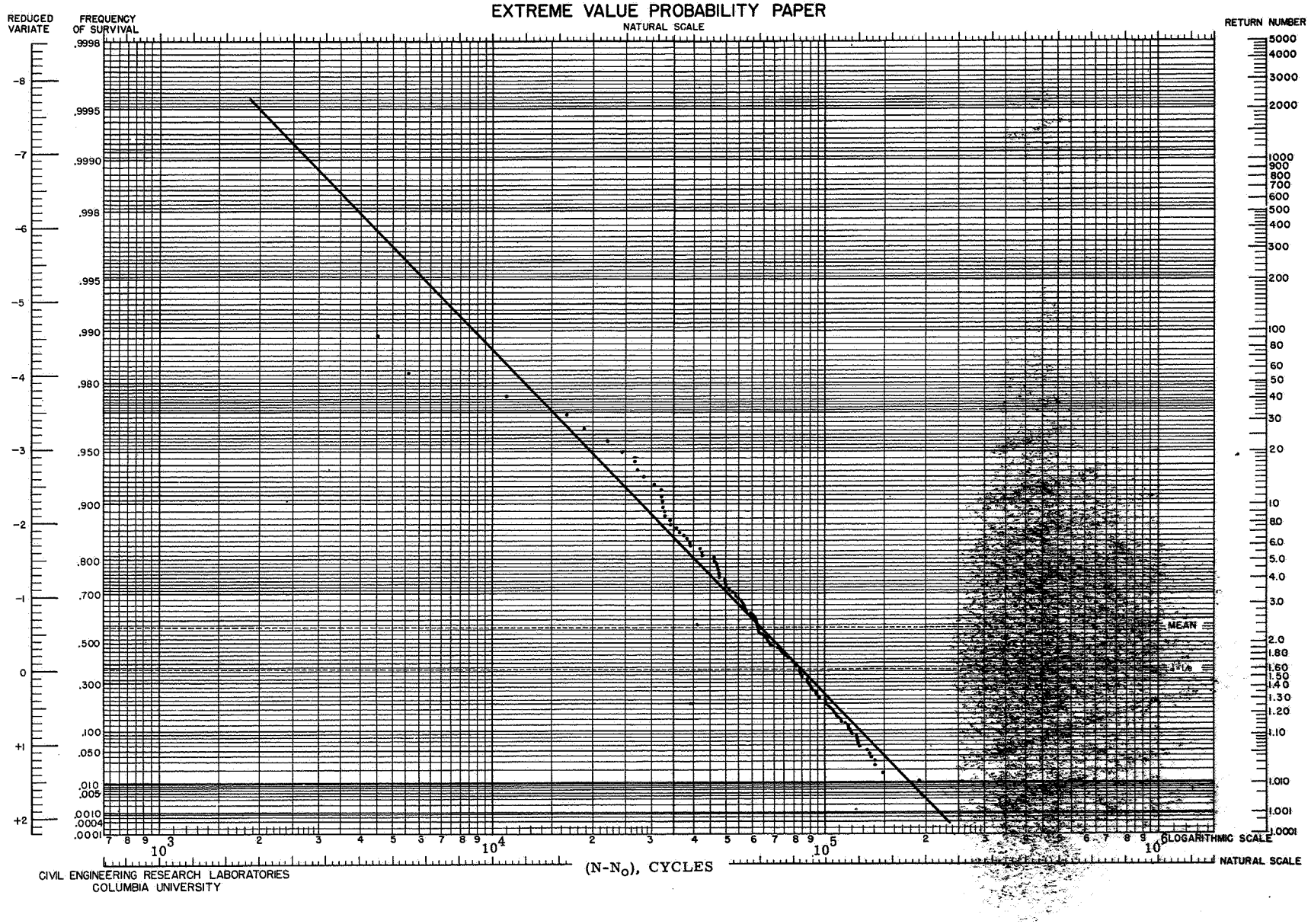

FIG. 8(a). WEIBULL PROBABILITY PLOT, SINGLE DISTRIBUTION. PARAMETERS CALCULATED BY UPPER VERTICAL MOMENT METHOD. 16.5 KSI, 150 SPECIMENS, r=0.98281.

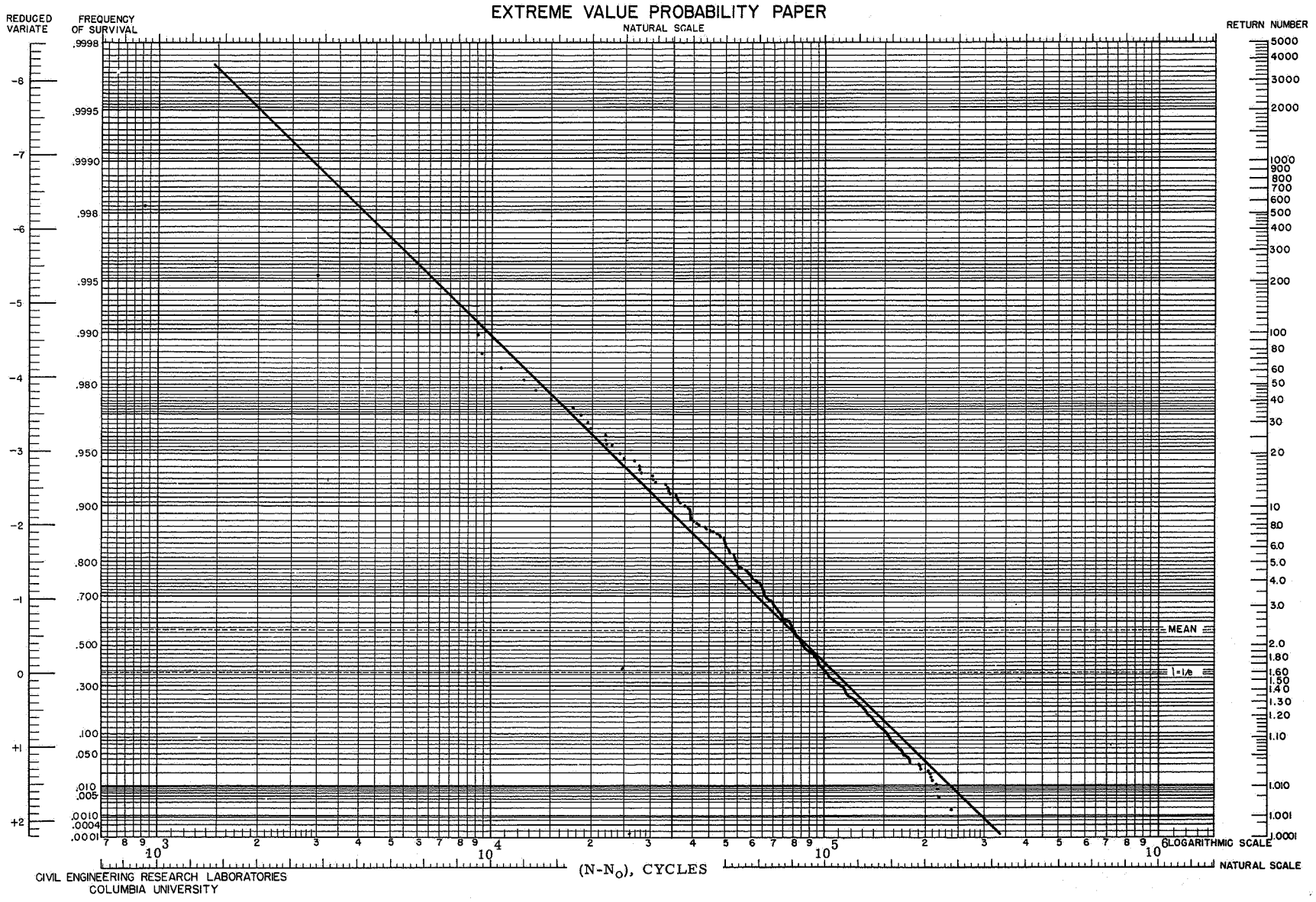

FIG. 8(b). WEIBULL PROBABILITY PLOT, SINGLE DISTRIBUTION. PARAMETERS CALCULATED BY UPPER VERTICAL MOMENT METHOD. 16.5 KSI, 350 SPECIMENS, r=0.98383.

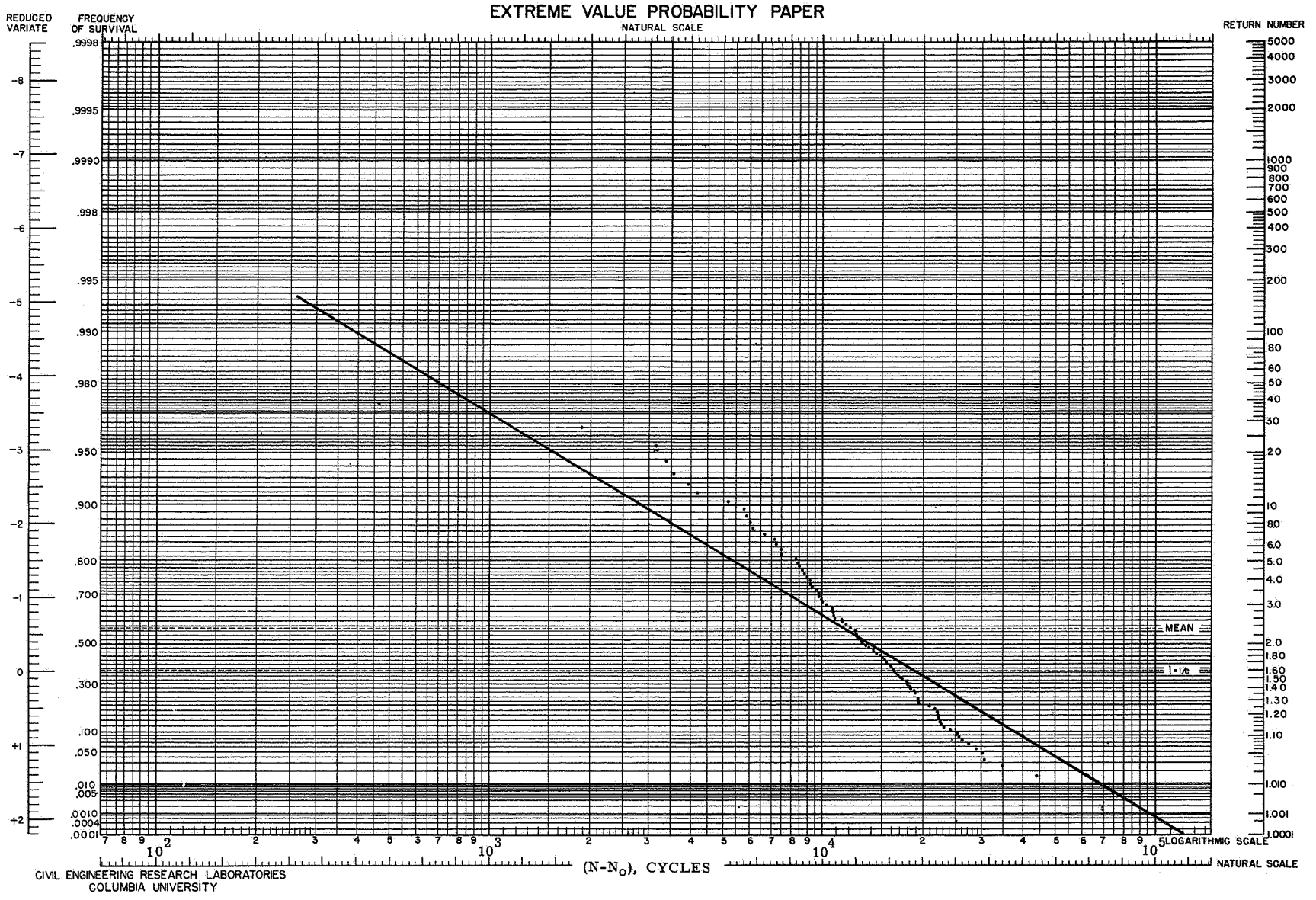

FIG. 8(c). WEIBULL PROBABILITY PLOT, SINGLE DISTRIBUTION. PARAMETERS CALCULATED BY UPPER VERTICAL MOMENT METHOD. 19.0 KSI, 100 SPECIMENS, r=0.88723.

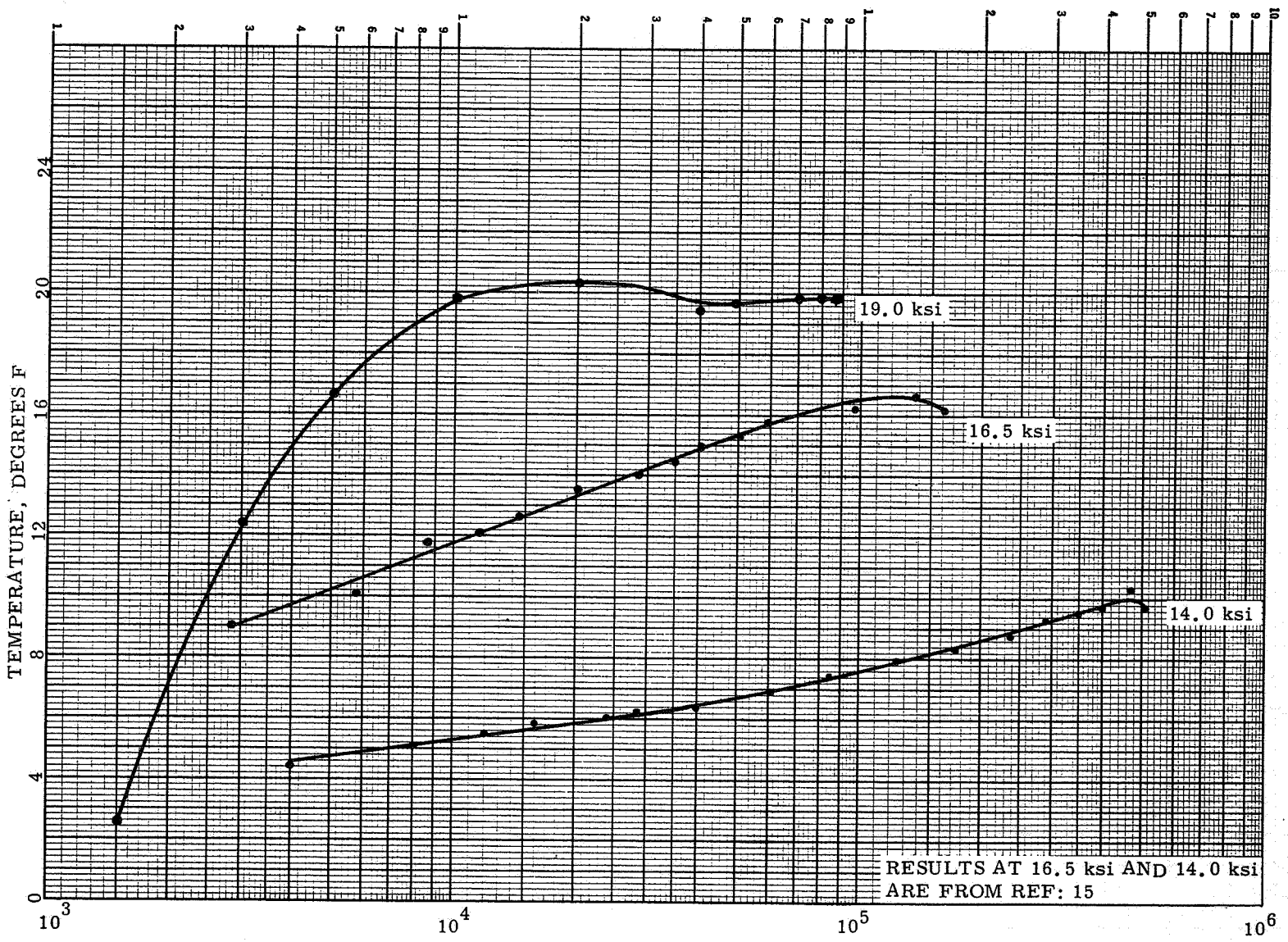

FIG. 9 TEMPERATURE INCREASE (ABOVE ROOM TEMPERATURE) IN A TYPICAL SPECIMEN FATIGUED AT 19.0 ksi

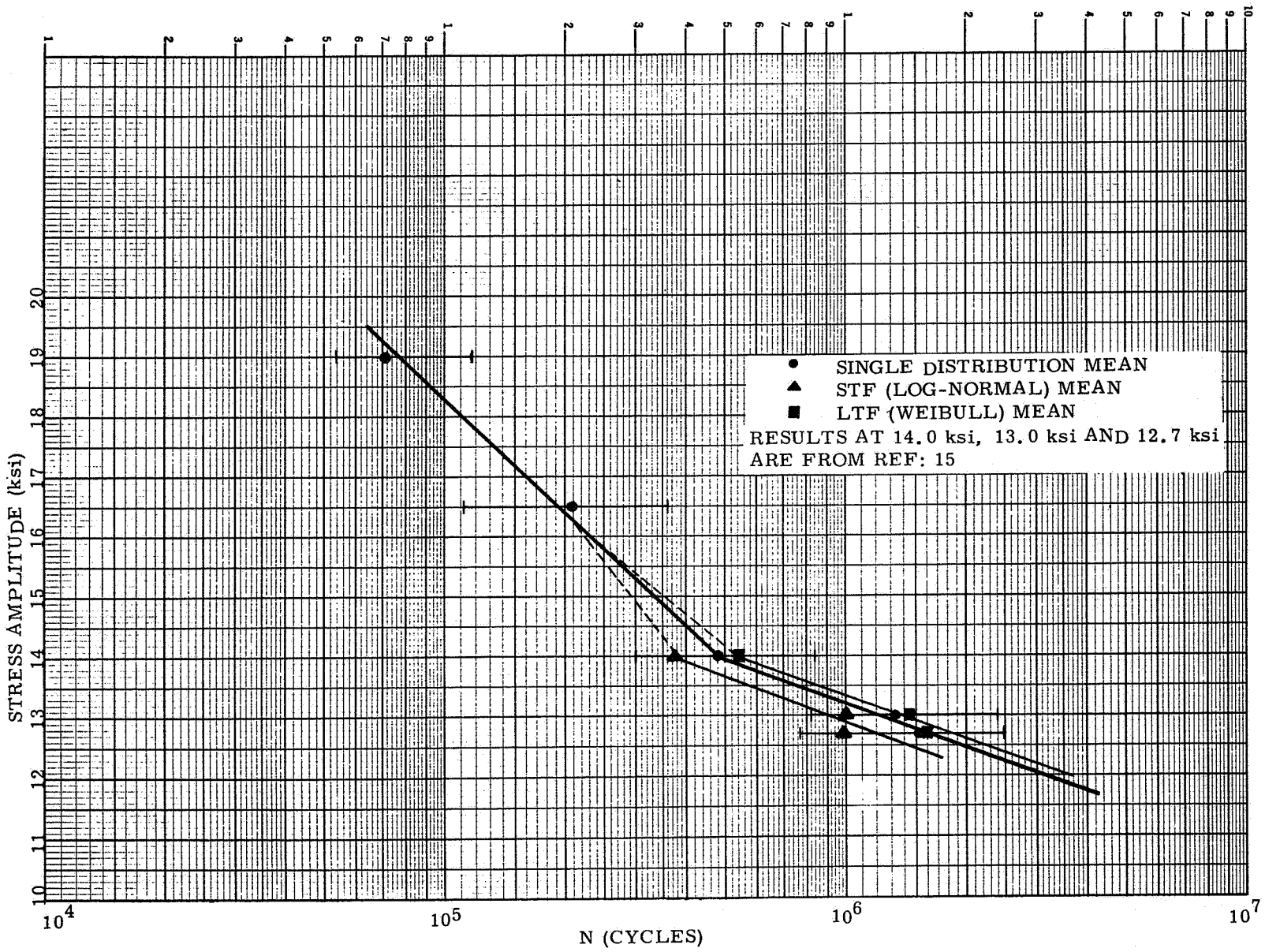

FIG. 10 SCHEMATIC REPRESENTATION OF S-N CURVE WITH SCATTER RANGES AND DISTRIBUTION MEANS.

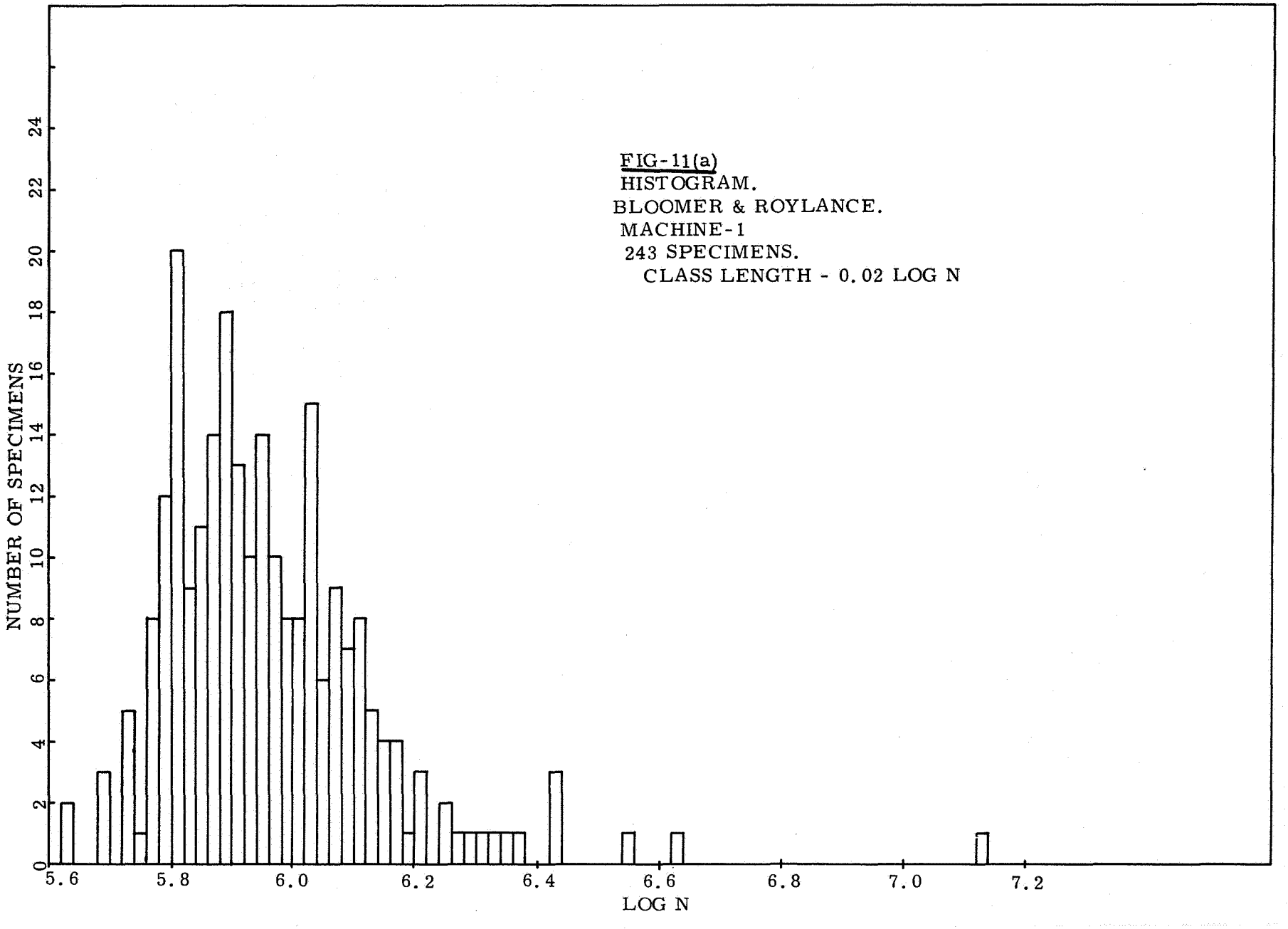
FIG-11(a)
HISTOGRAM.
BLOOMER & ROYLANCE.
MACHINE-1
243 SPECIMENS.
CLASS LENGTH - 0.02 LOG N
NUMBER OF SPECIMENS
0
2
4
6
8
10
12
14
16
18
20
22
24
5.6
5.8
6.0
6.2
6.4
6.6
6.8
7.0
7.2
LOG N

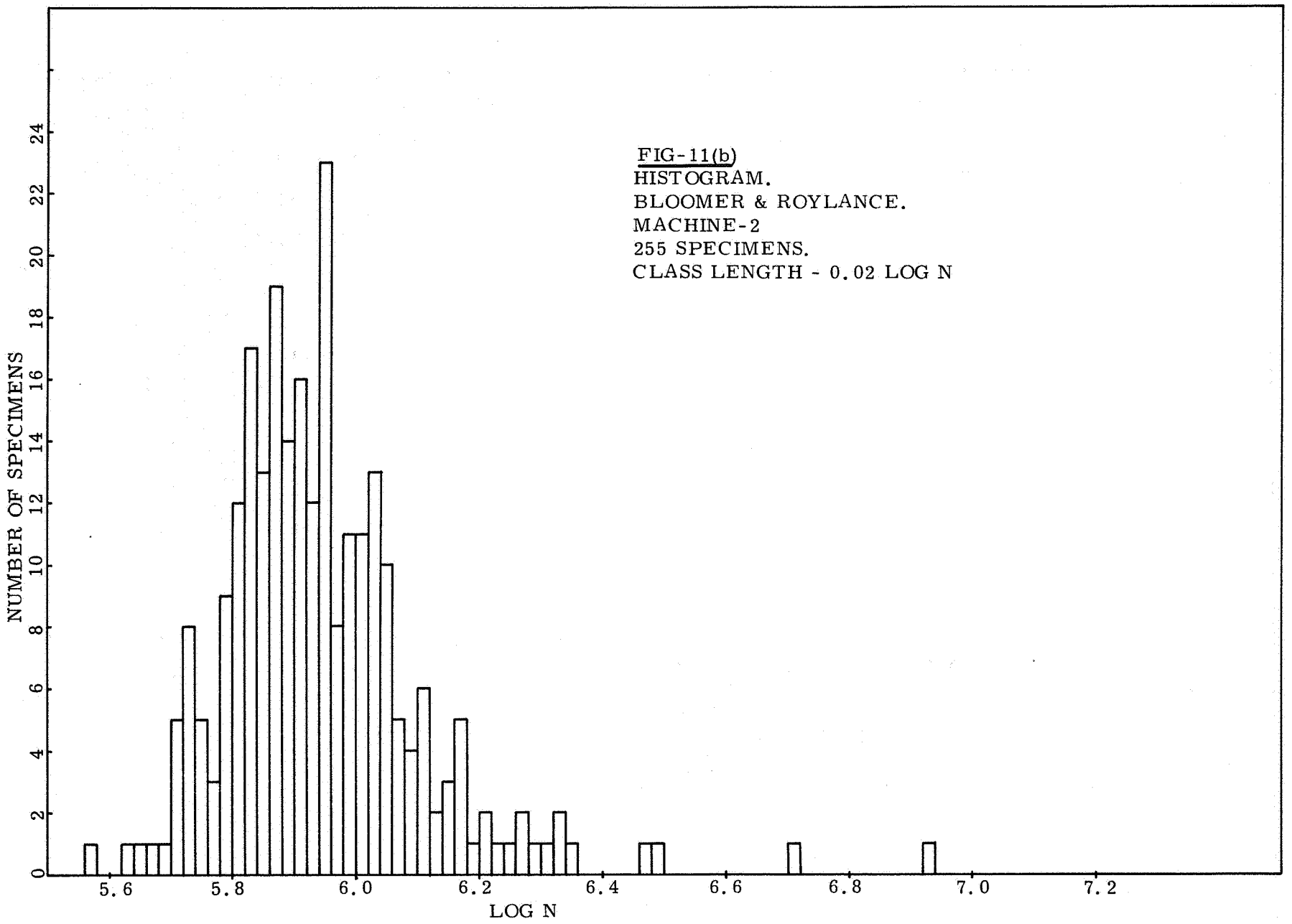

FIG-11(b)
HISTOGRAM.
BLOOMER & ROYLANCE.
MACHINE-2
255 SPECIMENS.
CLASS LENGTH - 0.02 LOG N

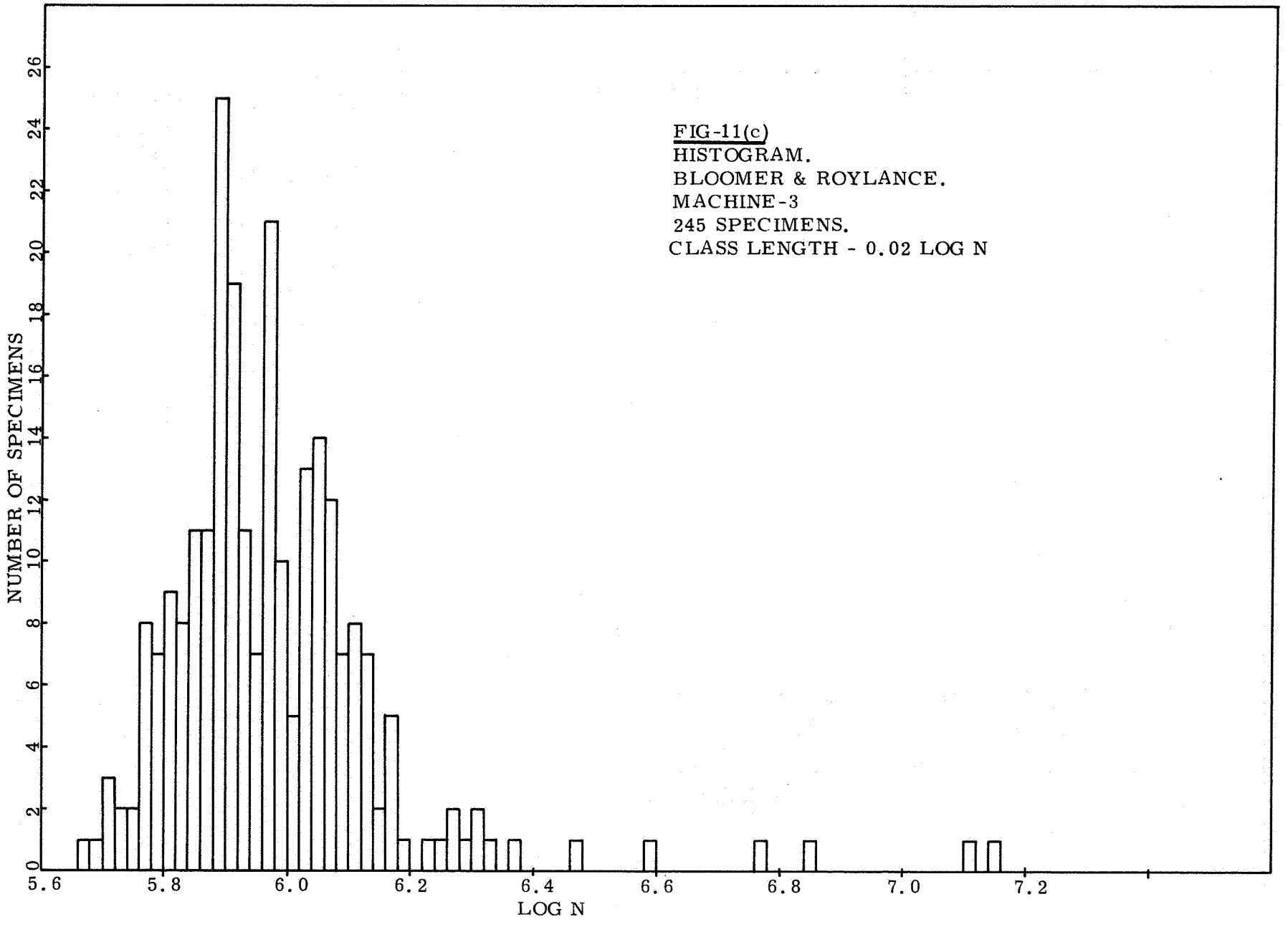

FIG-11(c)
HISTOGRAM.
BLOOMER & ROYLANCE.
MACHINE-3
245 SPECIMENS.
CLASS LENGTH - 0.02 LOG N

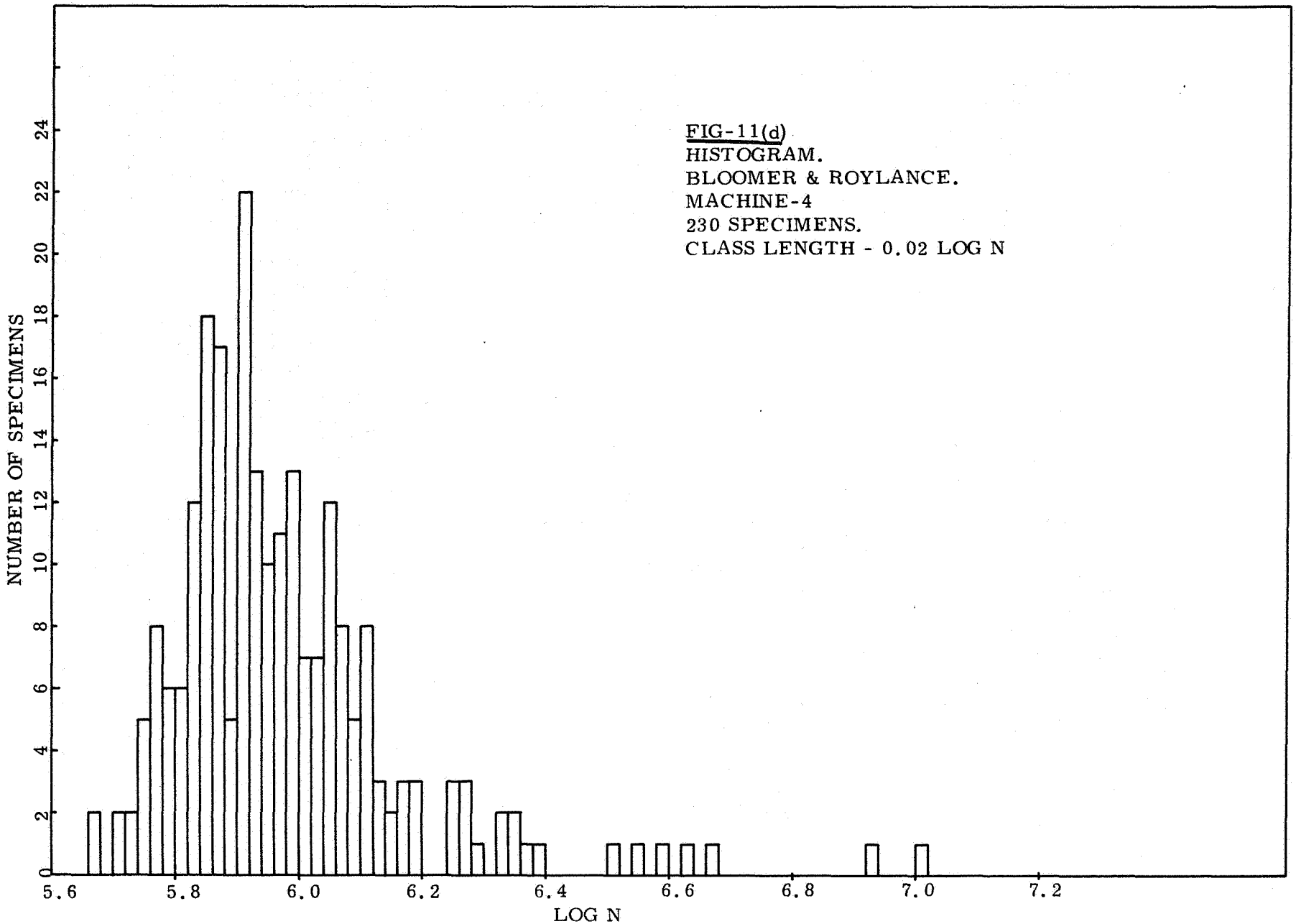
FIG-11(d)
HISTOGRAM.
BLOOMER & ROYLANCE.
MACHINE-4
230 SPECIMENS.
CLASS LENGTH - 0.02 LOG N
NUMBER OF SPECIMENS
0
2
4
6
8
10
12
14
16
18
20
22
24
5.6
5.8
6.0
6.2
6.4
6.6
6.8
7.0
7.2
LOG N

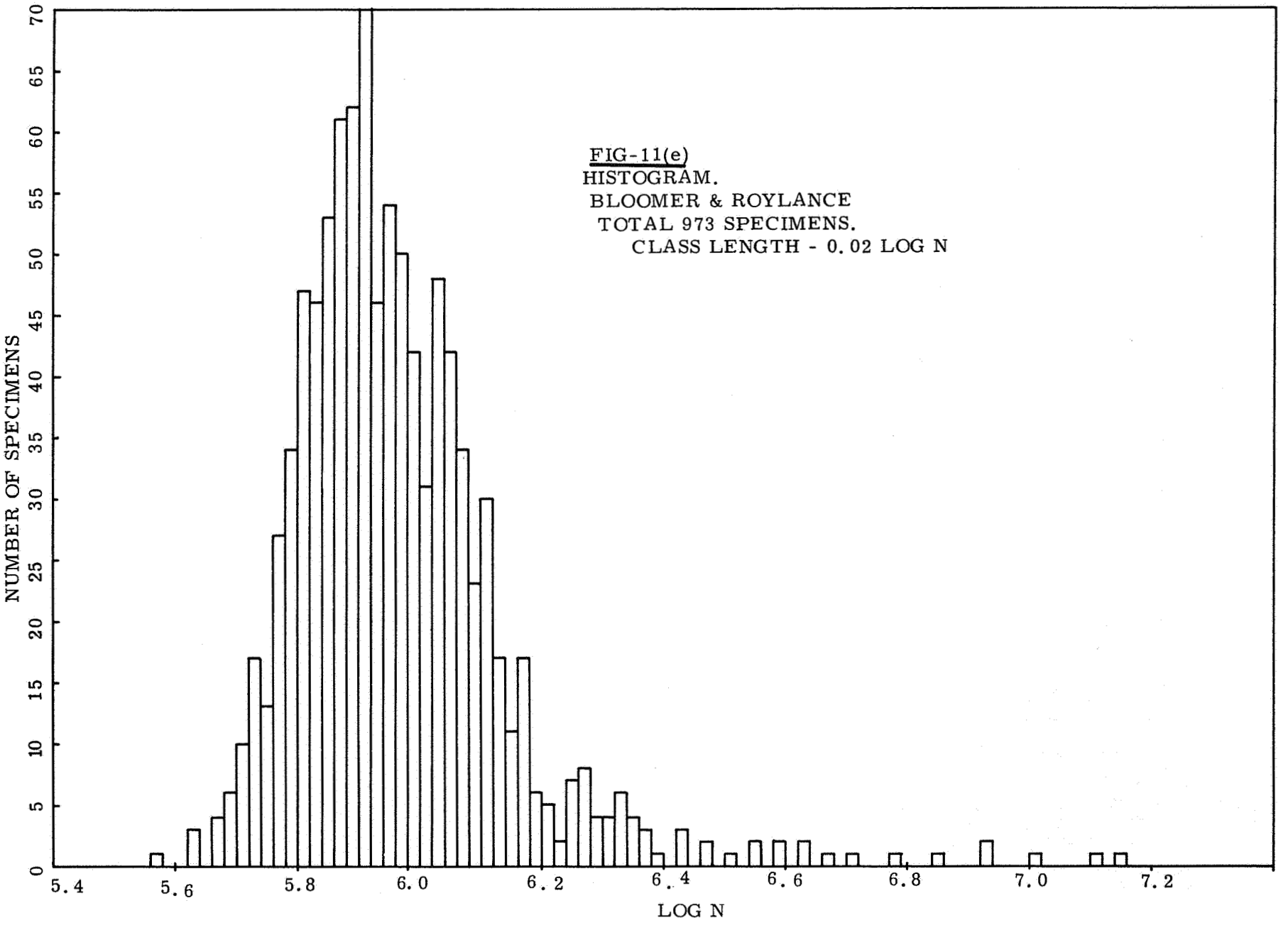
FIG-11(e)
HISTOGRAM.
BLOOMER & ROYLANCE
TOTAL 973 SPECIMENS.
CLASS LENGTH - 0.02 LOG N
NUMBER OF SPECIMENS
0
5
10
15
20
25
30
35
40
45
50
55
60
65
70
5.4
5.6
5.8
6.0
6.2
6.4
6.6
6.8
7.0
7.2
LOG N

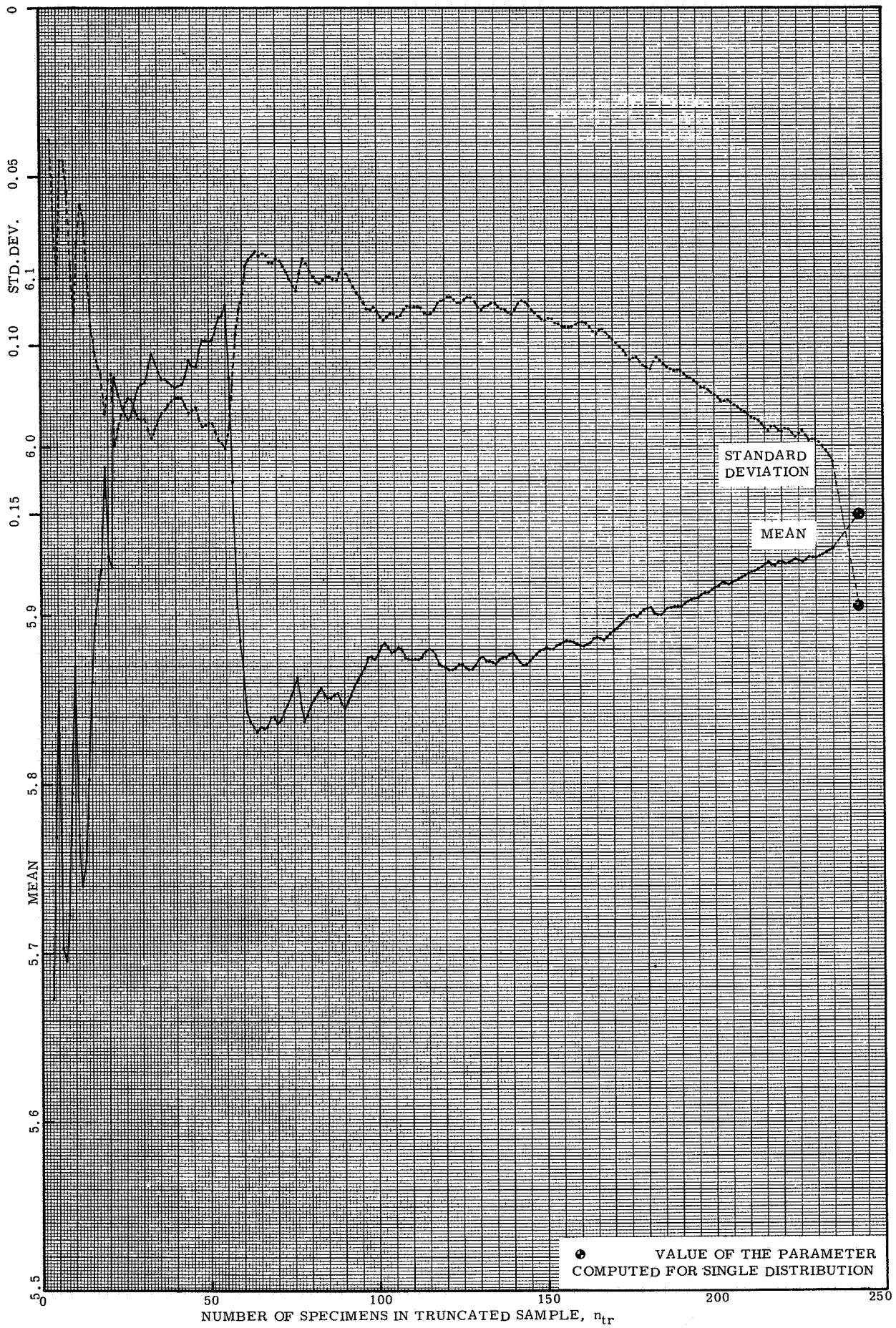

FIG. 12(a). PARAMETERS OF THE TRUNCATED LOG-NORMAL DISTRIBUTION. HIGH ENDURANCE PART EXCLUDED. BLOOMER & ROYLANCE, MACHINE- 1.

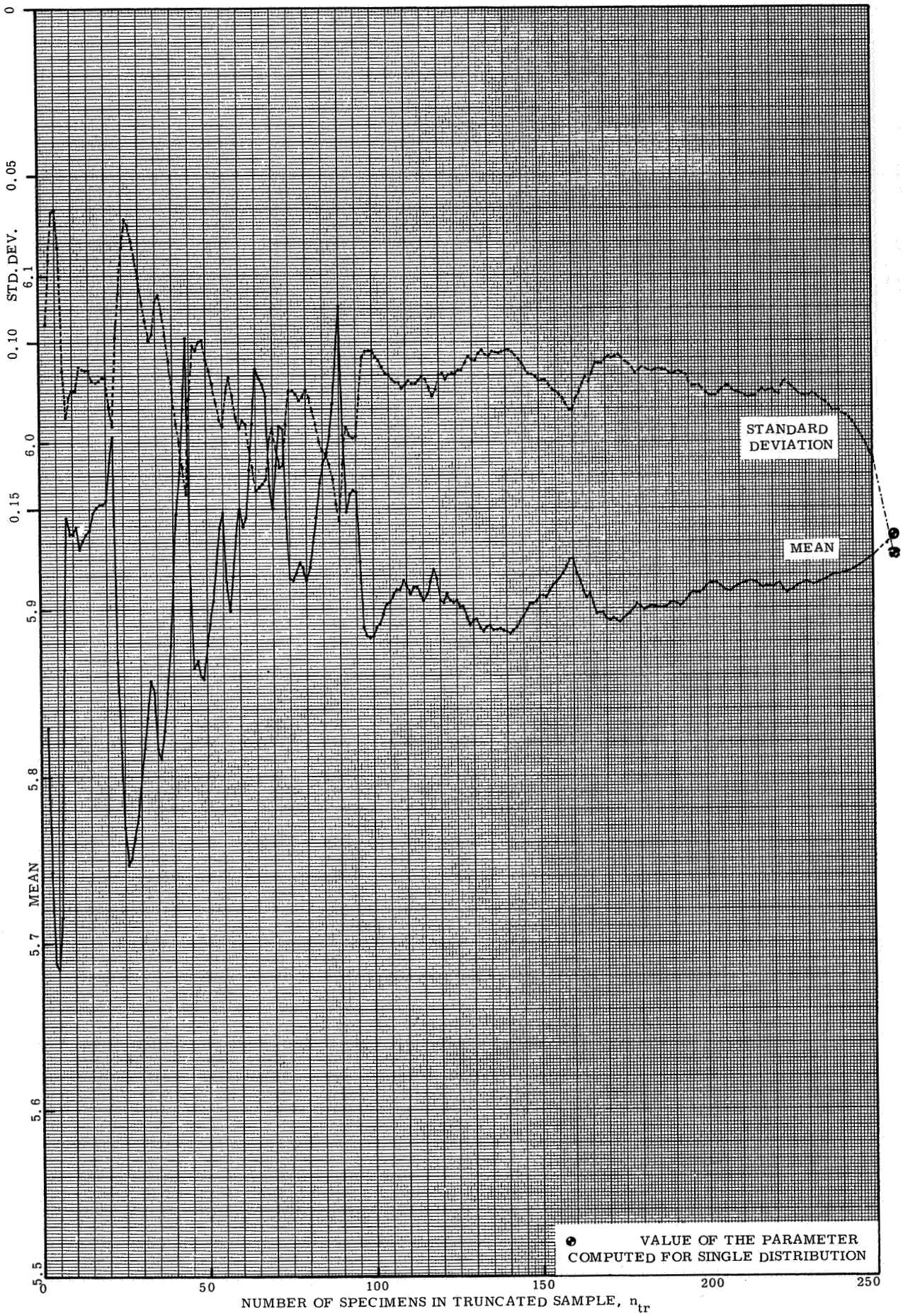

FIG. 12(b). PARAMETERS OF THE TRUNCATED LOG-NORMAL DISTRIBUTION. HIGH ENDURANCE PART EXCLUDED. BLOOMER & ROYLANCE, MACHINE- 2.

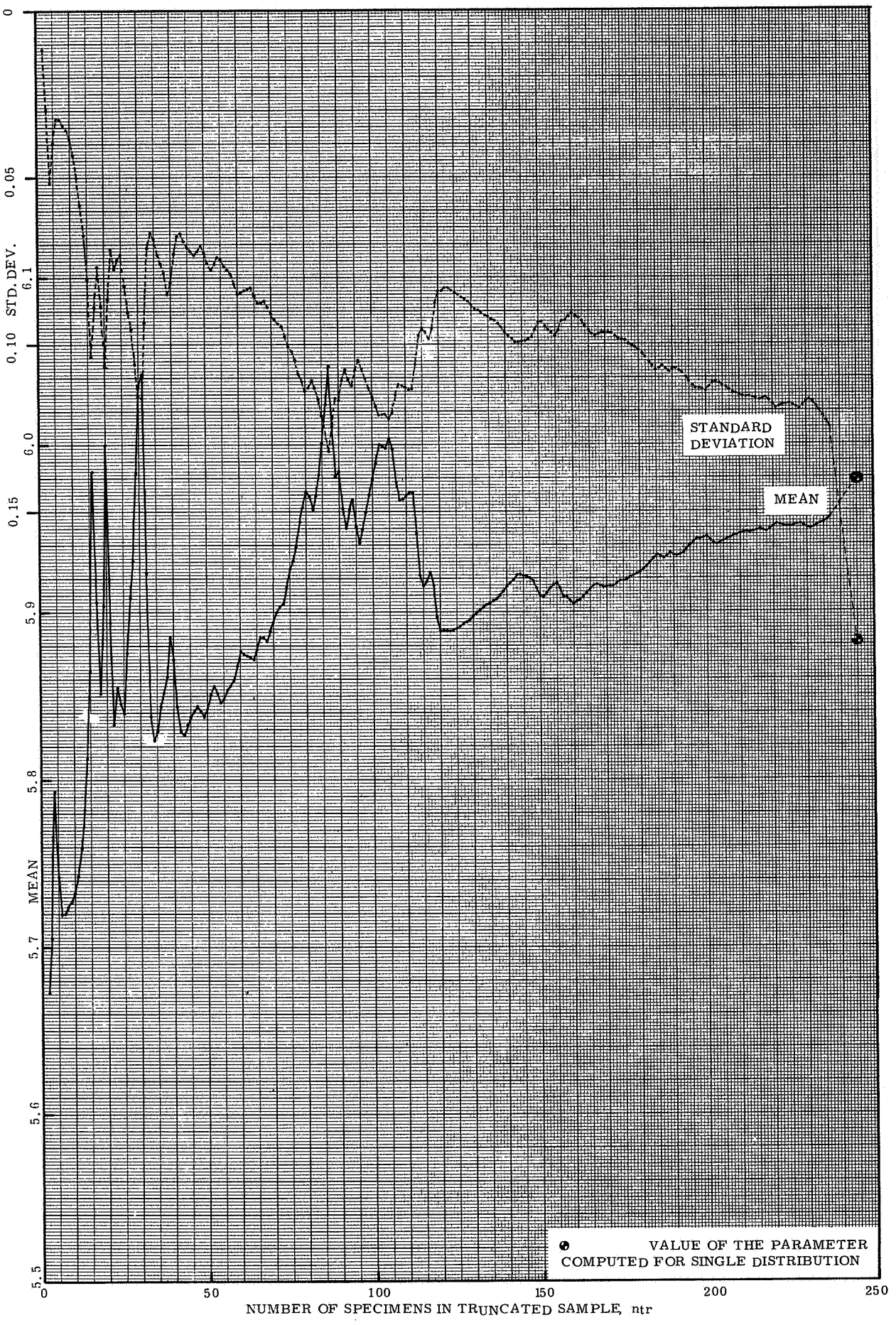

FIG. 12(c). PARAMETERS OF THE TRUNCATED LOG-NORMAL DISTRIBUTION. HIGH ENDURANCE PART EXCLUDED. BLOOMER & ROYLANCE, MACHINE- 3.

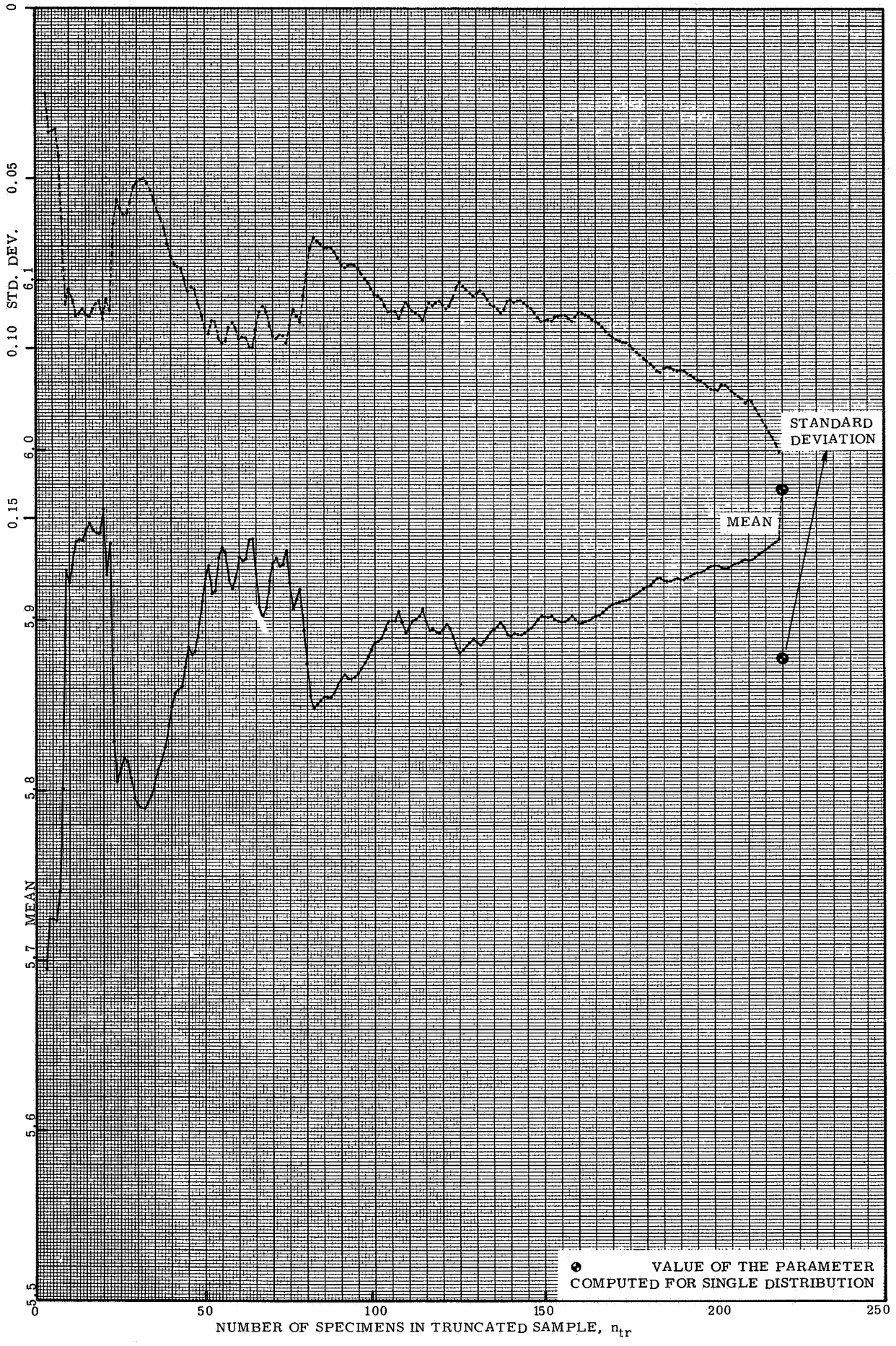

FIG. 12(d). PARAMETERS OF THE TRUNCATED LOG-NORMAL DISTRIBUTION. HIGH ENDURANCE PART EXCLUDED. BLOOMER & ROYLANCE, MACHINE- 4.

FIG. 12(e). PARAMETERS OF THE TRUNCATED LOG-NORMAL DISTRIBUTION. HIGH ENDURANCE PART EXCLUDED. BLOOMER & ROYLANCE, TOTAL.
$0 < n_{tr} < 250$.

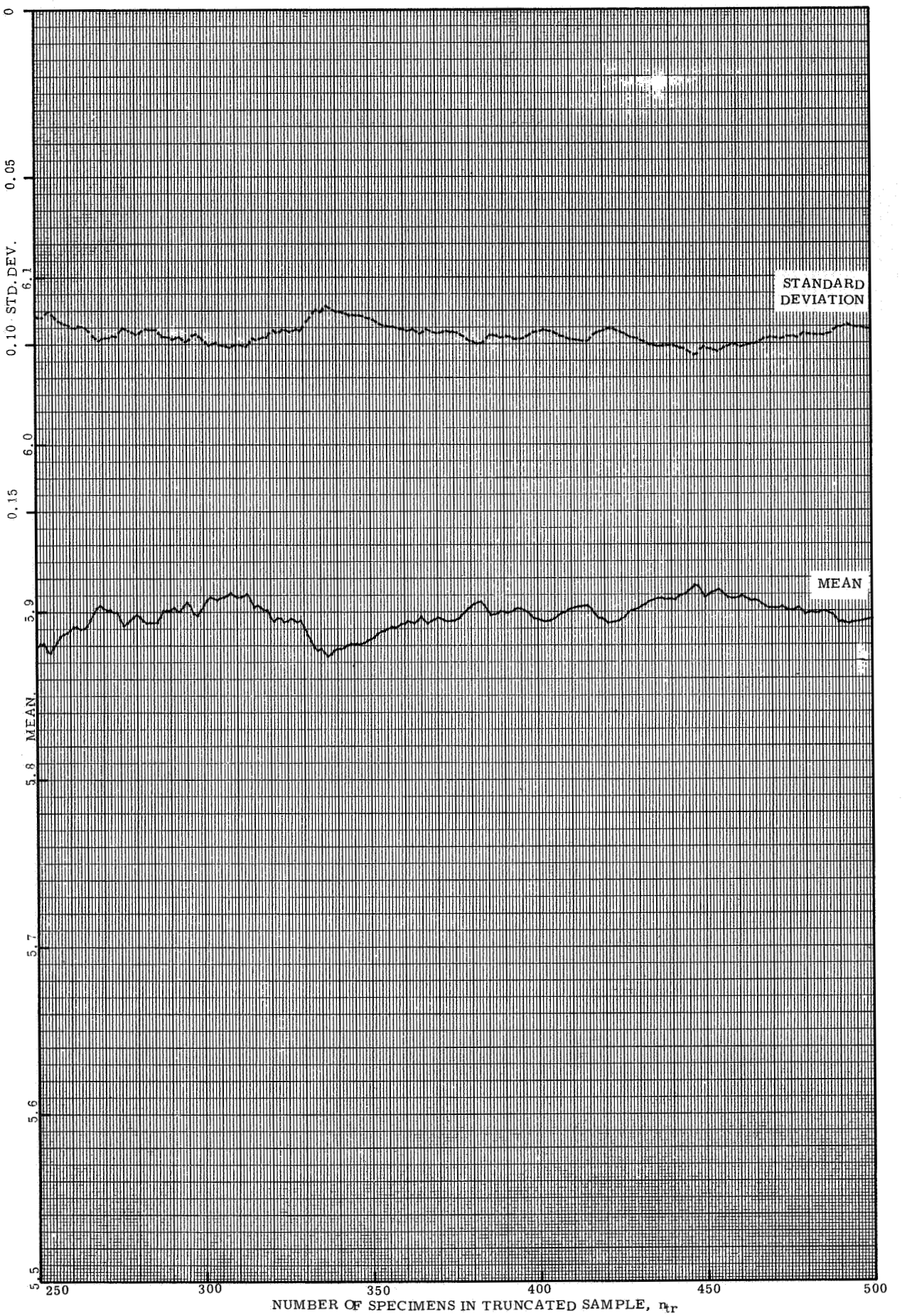

FIG. 12(e). PARAMETERS OF THE TRUNCATED LOG-NORMAL DISTRIBUTION. HIGH ENDURANCE PART EXCLUDED. BLOOMER &ROYLANCE, TOTAL.
$250 < n_{tr} < 500$.

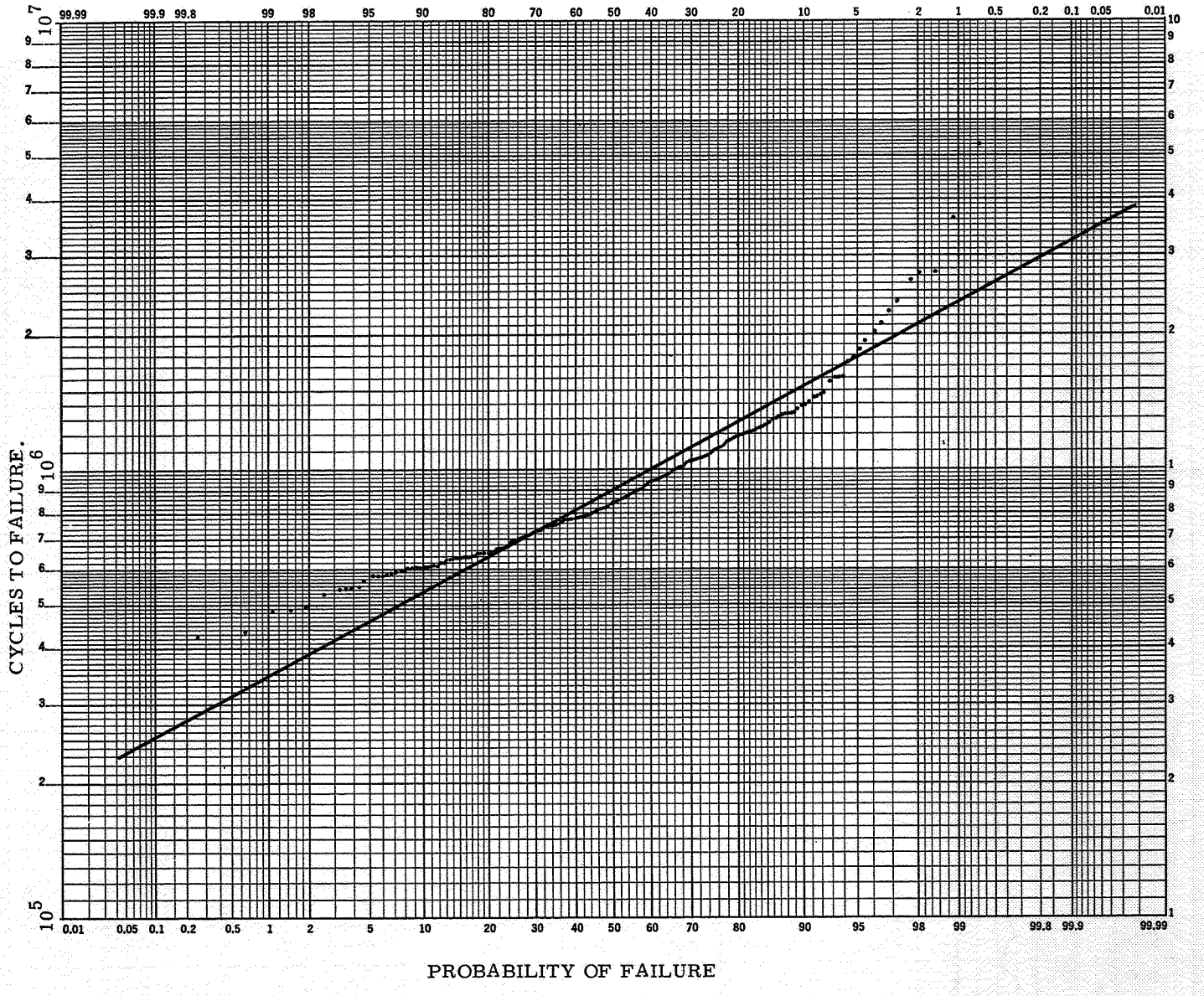

FIG. 13(a). LOG-NORMAL PROBABILITY PLOT. SINGLE DISTRIBUTION. BLOOMER & ROYLANCE, MACHINE-1; 243 SPECIMENS, r=0.93047.

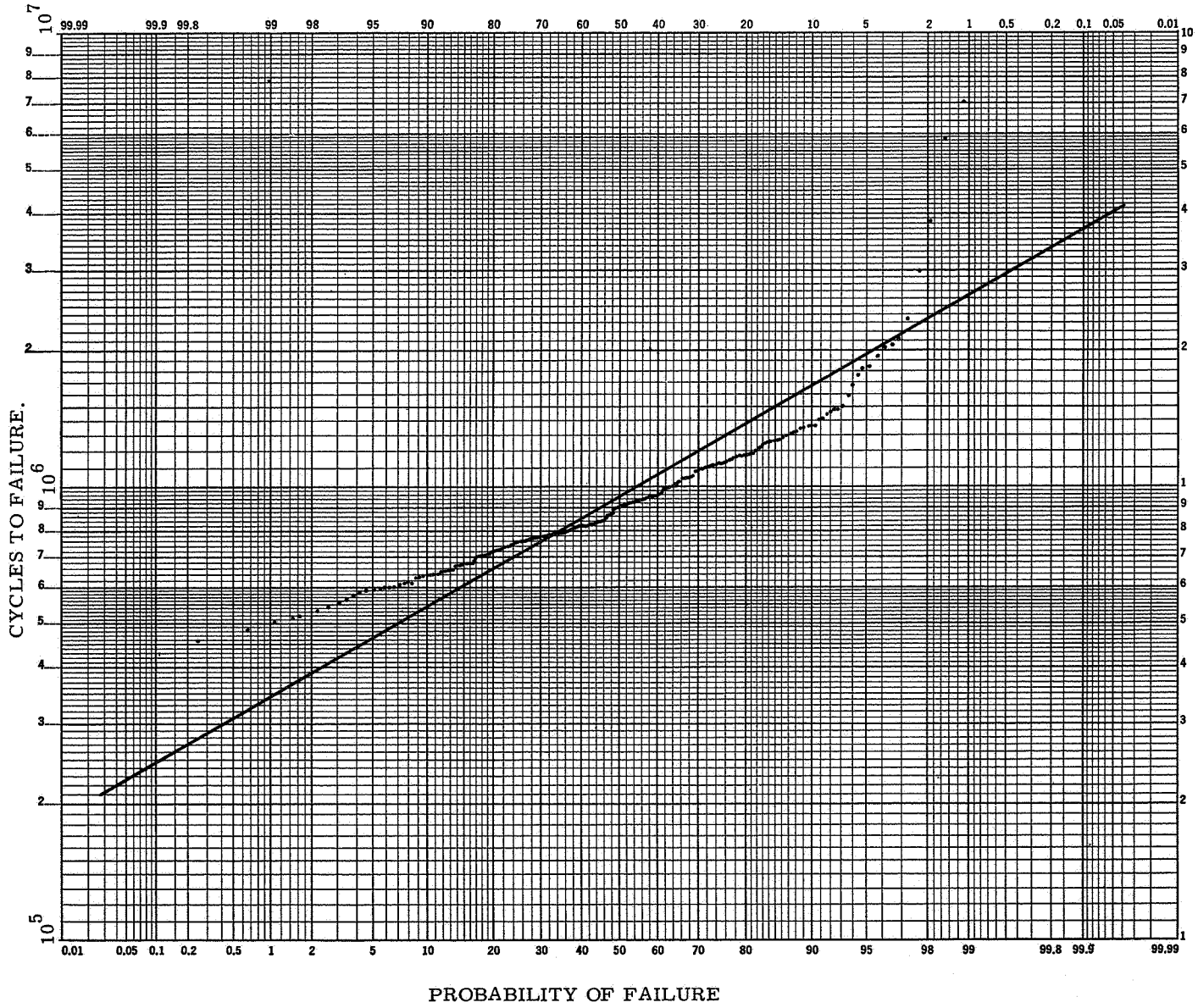

FIG. 13(c). LOG-NORMAL PROBABILITY PLOT. SINGLE DISTRIBUTION. BLOOMER & ROYLANCE, MACHINE-3; 245 SPECIMENS, r=0.88778.

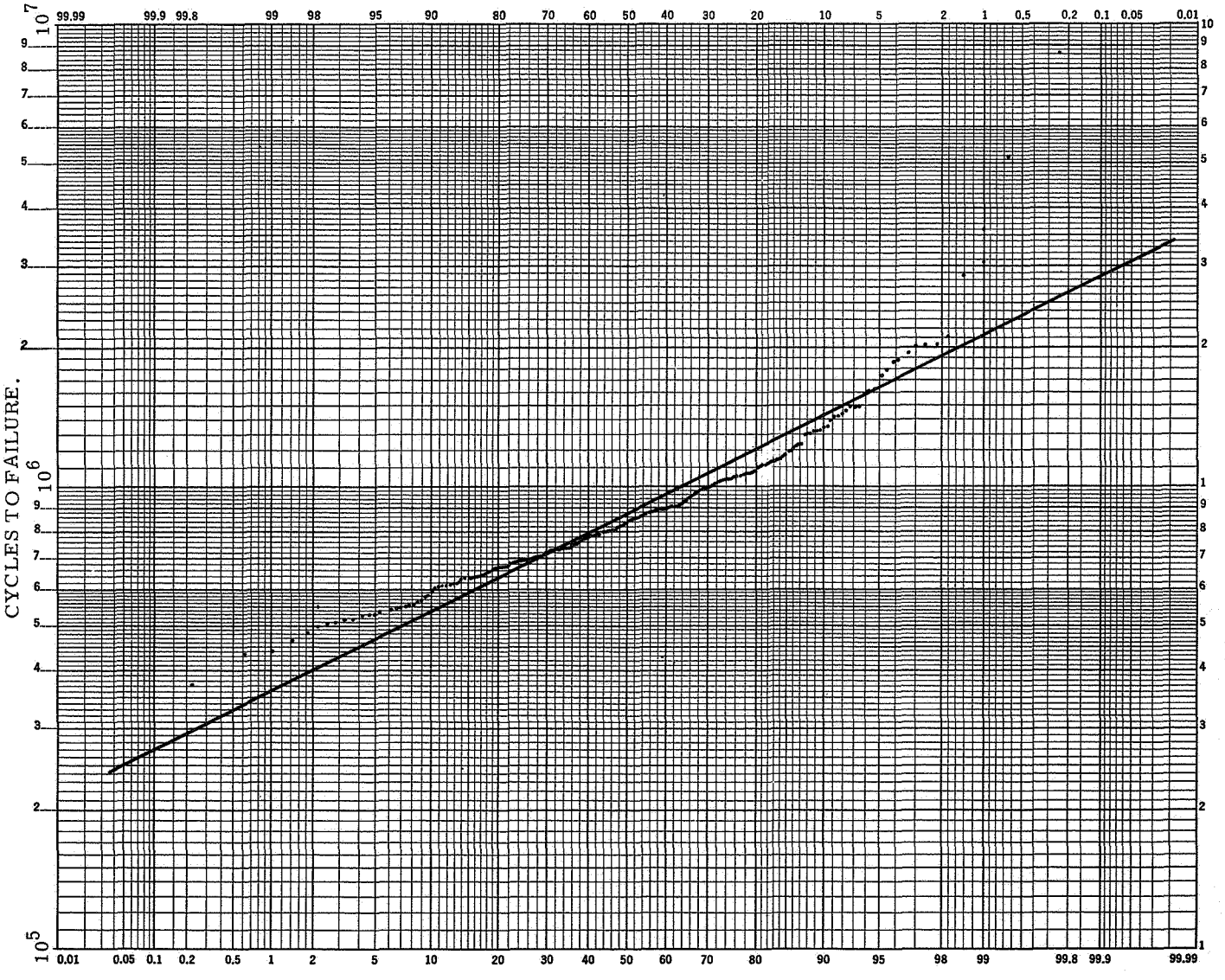

FIG. 13(b). LOG-NORMAL PROBABILITY PLOT. SINGLE DISTRIBUTION. BLOOMER & ROYLANCE, MACHINE-2; 255 SPECIMENS, r=0.94431.

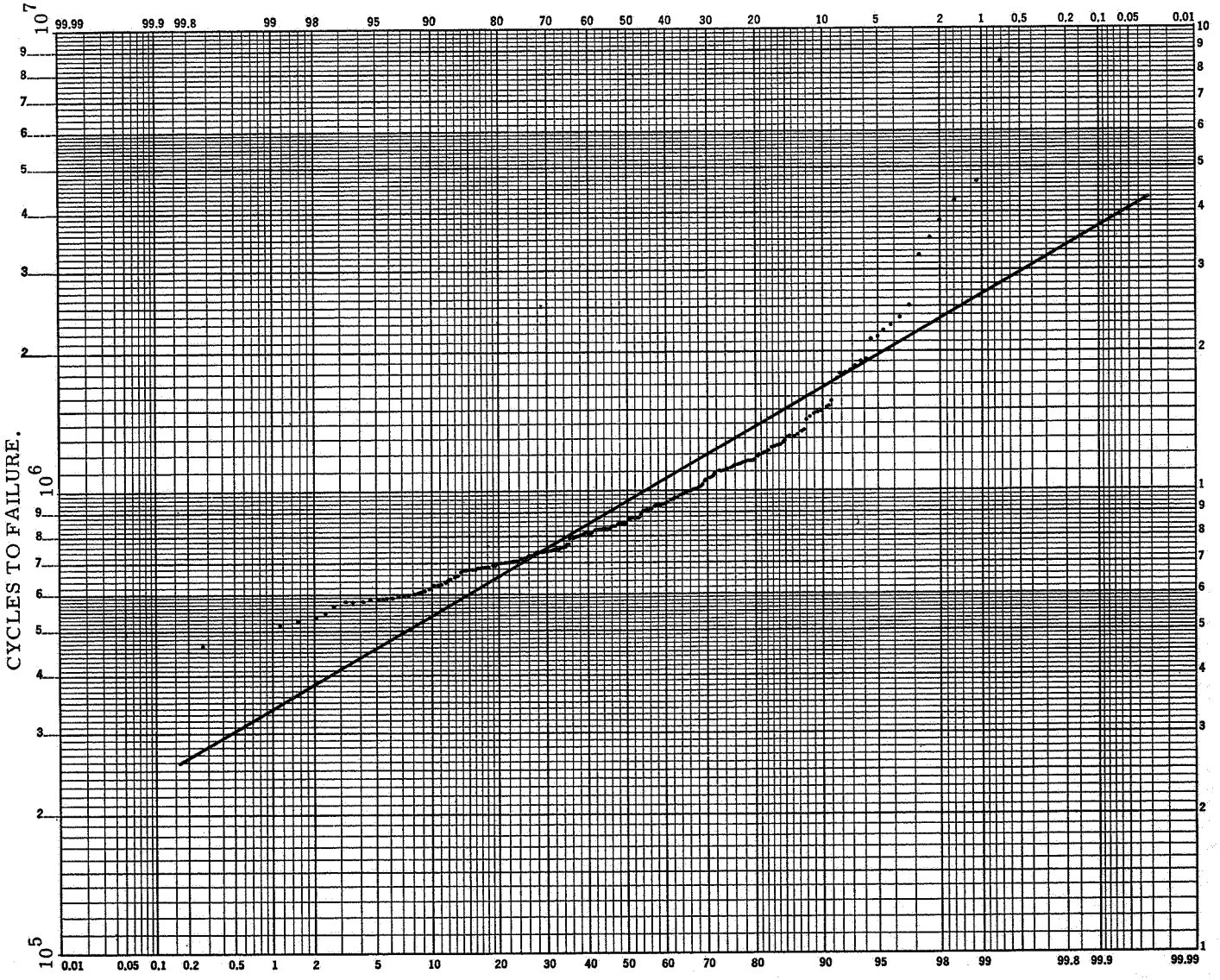

FIG. 13(d). LOG-NORMAL PROBABILITY PLOT. SINGLE DISTRIBUTION. BLOOMER & ROYLANCE, MACHINE-4; 230 SPECIMENS, r=0.91626.

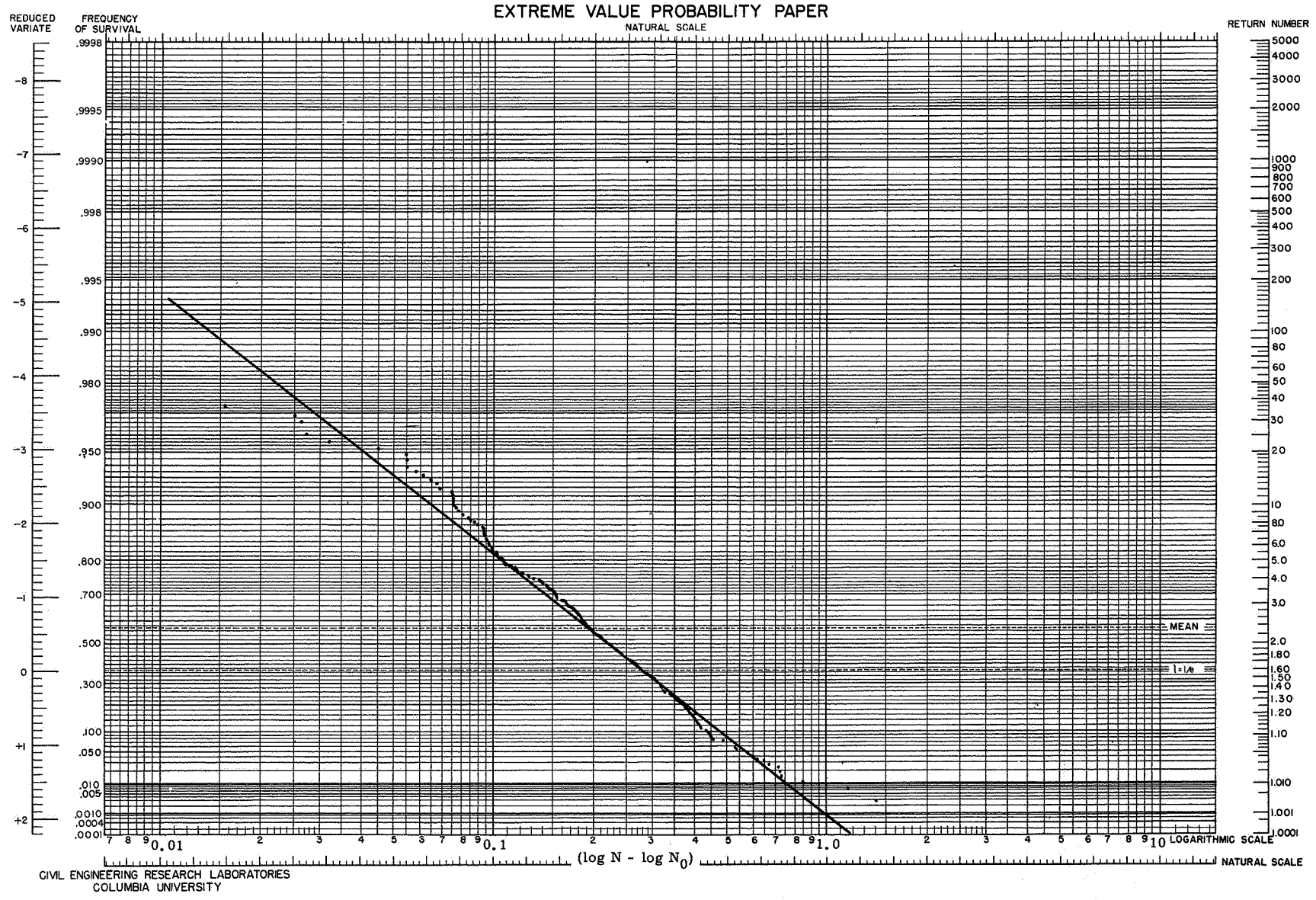

FIG. 14.a LOG-WEIBULL PROBABILITY PLOT. SINGLE DISTRIBUTION. PARAMETERS CALCULATED BY UPPER VERTICAL MOMENT METHOD. BLOOMER AND ROYLANCE, MACHINE-1, 243 SPECIMENS, $\log N_0 = 5.70737$.

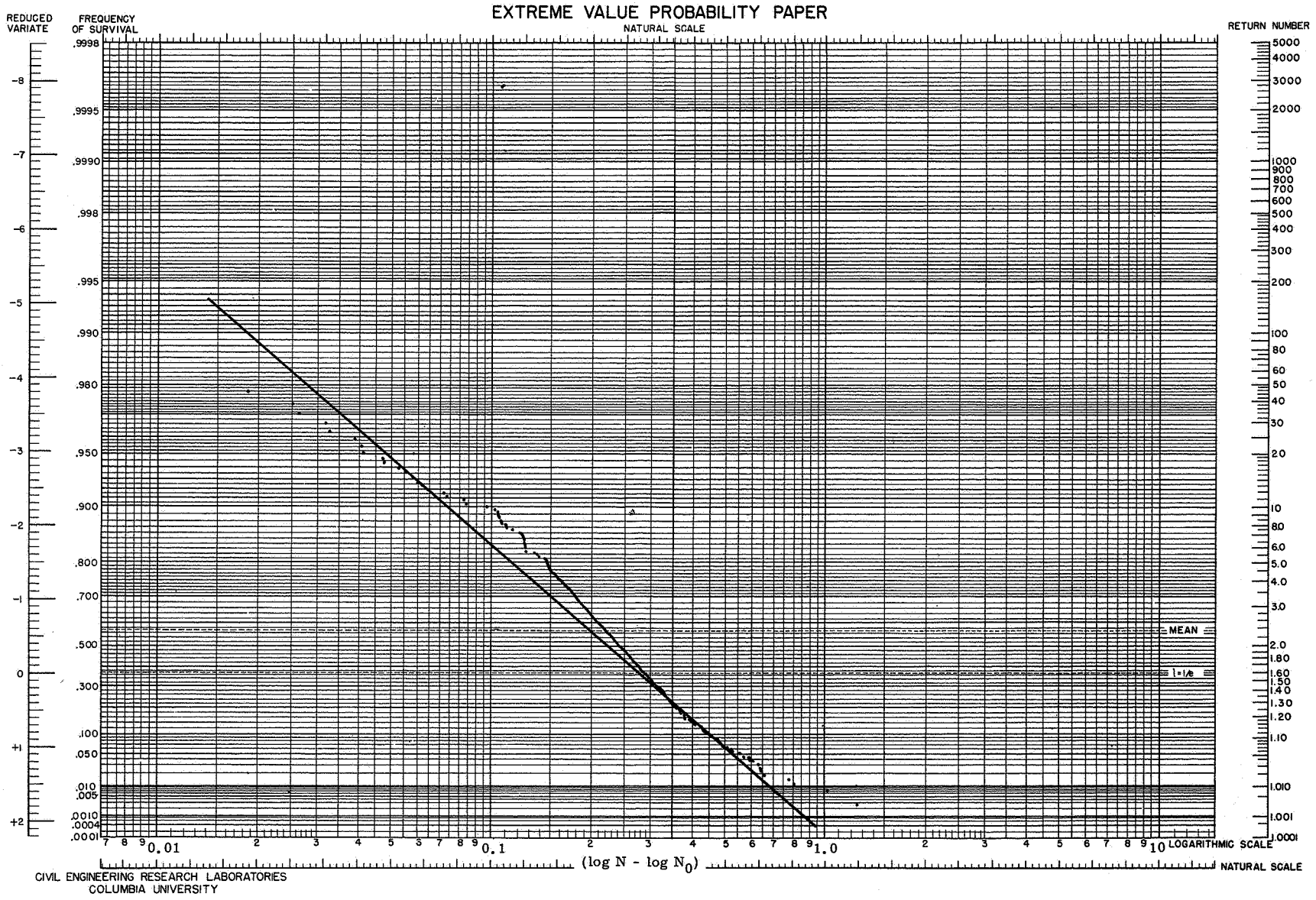

FIG. 14.b LOG-WEIBULL PROBABILITY PLOT. SINGLE DISTRIBUTION. PARAMETERS CALCULATED BY UPPER VERTICAL MOMENT METHOD. BLOOMER AND ROYLANCE, MACHINE-2, 255 SPECIMENS, $\log N_0 = 5.97763$.

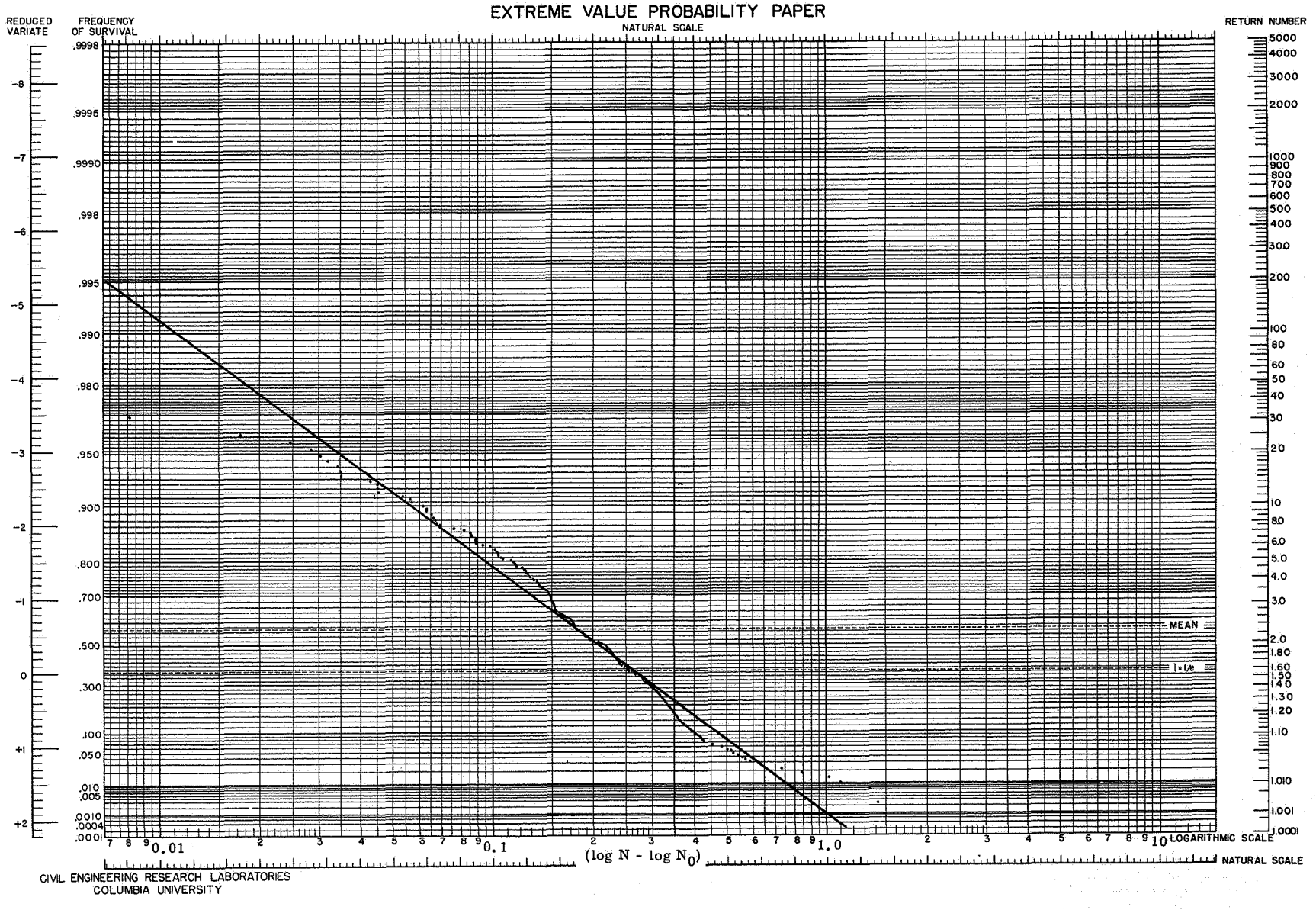

FIG. 14.c LOG-WEIBULL PROBABILITY PLOT. SINGLE DISTRIBUTION. PARAMETERS CALCULATED BY UPPER VERTICAL MOMENT METHOD. BLOOMER AND ROYLANCE, MACHINE-3, 245 SPECIMENS, $\log N_0 = 6.00701$.

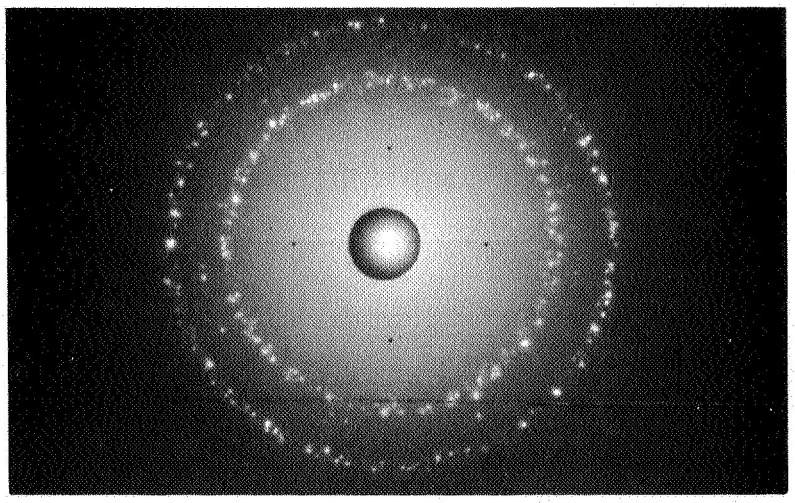

FIG. 15.a X-RAY BACK REFLECTION PATTERN OF A SPECIMEN FATIGUED AT S_a=10.0 ksi (Cu RADIATION).

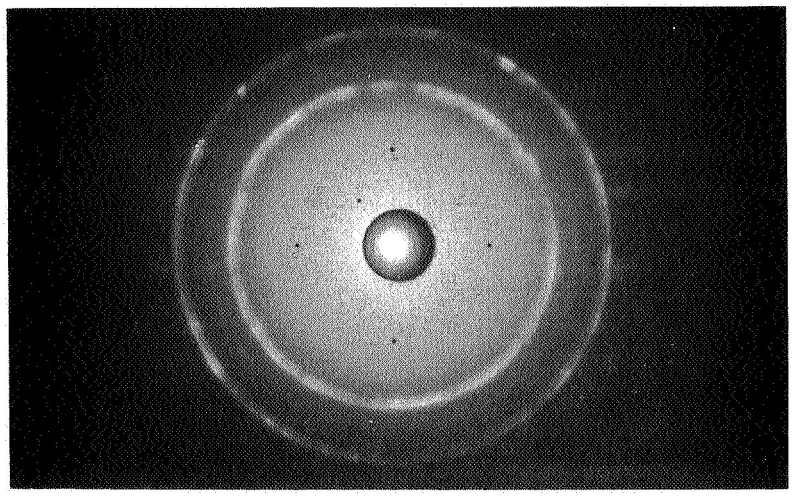

FIG. 15.b X-RAY BACK REFLECTION PATTERN OF A SPECIMEN FATIGUED AT S_a=16.5 ksi (Cu RADIATION).

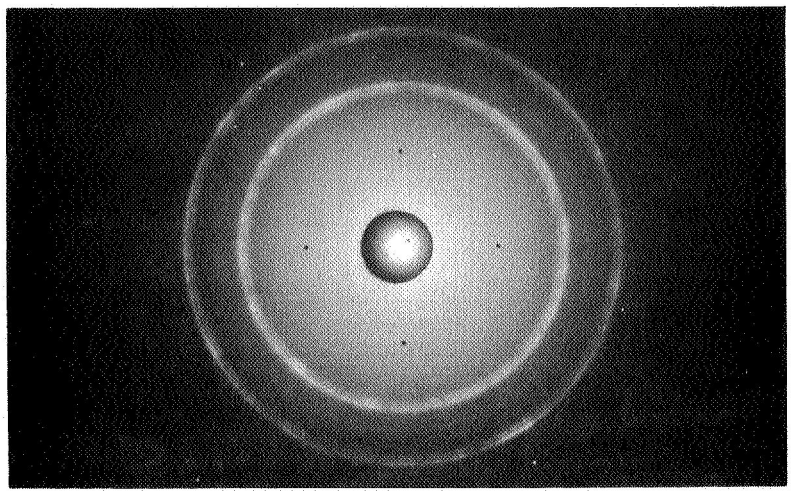

FIG. 15.c X-RAY BACK REFLECTION PATTERN OF A SPECIMEN FATIGUED AT S_a=19.0 ksi (Cu RADIATION).

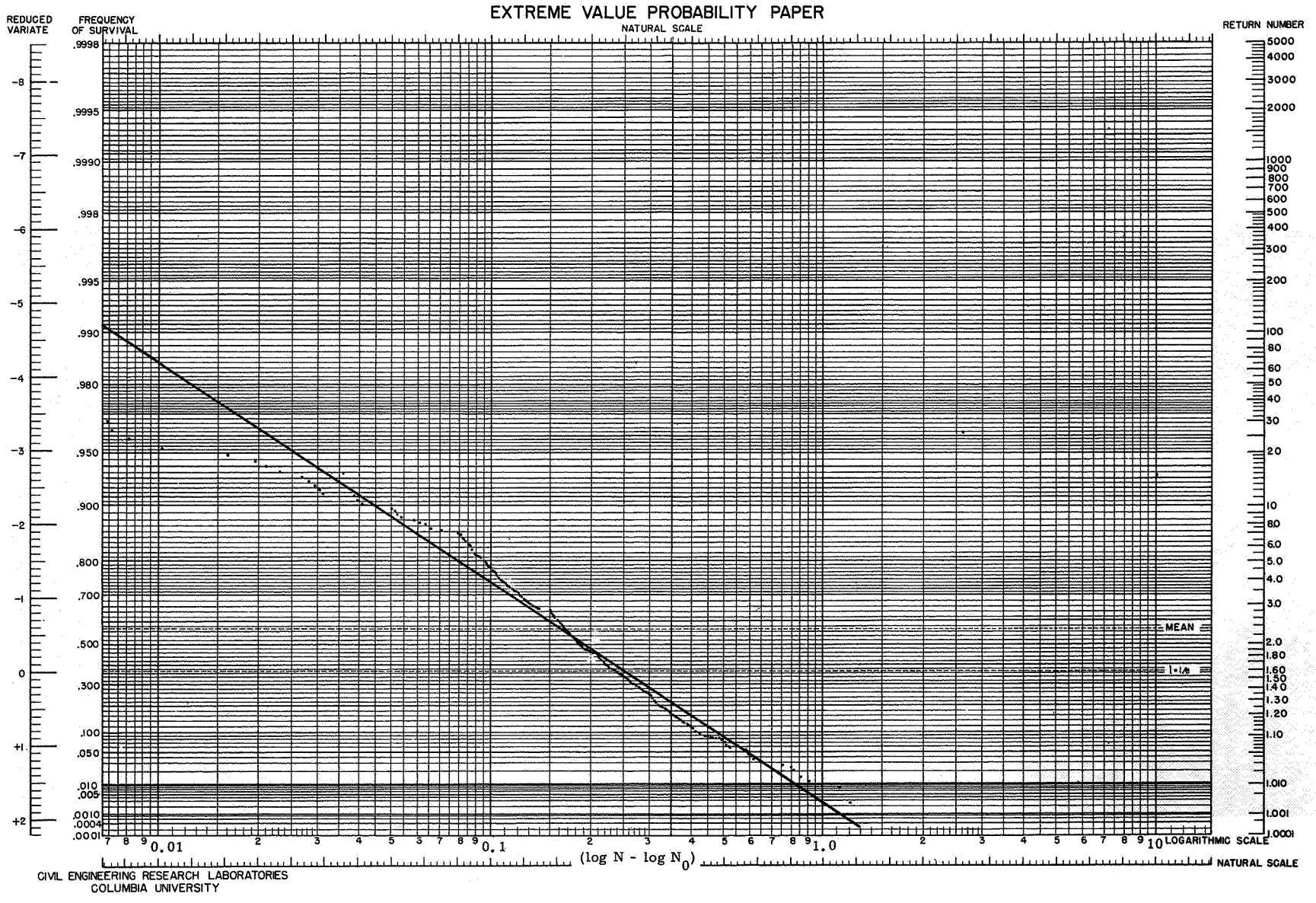

FIG. 14.d LOG-WEIBULL PROBABILITY PLOT. SINGLE DISTRIBUTION. PARAMETERS CALCULATED BY UPPER VERTICAL MOMENT METHOD. BLOOMER AND ROYLANCE, MACHINE-4, 230 SPECIMENS, $\log N_0 = 5.99812$.

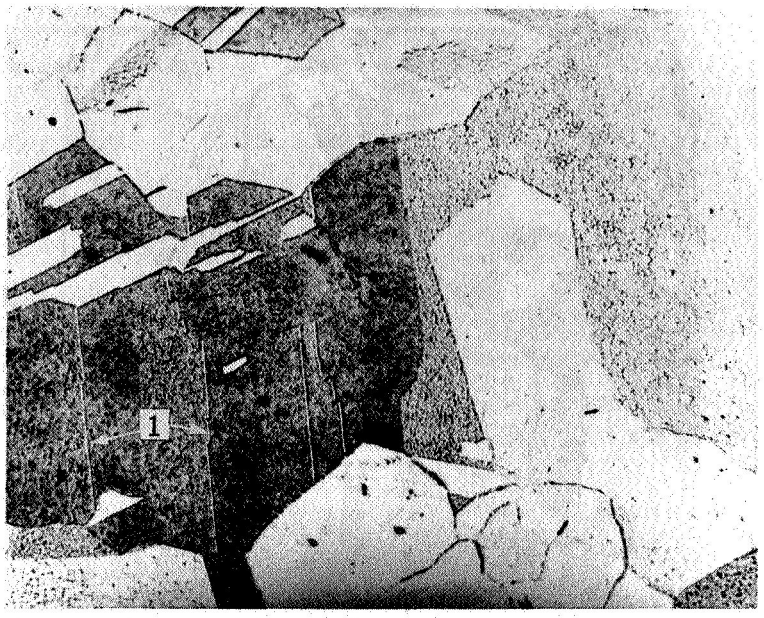

FIG. 16.a ETCHED-UP FATIGUED SLIP ZONES (F-14, ±10.0 ksi, x 500).
1. Distorted slip zones.

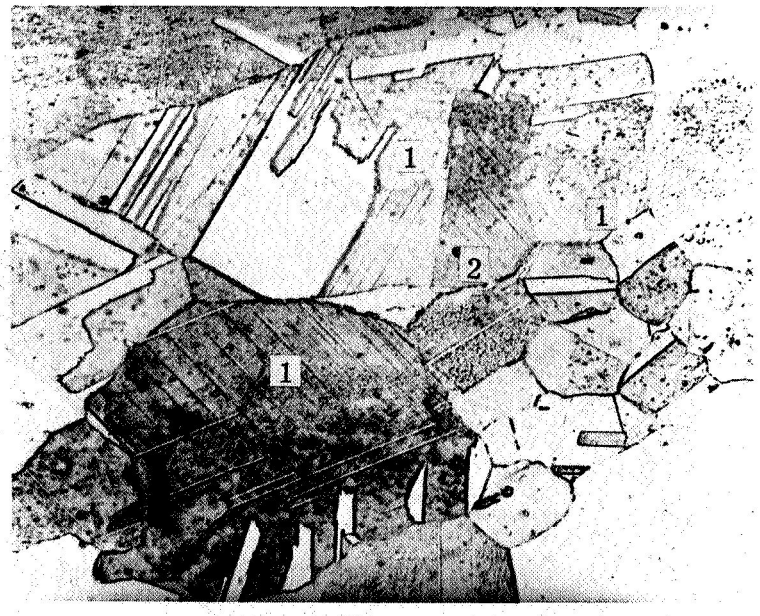

FIG. 16.b TYPICAL F-RANGE DAMAGE, STRAIGHT SLIP AND CROSS SLIP (F-13, ±10.0 ksi, x 500).
1. Cross slip
2. Straight slip.

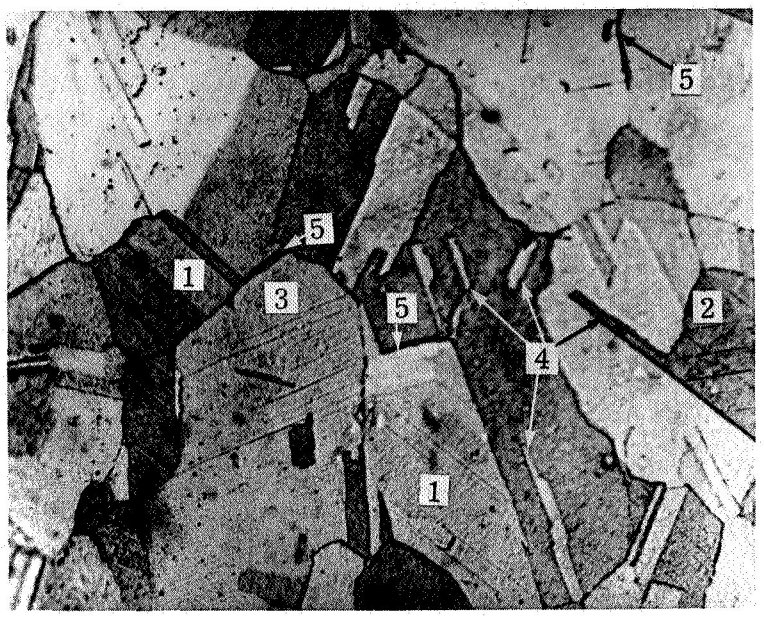

FIG. 16.c TYPICAL F-RANGE DAMAGE, STRAIGHT SLIP AND CROSS SLIP (F-14, ±10.0 ksi, x 500).
1. Straight slip 2. Cross slip 3. Distorted slip zones
4. Twin boundary distortion 5. Grain boundary damage.

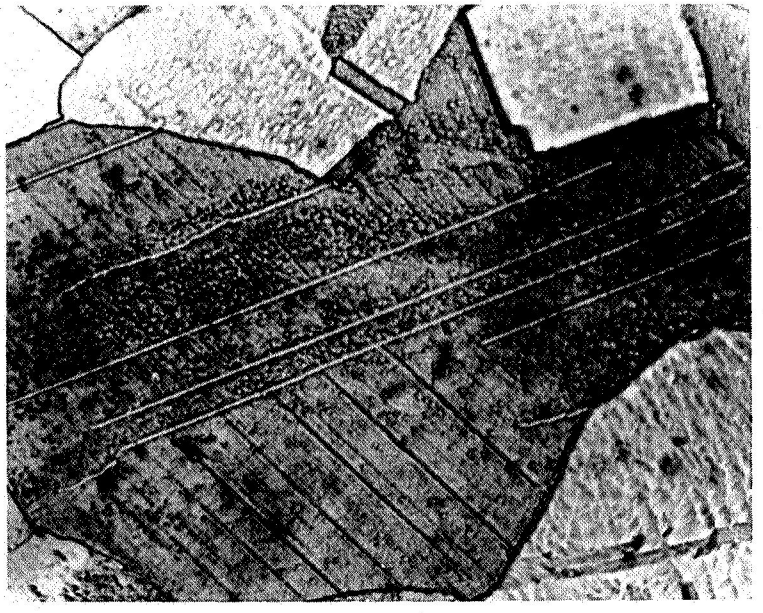

FIG. 16.d TYPICAL VIEW OF A GRAIN SHOWING CROSS SLIP AT HIGH MAGNIFICATION (F-13, ±10.0 ksi, x 1000).

FIG. 16.e TYPICAL F-RANGE DAMAGE, CROSS SLIP (F-13, ±10.0 ksi, x 500).
1. Cross slip.

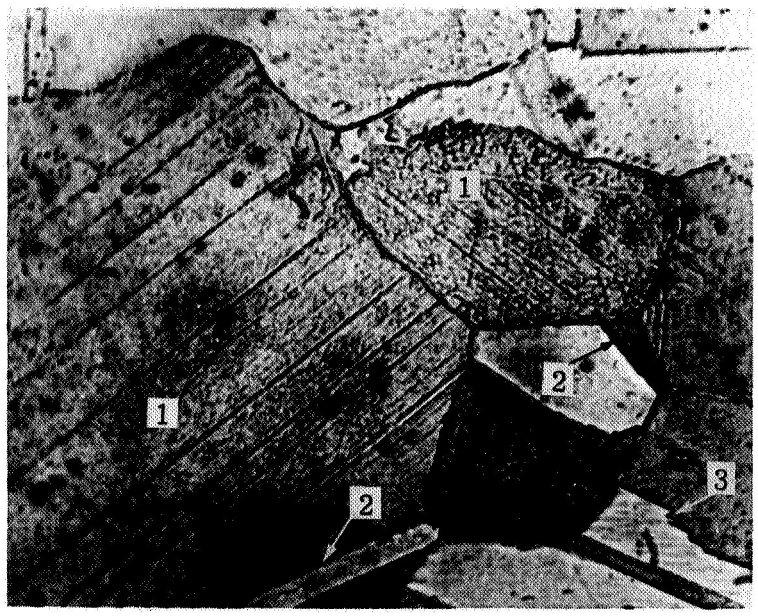

FIG. 16.f FATIGUED SLIP ZONES, TWIN BOUNDARY DAMAGE AND TWIN BOUNDARY DISTORTION (F-13, 10.0 ksi, x 1000)
1. Fatigued slip zones 2. Twin boundary damage
3. Twin boundary distortion.

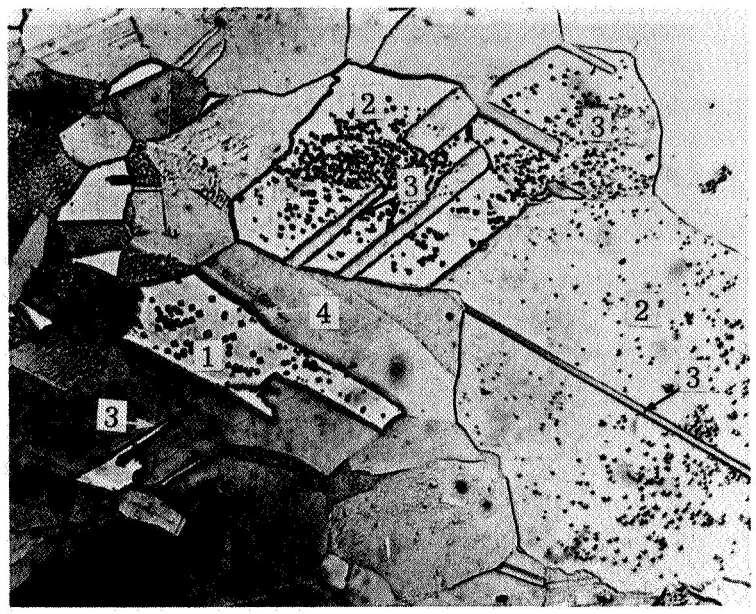

FIG. 17.a TYPICAL H-DAMAGE IN SEVERAL GRAINS (E-87, ±19.0 ksi, x 500)
1. Twin with H-damage showing etch pits
2. Grains with H-damage showing etch pits
3. Distorted twins 4. Twin boundary damage.

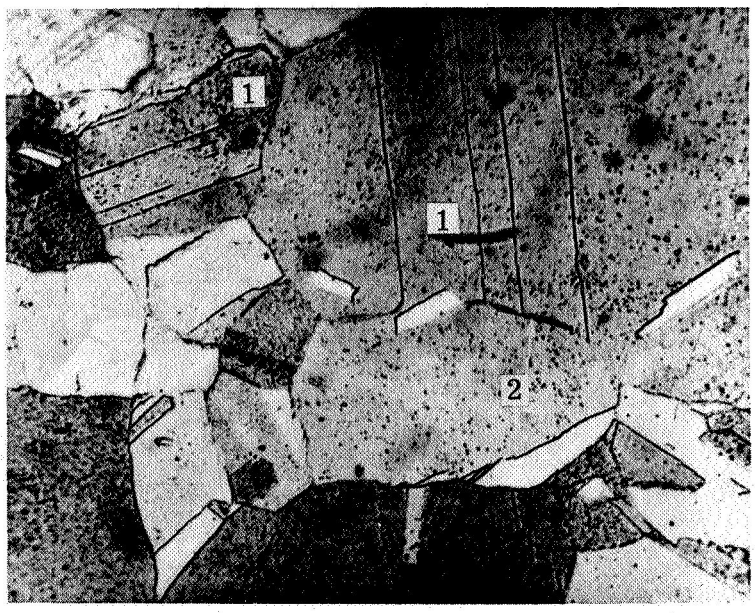

FIG. 17.b TYPICAL F-DAMAGE AT HIGH STRESS AMPLITUDES (E-83, ±19.0 ksi, x 1000).
1. Fatigued slip zones 2. Cell boundary damage.

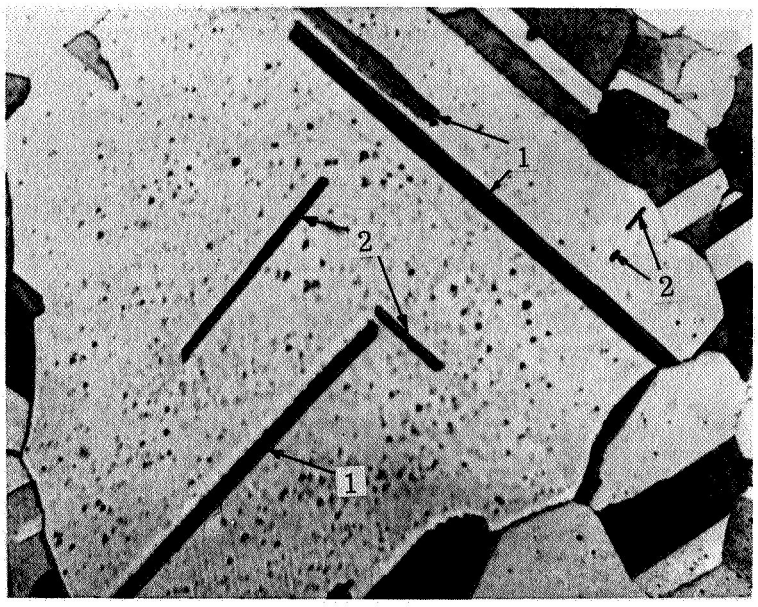

FIG. 17.c GRAIN WITH DISTORTED TWINS (E-83, ±19.0 ksi, x 1000).
1. Distorted twins with boundary damage 2. Cross slip.

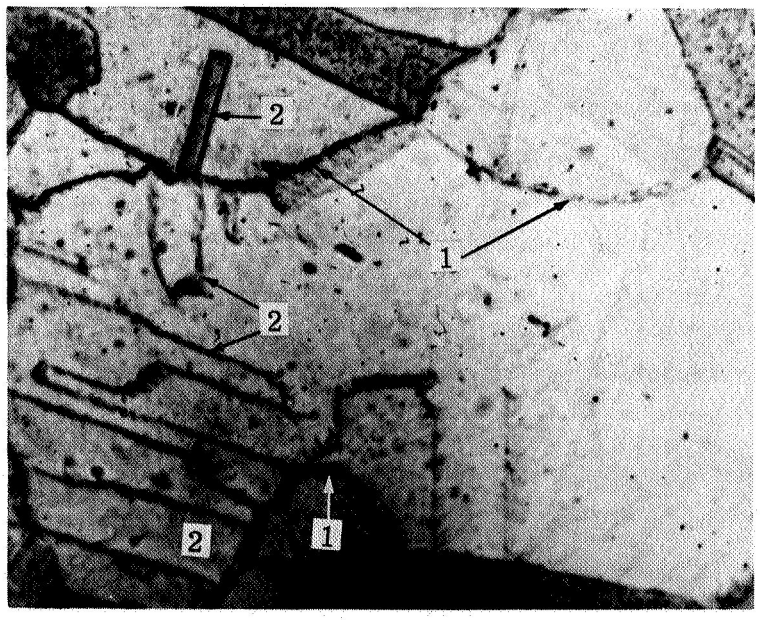

FIG. 17.d TYPICAL H-DAMAGE SHOWING CELL BOUNDARY DAMAGE (E-87, ±19.0 ksi, x 1000).
1. Cell boundary damage
2. Distorted twins with boundary damage.

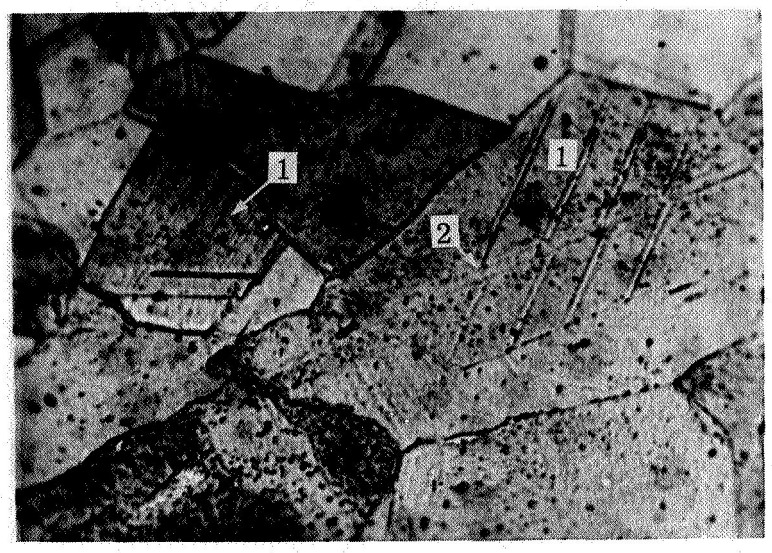

FIG. 17.e F-RANGE DAMAGE PRESENT AT HIGH STRESS AMPLITUDES (E-83, ±19.0 ksi, x 500)
1. Fatigued slip zones
2. Interaction between a twin and slip zones.

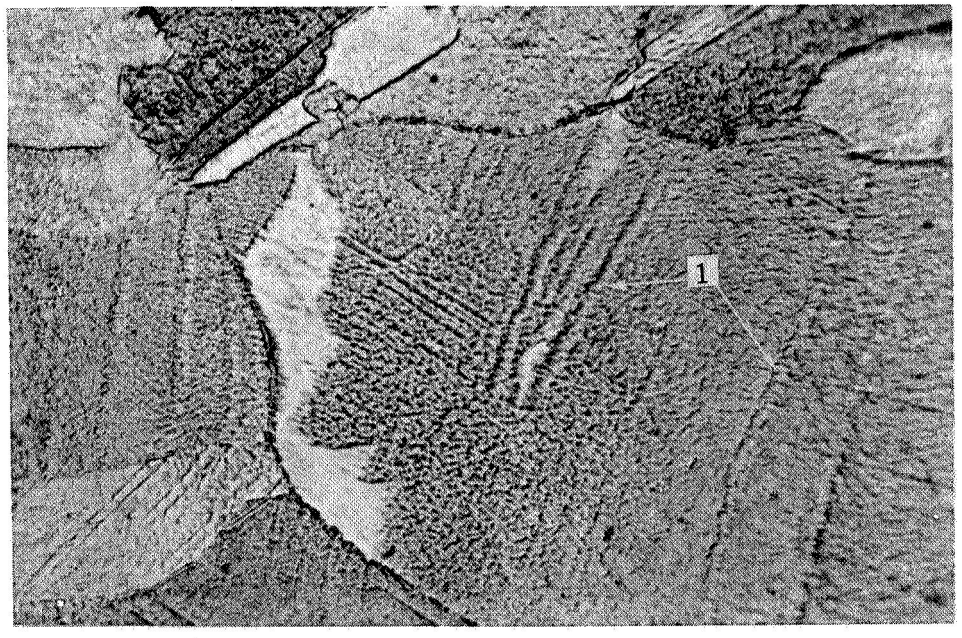

FIG. 18.a DISTORTED SLIP ZONES IN THE NEIGHBOURHOOD OF THE WORK HARDENED SURFACE LAYER (D-147, ±12.7 ksi, x 1500).
1. Distorted slip zones.

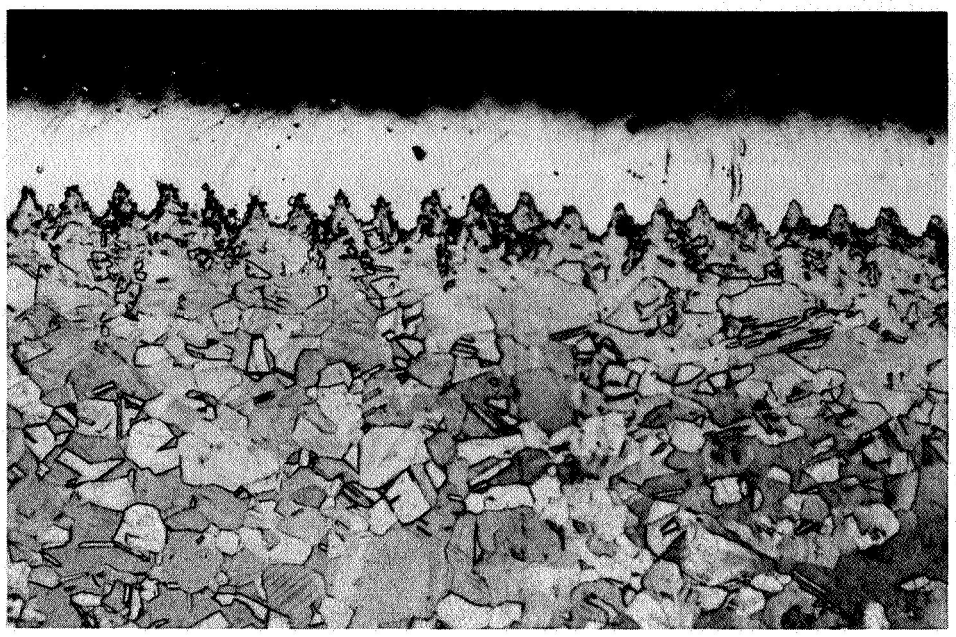

FIG. 18.b GROOVES LEFT BY FINAL MACHINING. EXTENSIVE TWINNING AND SOME SLIP CAN BE OBSERVED. (D-147, ±12.7 ksi, x 150)

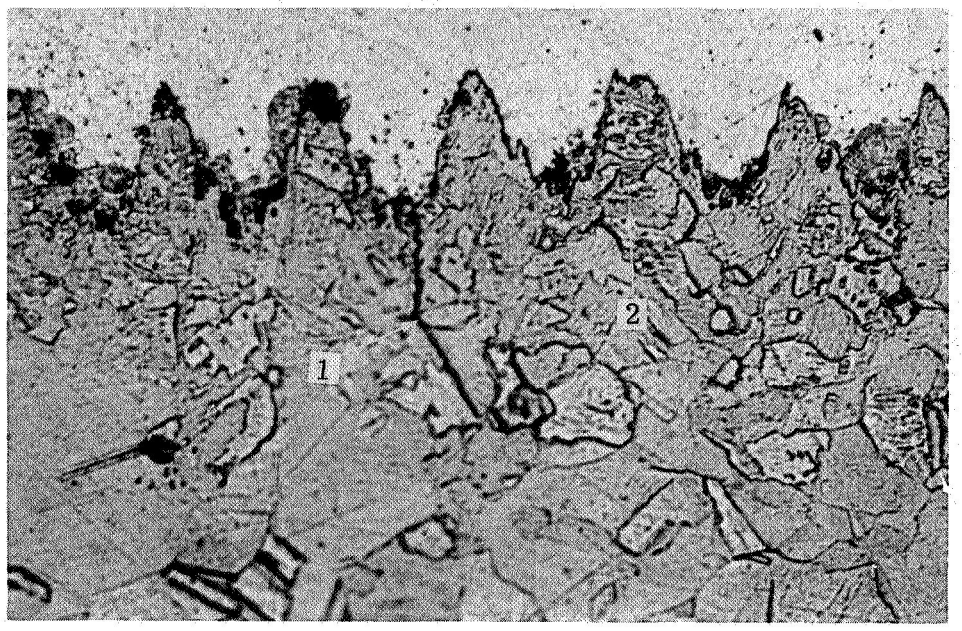

FIG. 18.c GROOVES LEFT BY FINAL MACHINING (D-147, ±12.7 ksi, x 500).
1. Microcrack from the groove
2. Work hardened surface layer.

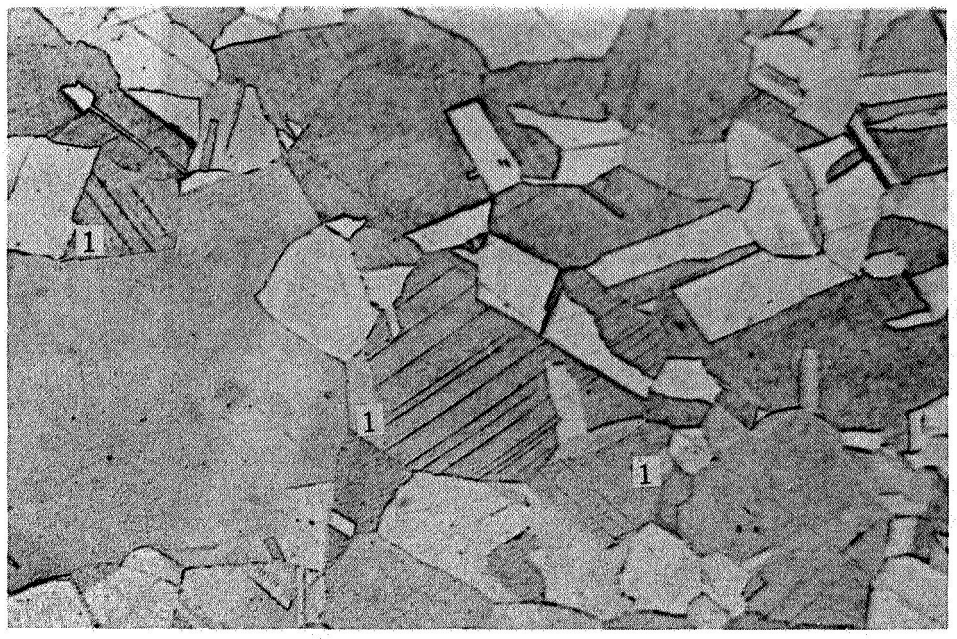

FIG. 18.d TYPICAL F-DAMAGE IN THE NEIGHBOURHOOD OF THE WORK HARDENED SURFACE LAYER (D-147, ±12.7 ksi, x 500).
1. Distorted slip zones.

FIG. 18.e EFFECT OF IMPROPER POLISHING PROCEDURE. NOTE THE THIN WORK HARDENED LAYER LEFTOVER BY POLISHING IN THE FORM OF BLACK PATCHES (D-147, +12.7 ksi, x 500)
1. Area shown at high magnification in Fig. 18.a

FIG. 19. a ABSENCE OF MICROCRACKS USUALLY DEVELOPING FROM GROOVES LEFT BY FINE-MACHINING. (A-21, ± 14 ksi, x150).

FIG. 19. b MICROCRACKS DEVELOPING AT THE ROOTS OF GROOVES LEFT BY FINE-MACHINING. (A-39, ±14 ksi, x150).

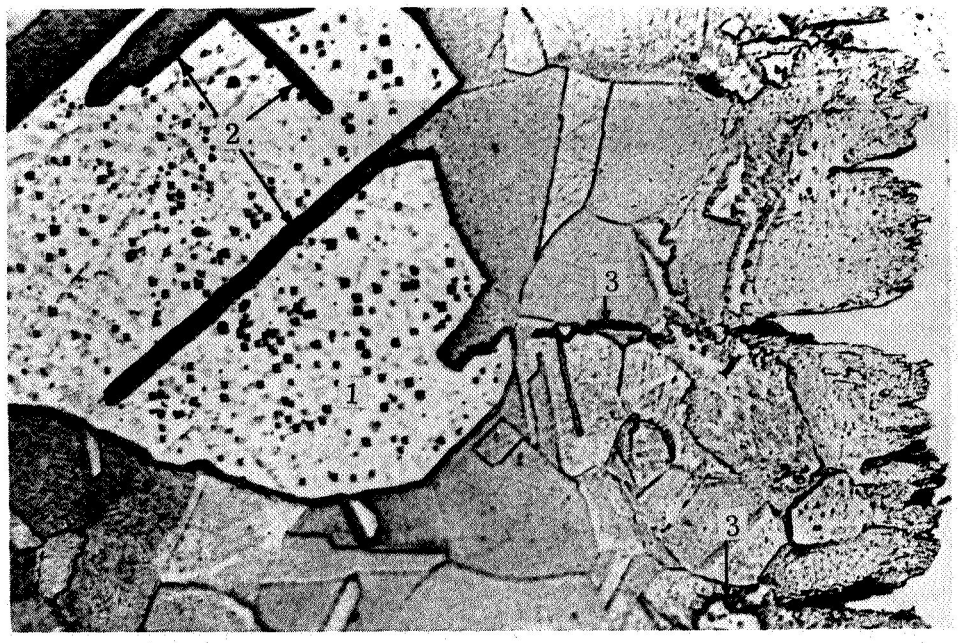

FIG. 19.c A TYPICAL GRAIN WITH H-RANGE DAMAGE IN THE VICINITY OF THE WORK HARDENED SURFACE LAYER (A-39, ±14.0 ksi x 500).
1. H-Range damage and etch pits
2. Distorted twins with boundary damage
3. Microcracks.

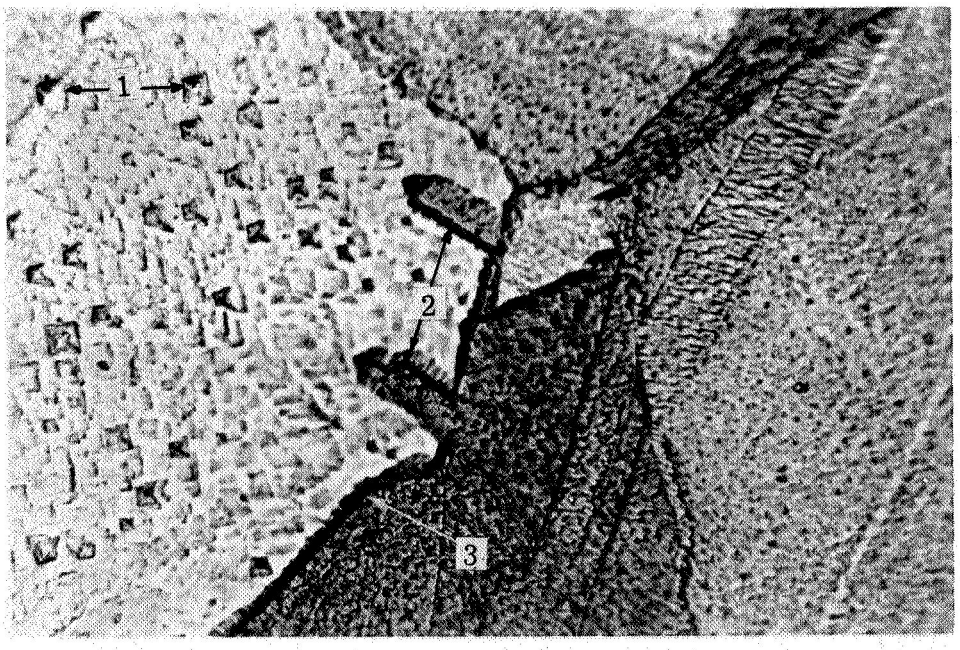

FIG. 19.d A GRAIN WITH H-RANGE DAMAGE AT HIGH MAGNIFICATION (A-39, ±14.0 ksi, x 1500).
1. Etch pits
2. Distorted twins with boundary damage
3. Grain boundary damage.

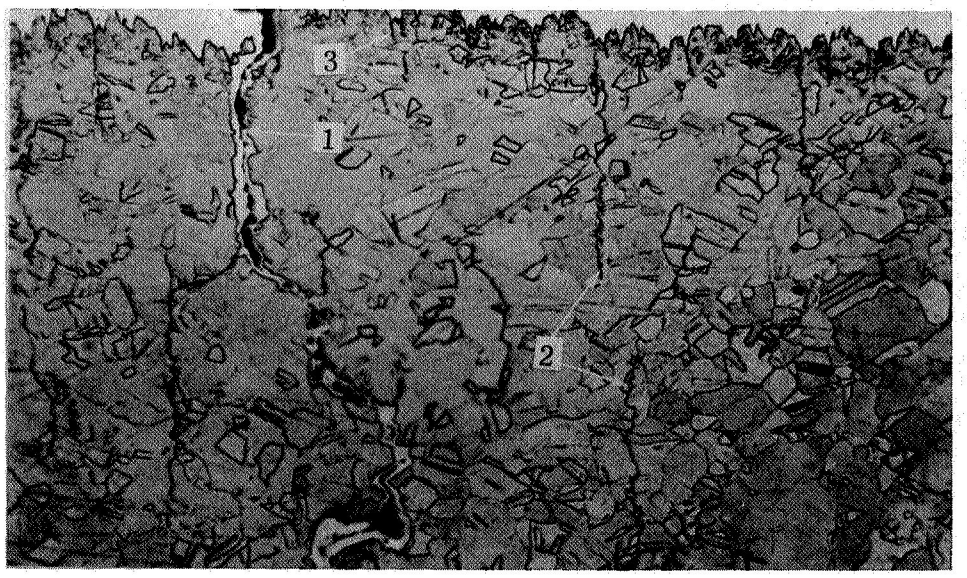

FIG. 20.a A TYPICAL VIEW SHOWING A NUMBER OF MICROCRACKS AND SEVERAL MACROCRACKS IN THE NEIGHBOURHOOD OF THE WORK HARDENED SURFACE LAYER (E-86, ±19.0 ksi, x 150).

1. Macrocrack which caused final failure 2. Macrocracks 3. Microcracks.

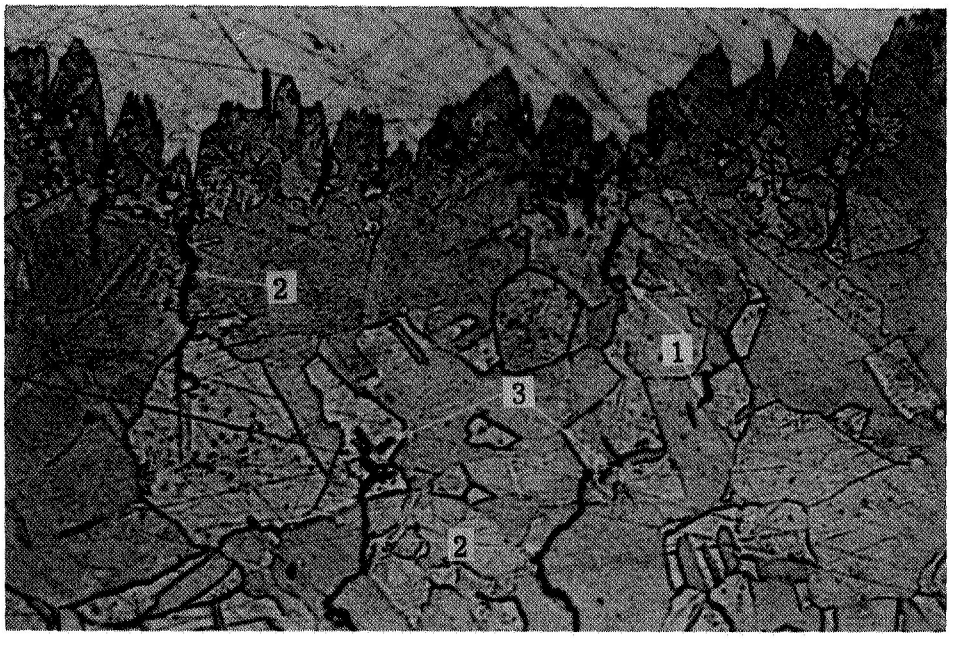

FIG. 20.b A TYPICAL VIEW SHOWING MICROCRACKS DEVELOPING FROM GROOVES LEFT BY FINAL MACHINING AND THE DEVELOPMENT OF MACROCRACKS BY LINKING-UP OF MICROCRACKS (E-86, 19.0 ksi, x 500).

1. Microcracks 2. Macrocracks 3. Microcracks about to link up with the neighbouring macrocracks.

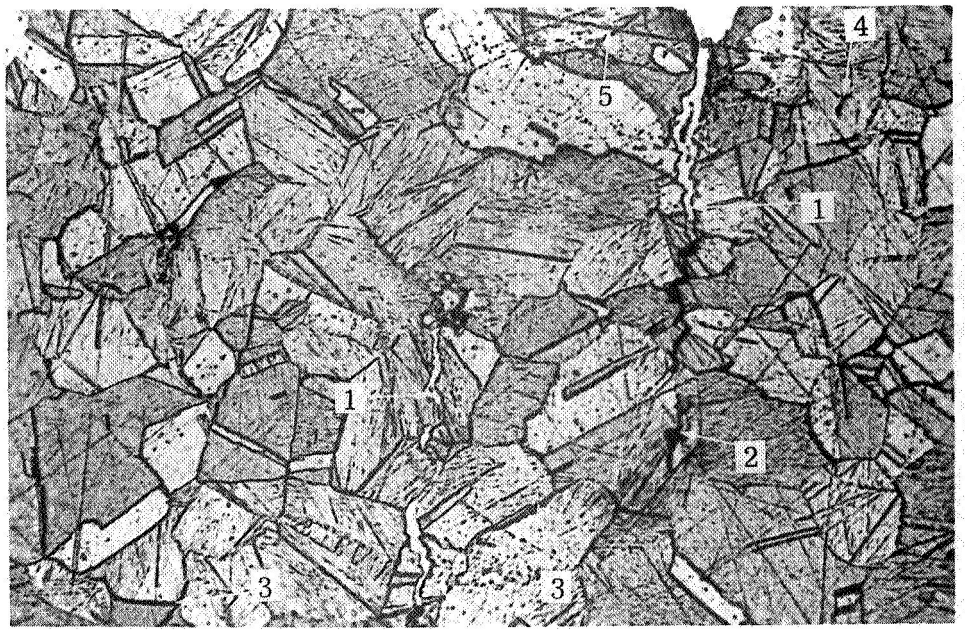

FIG. 20.c ORIGIN OF MICROCRACKS IN THE VICINITY OF THE WORK HARDENED SURFACE LAYER (E-51, ±19.0 ksi, x 500).
1. Macrocrack 2. A microcrack about to link up with the macrocrack 3. Grain boundary damage, about to open up into cracks 4. Microcracks in the interior of a grain 5. Polishing marks.

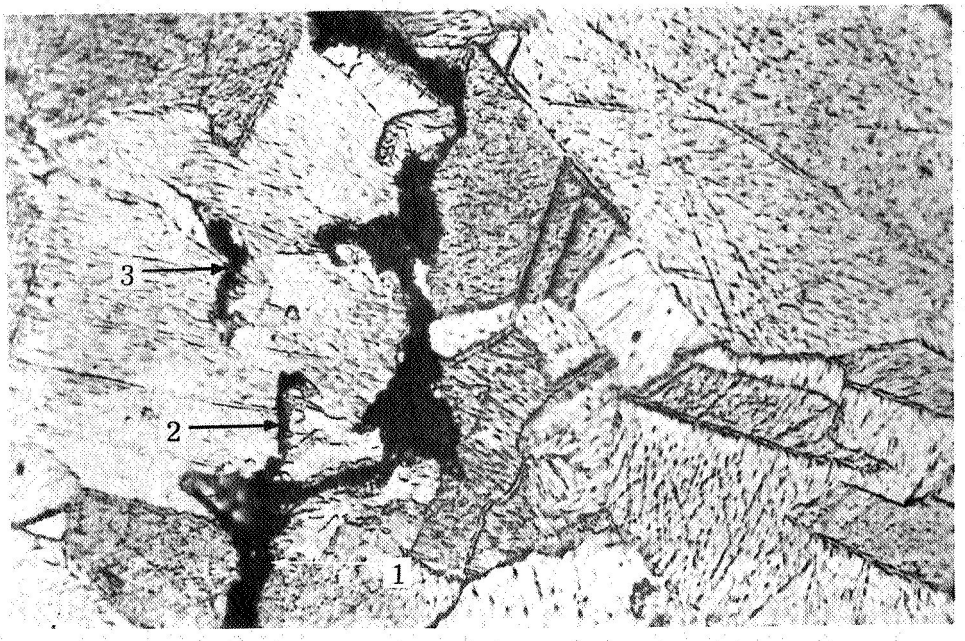

FIG. 20.d EVIDENCE OF LINK UP OF MICROCRACKS WITH THE MACROCRACK (E-51, ±19.0 ksi, x 1500).
1. Macrocrack running along the grain boundary 2. A microcrack which has just linked up with the macrocrack 3. A microcrack which was likely to link up with (2) if there had been further cycling.

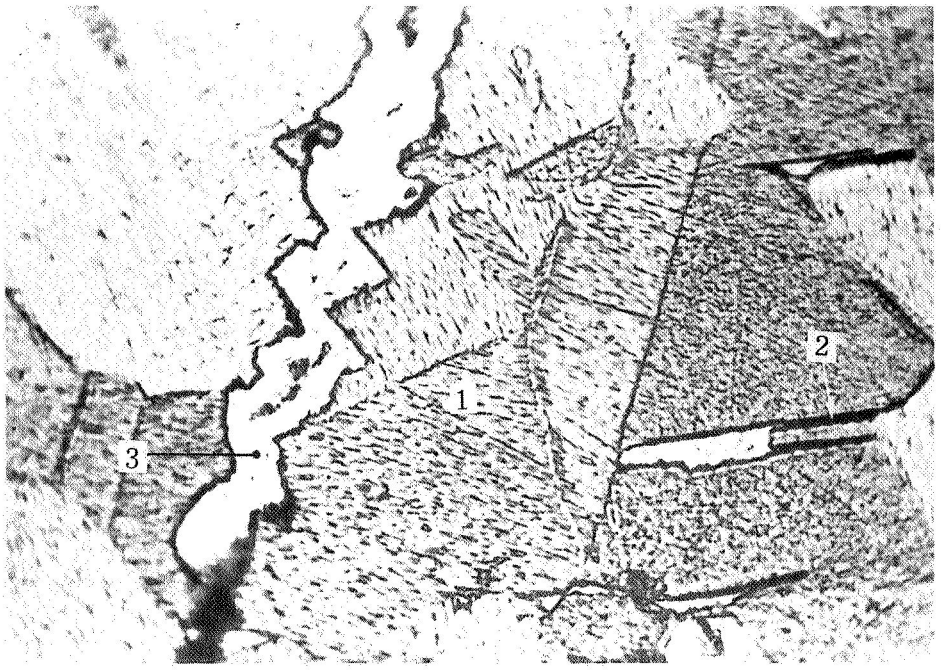

FIG. 20.e A TYPICAL MACROCRACK AT HIGH MAGNIFICATION (E-51, ±19.0 ksi, x 1500).
1. Macrocrack 2. Twin boundary damage 3. Silver deposit.

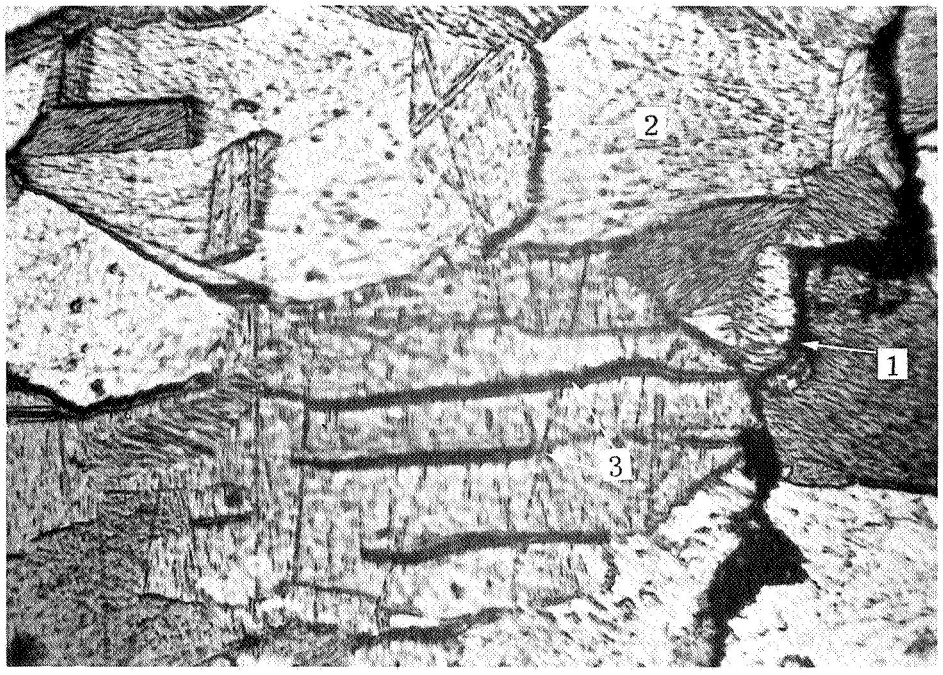

FIG. 20.f FATIGUED SLIP ZONES AT HIGH MAGNIFICATION (E-51, ±19.0 ksi, x 1500).
1. Macrocrack 2. Cell boundary damage 3. Fatigue slip zones about to open up into cracks.